Dynamics of Clustering in Systems of Granular and Active Particles

A Thesis

Submitted for the Degree of

DOCTOR OF PHILOSOPHY

in the Faculty of Science

by

Subhajit Paul

THEORETICAL SCIENCES UNIT
JAWAHARLAL NEHRU CENTRE FOR ADVANCED SCIENTIFIC RESEARCH
Bangalore – 560 064

JUNE 2017

To my family

DECLARATION

I hereby declare that the matter embodied in the thesis entitled "**Dynamics of Clustering in Systems of Granular and Active Particles**" is the result of investigations carried out by me at the Theoretical Sciences Unit, Jawaharlal Nehru Centre for Advanced Scientific Research, Bangalore, India under the supervision of Prof. Subir K. Das and that it has not been submitted elsewhere for the award of any degree or diploma.

In keeping with the general practice in reporting scientific observations, due acknowledgement has been made whenever the work described is based on the findings of other investigators.

Subhajit Paul.

Subhajit Paul

CERTIFICATE

I hereby certify that the matter embodied in this thesis entitled "**Dynamics of Clustering in Systems of Granular and Active Particles**" has been carried out by Mr. Subhajit Paul at the Theoretical Sciences Unit, Jawaharlal Nehru Centre for Advanced Scientific Research, Bangalore, India under my supervision and that it has not been submitted elsewhere for the award of any degree or diploma.

Prof. Subir K. Das
(Research Supervisor)

Acknowledgements

First and foremost, I would like to express my sincere and warmest gratitude towards my thesis supervisor Prof. Subir K. Das, for giving me the opportunity to pursue Ph.D. under his guidance. I am thankful to him for his help, encouragement, important suggestions, and guidance throughout my Ph.D. years. He has introduced me to a diverse set of problems. I feel great respect for his brilliance, hard work, and honesty. Working with him was really a nice experience.

I would like to acknowledge all other faculty members of Theoretical Sciences Unit (TSU) - Prof. Swapan K. Pati, Prof. N.S. Vidhyadhiraja, Prof. Umesh V. Waghmare, Prof. K.B. Sinha, Prof. Shobhana Narasimhan, Prof. Kavita Jain, Prof. Srikanth Sastry, and Dr. Meher K. Prakash - for various important scientific discussions.

I would like to express my gratitude to all my course instructors from JNCASR - Prof. Subir K. Das, Prof. Swapan K. Pati, Prof. N.S. Vidhyadhiraja, Prof. Kavita Jain, Prof. Shobhana Narasimhan, Prof. Umesh V. Waghmare, Prof. Balasubramanian Sundaram, and Prof. Rajesh Ganapathy - for all the wonderful courses they have taught.

Particular mention should be made of one of my school teachers Dr. Uttam Ghosh, who taught me mathematics during higher secondary. I am also very much thankful to a few of my former teachers - Late Mr. Ramchandra Ghosh, Mr. Kalyan Majumdar, Dr. Subir Sarkar, Mr. Dipak Dey, Dr. Dipak Ghose, Dr. Chandramadhab Pal, Dr. Abhijit Chakraborty, Dr. Basudeb Ghosh, and Mr. Subhash Lahiri - for their teaching as well as for all the encouragements and support to pursue higher studies.

I am thankful to all the members from Hostel, Complab, Library, Administration, Academic section, and other departments as well, for all their help. I am also thankful to all the doctors from Dhanvantari for their immense help in last three years.

I acknowledge JNCASR and University Grants Commission (UGC) for the financial supports during my Ph.D. years.

I thank all my past and present lab members - Dr. Suman Majumder, Dr. Sutapa Roy, Dr. Shaista Ahmed, Saugata Patra, Saikat Chakraborty, Dr. Jiarul Midya, Dr. Sunita, Nalina V., Jyoti Prasad Banerjee, Arabinda Bera, and Koyel Das - for various scientific and non-scientific discussions and for creating a research-friendly atmosphere in the lab. In addition, I am thankful to my friends in JNCASR - Jiaul Hoque, Dr. Avijit Saha, Dr. Sudeshna Sen, Koushik Pal, Dr. Dibyajyoti Ghosh, Debdipto Acharya, Sourav Mondal, Dr. Ritesh Haldar, Somnath Ghara, Arpan De, Chandan De, and Sisir Maity - for making my stay here an enjoyable one. I am also thankful to all my other friends from JNCASR for all their help whenever needed. I am really thankful to Nabadyuti for all the silent sacrifices she has made for me to make my life easier.

Finally, I would like to express my deepest gratitude towards my parents, my brother and all the other family members for their unconditional love, support and encouragement. Their care is always a source of my strength and happiness.

SYNOPSIS OF THE THESIS

The objective of this thesis is to study the dynamics of clustering in granular and active matter models. In **Chapter 1**, we provide the necessary background for the works presented in the subsequent chapters. Various scaling properties related to spatiotemporal pattern formation and their relevance in the context of dynamics in aforementioned systems have been discussed in detail. In this chapter, we also provide discussions on a number of relevant computational techniques and introduce a few methods which are used later to analyze the simulation data.

In **Chapter 2** we have studied the dynamics of clustering in a freely cooling granular gas model (GGM), where particles collide inelastically, in space dimension $d = 2$, via the event driven molecular dynamics (EDMD) simulations. Emergence of particle-rich and particle-poor domains in the system at late time resembles the pattern formation in a vapor-liquid phase transition. The primary objective has been to understand the growth behavior. We have identified a power-law time (t) dependence of average cluster or domain size and accurately quantified the corresponding exponent via a finite-size scaling technique. It has been demonstrated that the finite-size effects are much stronger in GGM compared to the standard phase transition scenario.

Chapter 3 contains results for the energy decay, growth and aging in GGM as well as in a ballistic aggregation model (BAM). In the BAM the particles move ballistically and stick to each other following collisions. In this chapter the focus has been on space dimension $d = 1$. Growth of average mass (m) of clusters in BAM has been shown to be inversely proportional to

the decay of energy (E), i.e., $m \sim 1/E \sim t^{\xi}$. The value of the exponent ξ is estimated to be 2/3, that obeys a d- dependent scaling theory prediction $\xi = 2d/(d+2)$. Via a renormalization-group method of analysis of the EDMD simulation results, we show that the exponent in the GGM has nearly the same value as in the BAM. Furthermore, via more direct investigation we demonstrated that the growth mechanism in GGM is same as that in the BAM. For the investigation of aging, we have studied the decay of the density autocorrelation function with the progress of time. Quantitative similarity of the decay in the two models further establishes the close equivalence between the GGM and BAM.

In **Chapter 4** we have studied the kinetics in $d = 2$, for clustering in the same models as in chapter 3. Unlike in $d = 1$, here we show that GGM and BAM are not equivalent. Furthermore, it has been demonstrated, from accurate analyses, that the scaling theory prediction related to the energy decay and cluster growth does not hold for BAM, in this dimension, when the packing fraction is low. The aging property for the BAM has been shown to obey the similar scaling property as in $d = 1$. The corresponding power-law exponent λ has been estimated. In both $d = 1$ and 2, it is observed that λ obeys a lower bound that depends upon the space dimension and structural property.

Chapter 5 deals with the dynamics of the BAM in $d = 2$ and 3, for various different densities. We have estimated the exponents for the (power-law) decay of the kinetic energy and growth of the average cluster mass for a wide range of the packing fraction. It is shown that these exponents follow a hyperscaling relation and their values are observed to approach the above

mentioned scaling theory prediction as the density increases.

Finally, in **Chapter 6**, we have presented results for the coarsening dynamics in a two-dimensional model active matter system. The model consists of passive inter-particle interaction and active alignment interaction. The passive and active interactions have been introduced via the well-known Lennard-Jones and Vicsek models. We perform molecular dynamics simulations for very low overall density of particles for which disconnected clusters form and grow with time. The influence of the self-propelling activity in the coarsening process has been quantified by comparing the results with those from the corresponding passive model that also undergoes phase transition.

List of Publications

- "Dynamics of clustering in freely cooling granular fluid", **Subhajit Paul** and Subir K. Das, Europhys. Lett. **108**, 66001 (2014).
- "Ballistic aggregation in systems of inelastic particles: Cluster growth, structure and aging", **Subhajit Paul** and Subir K. Das, to appear in Phys. Rev. E (2017).
- "Density dependence of ballistic aggregation in 2 and 3-dimensions", **Subhajit Paul** and Subir K. Das, to be submitted.
- "A comparative study of kinetics of phase separation in passive and active matter systems", **Subhajit Paul** and Subir K. Das, to be submitted.

List of Figures

List of Tables

Contents

Chapter 1

Introduction

1.1 Nonequilibrium systems

Thermodynamics and equilibrium statistical mechanics have been used widely in various situations for the understanding of systems in equilibrium [1]. But, most of the natural systems are inherently not in equilibrium. Examples include systems from microscopic scale to the scale of the universe. Granular flows, turbulent motion in fluids, motion of active microswimmers as well as formation and breakdown of cosmic particles are all examples of out-of-equilibrium systems. In our daily life also, most of the systems we deal with are out of equilibrium. Though lots of studies have been done to understand various nonequilibrium systems, a compact and general theory is missing due to ample diversity in the exhibited phenomena [2]. In this thesis, we will primarily deal with granular and active matter systems, examples of typical nonequilibrium systems, detailed introduction about which will be given in following sections.

1.2 Granular systems

Granular materials, very common in nature, show diverse properties [3] in various situations. There have been much recent interest to study the structure and dynamical properties of granular systems. They consist of large number of particles with typical size of grains within the range between μm to cm. These materials can be found in different places in nature, examples ranging from powders to life-saving drugs to the daily necessary commodities like rice, sugar, coffee beans etc. to the cosmicdust particles in the planetary rings. They are widely used in various industries like pharmaceutical, agricultural and mining. Natural calamities and various geological processes, viz., earthquakes, landslides, erosions, dune migration, etc. occur due to distinctive properties of soil, sand, etc.

Though common, as evident from the previous paragraph, understanding of their structural and dynamic behavior is still a challenge. The size of the particles are such that the Brownian motion is often irrelevant for its description. As an example, energy of a typical grain of size $1mm$, moving with a velocity $1cm/sec$ can exceed the thermal energy k_BT by few orders of magnitude, where k_B is the Boltzmann constant and T is the typical room temperature. The collective behavior of granular particles is also interesting and can be very much different from the properties of the three common phases of matter, i.e., solid, liquid and gas, mostly due to the dissipative nature of forces acting among the grains, such as inelastic collisions and friction [3]. Since thermal energy is not sufficient for the motion of the grains, thermodynamic fluctuations play negligible role on its dynamics. Thus, to

keep the system alive, these grains need to gain energy from external sources, viz., gravity, electric or magnetic fields, etc. Understanding fundamental behavior of these systems can give insights to some of those aforementioned natural phenomena.

Studies on granular systems are not new [4–10]. In the last century, most of these research were done in the applied engineering field, keeping various industrial applications in mind. But, in last few decades physicists became interested to study the dynamical properties as well as pattern formation in these systems [9, 10] under various conditions. A seminal work in this regard was done by P. K. Haff [4], where the temporal decay of temperature for such a system, which is a collection of homogeneously distributed grains colliding inelastically among themselves, has been predicted. The temperature mentioned above is called the "granular temperature", which is essentially the average kinetic energy of the particles. We can see that granular system is a rich area of research in non-equilibrium statistical physics [9] and also in the context of pattern formation about which some discussions will be provided in the following sections.

As already mentioned, there are two important aspects which make the granular systems unique from the conventional states of matter. First, the non-Brownian behavior of the grains. The second is the dissipative nature of collisions among the grains. Numerous experiments have been performed to understand their various collective complex behavior, e.g., formation of convection rolls, brazil-nut effects, size segregation and pattern formation under vertical vibration [11–16], etc.

1.2.1 Granular gas

A dilute assembly of granular particles is known as granular gas. Particles move ballistically until they make momentum conserving inelastic collisions. During the nonequilibrium evolution, granular gases form various patterns depending on the details of the problem [9]. There is a fluid-like behavior due to the flow of the grains from one part of the system to another. As an idealization, granular flow can be thought of a fluid composed of solid hard particles or grains. The behavior of the motion of the flow is entirely determined by particle collisions [3–5]. There exist works on granular gas flows where continuum dynamical descriptions have been obtained for the evolution of mass, momentum and energy [17]. This leads to describe the system via hydrodynamic equations [17, 18], viz., Navier-Stokes equations, like molecular fluid. But, due to continuous decrease of energy of the system, a dissipative term needs to be considered in the energy equation. Though many experimental [11, 12] and theoretical [5] works are related to dilute granular media, in nature granular matter can be rather dense.

Two cases

Depending on whether any external drive is present or not, granular gas generally falls into two categories [19, 20].

(i) Freely cooling granular gas (FCGG), in which there is no external drive to compensate for the energy dissipation due to inelasticity and friction. Thus, due to continuous decrease of velocities, particles can come to rest. Even the simplest and well-studied model of spherical particles capture many basic

features of the real dynamics and is a good example of a phase ordering system showing non-trivial coarsening behavior [21–23].

(ii) The second one is driven granular gas. As the name suggests there is an external drive on the system. There are various ways to agitate a granular system, viz., by applying electric or magnetic fields, gravity, vibration of the system with some frequency, rotation, etc. [15, 24]. In this case, the dissipation of energy gets compensated by external input and the system reaches a (nonequilibrium) steady state. A typical example is emergence of various structures due to vertical vibration of the base, depending upon the amplitude and frequency of vibration [16]. Another example is a polydisperse system where size segregation among different species occurs [12], when the system is subjected to horizontal and vertical vibrations.

In this thesis we confine ourselves in FCGG only.

1.2.2 Modeling via coefficient of restitution

As already mentioned, one basic fact that makes the granular gas different from other systems is the dissipation of energy due to inelastic collisions among the grains [20, 25]. As the simplest case, the system can be thought of as made of hard spherical particles. In this thesis we will refer to this as the granular gas model (GGM). Inelastic collisions suggest that the coefficient of restitution (e) should be in the range $0 \leq e < 1$. For $e = 0$, i.e., when collisions are perfectly inelastic, particles stick to each other upon collision [26]. This model will be referred to as the ballistic aggregation model (BAM). Now, the value of e solely determines the rate of energy dissipation, which is

proportional to $(1-e^2)$ in each collision which sets various time scales in the problem. For realistic system, instead of being a constant quantity, value of e depends upon the relative velocities of the colliding particles ($\vec{v}_{\rm rel}$) [23,27,28] such that the effective coefficient of restitution ($e_{\rm eff}$) is written as

$$e_{\rm eff} = 1 - D_1|\vec{v}_{\rm rel}.\hat{n}|^{1/5} + D_2|\vec{v}_{\rm rel}.\hat{n}|^{2/5} \mp .... , \tag{1.1}$$

where values of D_1 and D_2 depend on the materials, $\hat{n}$ is the unit vector along the direction joining two colliding particles at the time of collision. These are known as viscoelastic particles. In this case, $e_{\rm eff} \to 1$ when $\vec{v}_{\rm rel} \to 0$. But, in the simplest case one can take e as constant, which is sufficient to see the nontrivial effect of inelasticity in the system. In this thesis we will use a version of the GGM that considers fixed value of e, with no friction.

The general equation of motion of the i'th particle in an N-particle system can be written as [29]

$$m_i\ddot{\vec{r}}_i = \vec{F}(\vec{r}_1, ...\vec{r}_N, \vec{v}_1, ..., \vec{v}_N) , \tag{1.2}$$

where $\vec{r}_i$'s and $\vec{v}_i$'s are the positions and velocities of the particles. These give rise to N coupled differential equations for all the particles. $\vec{F}$ is the force acting on the i-th particle. In granular gas systems, the forces are very short-ranged. Particles exert repulsive forces on each other only when they are in contact. Particles move ballistically between two successive collisions, when there is no force. The duration of a collision is very small compared to the mean free time of the particles [19]. Thus the collisions can be thought as instantaneous. In dilute systems, simultaneous collisions among three or

more particles are extremely rare. Thus for a binary collision between i and j the equation of motion can be written as

$$m_{\text{eff}}\ddot{\vec{r}}_{ij} = \vec{F}(\vec{r}_{ij}, \vec{v}_{ij})\,, \tag{1.3}$$

where $\vec{r}_{ij} = \vec{r}_i - \vec{r}_j$ and $\vec{v}_{ij} = \vec{v}_i - \vec{v}_j$. Thus, it becomes a two-particle problem from an N-particle one. The full solution of Eq. (1.3) can describe the collision accurately with appropriate boundary conditions. To describe the dynamics, the details of a collision is not necessary. Only the outcome is important. We need to know the post-collisional velocities $\vec{v}_i{}'$ and $\vec{v}_j{}'$ from the prior knowledge of pre-collisional velocities $\vec{v}_i$ and $\vec{v}_j$. The relation between pre- and post-collisional velocities can be written as [9, 19, 20, 25]

$$\vec{v}_i{}' = \vec{v}_i - \Big(\frac{1+e}{2}\Big)[\hat{n}\cdot(\vec{v}_i - \vec{v}_j)]\hat{n}\,, \tag{1.4}$$

$$\vec{v}_j{}' = \vec{v}_j - \Big(\frac{1+e}{2}\Big)[\hat{n}\cdot(\vec{v}_j - \vec{v}_i)]\hat{n}\,, \tag{1.5}$$

where $0 < e < 1$ describes the GGM. So knowledge of e, to a good degree, is sufficient for the description of granular gas dynamics [20].

Being a main model of our studies, first we will give an overview of the GGM.

1.2.3 Review of GGM

In this section we will briefly describe some of the well-known results related to GGM. Consider a system of homogeneously distributed particles with their velocities drawn from some distribution (say, Gaussian). During

its evolution via inelastic collisions, at initial stage, though the energy of the system decreases, particle density remains uniform. This is known as homogeneous cooling state (HCS) [4,6]. At a later stage, there is a crossover from HCS to a state with particle-rich and particle-void regions, i.e., there is emergence of clusters leading to a density inhomogeneity in the system, referred to as the inhomogeneous cooling state (ICS) [5,6,21,22]. The case of ICS is poorly understood, even though there exists a large set of numerical simulations [5–7, 21–23, 30–33].

(a) Homogeneous cooling state

Energy decay in HCS: The average energy (granular temperature) is defined for a system of N particles (with unit mass) as

$$E(t) = \frac{1}{N}\sum_{i=1}^{N} v_i^2 \,. \tag{1.6}$$

$E(t)$ follows t^{-2} behavior, independent of the dimension of the system. This is known as Haff's cooling law [4].

Dynamical equation for energy decay in d-dimensions can be written as [21]

$$\frac{dE(t)}{dt} = -\epsilon\omega(E)E/d \,, \tag{1.7}$$

where $\epsilon = (1 - e^2)$ is the rate of dissipation in each collision, $\omega(E)$ is the collision frequency with the form $\omega(E) = \pi^{-1/2}\Omega_d\chi(\rho)\rho\sigma^{d-1}E^{1/2}$, Ω_d being the solid angle in d- dimensions, $\chi(\rho)$ the pair correlation function of the hard particles in contact at density ρ and diameter σ. The solution for $\omega(E)$ with initial energy E_0 can be written as $\omega(E) = \omega(E_0)(E/E_0)^{1/2}$. Substituting

this in Eq.(1.7) we obtain the behavior of energy decay as

$$E(t) = E_0(1 + t/t_0)^{-2}\,, \tag{1.8}$$

where $t_0 = 2d/(\epsilon\omega(E_0))$. In hard sphere systems, instead of using real time t, sometimes it is helpful to use the collision time $\tau(t)$, which is the average number of collisions per particle until time t. The relation between $\tau(t)$ and t can be written as [21]

$$\tau(t) = \int_0^t \omega(t')dt' = \frac{2d}{\epsilon}\ln\left[1 + \frac{\epsilon\omega(E_0)}{2d}t\right]. \tag{1.9}$$

In terms of $\tau(t)$, the energy decay has the simple form, $E(\tau) = E_0 e^{-(\epsilon/d)\tau}$ [21,34]. This decay of energy, shown in Eq.(1.8), is valid for all d for the case when $\epsilon = (1 - e^2)$ is a constant. But for viscoelastic particles, the value of e depends on the relative impact velocity of the colliding particles ($e \equiv e(\vec{v}_{\rm rel})$), suggesting a dependence of e on the energy. In this case, energy decay takes the form [35]

$$E(t) = E_0(1 + t/t_0')^{-5/3}\,. \tag{1.10}$$

This result was first obtained by Pöschel taking the form of e as $e \simeq 1 - D_1|\vec{v}_{\rm rel}|^{1/5}$ [35]. Eq. (1.10) shows that $E(t)$ decays rather slowly for viscoelastic particles compared to the case with e = constant. Dependence of e on $\vec{v}_{\rm rel}$ is more realistic.

But these results are not valid in ICS, as clusters begin to form and velocity correlations start building up among the particles.

(b) Inhomogeneous cooling state

The HCS at late times becomes unstable to long wavelength density fluctuations and the system crosses over to ICS [5–7,21,33]. Spontaneous formation of high- and low-density regions of particles define ICS. These regions grow with time. Because of the reduction in normal relative velocity, following every collision, interesting pattern also forms in the velocity field, with emergence of topological defects like vortices, anti-vortices, etc.

Energy decay: Via numerical simulations, the ICS was first probed by Goldhirsch *et al.* [5] for the GGM that will be studied by us. One is interested to know the form of energy decay as Haff's law is no longer valid in ICS. Ben Naim *et al.* [8] studied energy decay in ICS for a granular gas in $d = 1$ and found the exponent θ for the decay of energy ($E(t) \sim t^{-\theta}$) to be $2/3$, independent of the value of e. X. Nie *et al.* [33] studied the GGM in $d = 2$ and found the exponent to be $\theta = 1$, independent of e. Miller and Luding did the simulation in $d = 3$ and studied energy decay and cluster-growth in ICS [36]. Though their data were not very much conclusive, they suggested that energy decay in $d = 3$ is faster than in the lower dimensions and estimated the exponent to be 1.1 ± 0.1. Instead of real time t, they used collision time τ, which has been defined earlier. A thorough study by Pathak *et al.* [37] showed that $\theta = 1.2$ in $d = 3$ and the energy decay in ICS is same as a mean field exponent for ballistic aggregation, details of which will be discussed in the next section. In Fig. 1.1, we plot the decay of energy for both HCS and ICS as a function of time in $d = 2$ for $e = 0.9$.

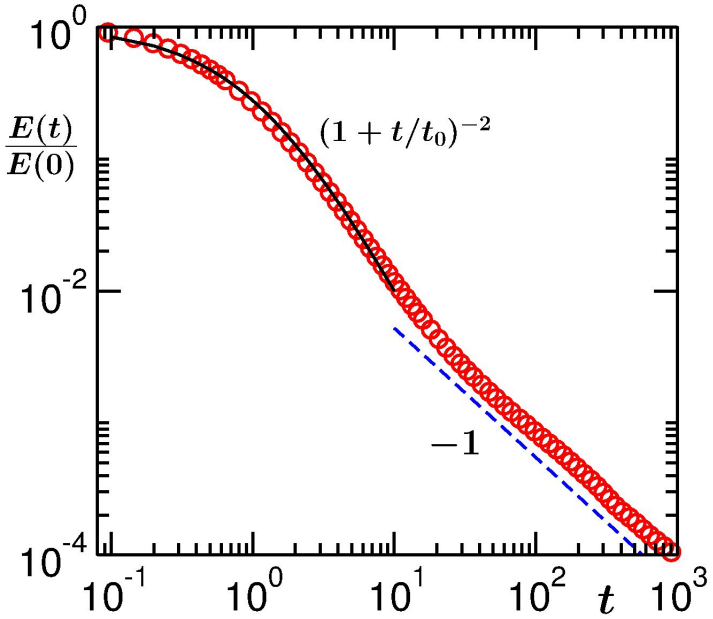

Figure 1.1: Plot of average kinetic energy $E(t)$, as a function of time (t), for a $2D$ granular gas for $e = 0.9$. In HCS, energy decay follows Haff's law, denoted by continuous curved line. In ICS, it follows a power-law t^{-1}, denoted by the dashed line. The deviation from $(1+t/t_0)^{-2}$ behavior marks the onset of HCS to ICS crossover.

Growth of clusters: Here, we discuss about the growth of clusters in ICS, which is a considerable part of our studies. Details about dynamics of growth and the corresponding exponents for granular gases will be presented in the subsequent chapters for different dimensions. Though the transition from HCS to ICS has probably no direct relevance with phase transitions, similarity of the pattern [22] with that for a critical quench in standard phase transition phenomena (e.g., vapor-liquid transition) [38] made us interested to look at various statistical quantities generally used in studies related to kinetics of phase transitions. Later in this chapter, we will discuss about different kinds of growth mechanisms present in phase transitions.

1.2.4 Ballistic aggregation

Ballistic aggregation mechanism is believed to be true for the description of granular gas in ICS in $d = 1$. A study by Carnevale *et al.*, via scaling arguments, predicted the time dependence of energy and mass of the clusters [26], viz., $m \sim 1/E \sim t^{2d/d+2}$, for this mechanism. Below we provide further details on the model on which the above predictions are based.

Consider two spherical particles, say, i and j, located at $\vec{r}_i$ and $\vec{r}_j$ with masses m_i and m_j moving with velocities $\vec{v}_i$ and $\vec{v}_j$, colliding and forming a new larger sphere (shape doesn't change). The position $\vec{r}\,'$ and velocity $\vec{v}\,'$ of the new particle of mass m' can be obtained from the conservation equations for mass, momentum and centre-of-mass which are written below

$$m' = m_i + m_j \,, \tag{1.11}$$

$$m'\vec{r}\,' = m_i\vec{r}_i + m_j\vec{r}_j \,, \tag{1.12}$$

and,

$$m'\vec{v}\,' = m_i\vec{v}_i + m_j\vec{v}_j \,. \tag{1.13}$$

In terms of diameter of the particles, Eq. (1.11) can be written as $a'^d = a_i^d + a_j^d$ (in space dimension d), where a' is the diameter of the new particle and a_i and a_j are the diameters of the colliding particles i and j, respectively. As the mass ($\equiv$ (diameter)^d) increases, the number density of clusters decreases with time, as well as the total kinetic energy. Scaling hypothesis predicts that the growth of mass of the clusters is inverse of the decay of energy. This model we will refer to as the ballistic aggregation model (BAM).

1.3 Active matter systems

Here we will give a brief introduction of active matter systems. 'Active matter' is a class of non-equilibrium systems made up of elements having self-propelling behavior [39, 40]. Examples are flocks of birds, schools of fish, slime molds, colonies of bacteria, etc. From the examples it is clear that clustering is commonly observed in active matter systems. Fig. 1.2 depicts that elements within a cluster show orientational ordering. Almost parallel movement of each of the elements, give rise to large scale spatio-temporal pattern. So, the fundamental questions that arise here are about the type of pattern and its evolution with time.

Figure 1.2: A school of fish. The picture demonstrates the tendency of each fish moving along the direction of others, while swimming. Source: www.googleimages.com

A seminal work in this regard was by Vicsek *et al.* [39], who, using a simple rule of the interaction of particles with its neighbors, showed the formation and growth of clusters. We will modify the Vicsek rule by incorporating an additional interaction among the particles in the system [41]. With this

model, which will be described in detail in Chapter 6 along with additional overview of this subject, we will study the cluster pattern and its dynamics. Here note that in the Vicsek model neighbors try to parallelize each other's velocity. That way there exists some similarity with the GGM.

Given that structure and dynamics in the above and other models of granular and active matters resemble those of ordering dynamics during phase transitions, below we provide a general discussion on it.

1.4 Ordering phenomena during phase transitions

Phase transition is common in nature and is of much research interest [39, 41–54]. Fig. 1.3 shows a schematic phase diagram or coexistence curve [42, 43] of a vapor-liquid transition in the temperature (T) vs density (ρ) plane, where ρ_c and T_c are the critical density and critical temperature, respectively [42]. For $T > T_c$, the equilibrium state of the system is a single-phase with "uniform" density. When the system is quenched inside the coexistence curve, it becomes unstable to fluctuations and moves to a new equilibrium state at that temperature, i.e., a phase-separated one, via the formation and growth of domains of like particles [42, 43]. In this diagram, the left branch of the coexistence curve corresponds to the low density vapor phase and the right branch to the high density liquid phase. This schematic diagram applies to the phase separation in a binary mixture ($A+B$) as well, if the abscissa variable is replaced by the concentration of one

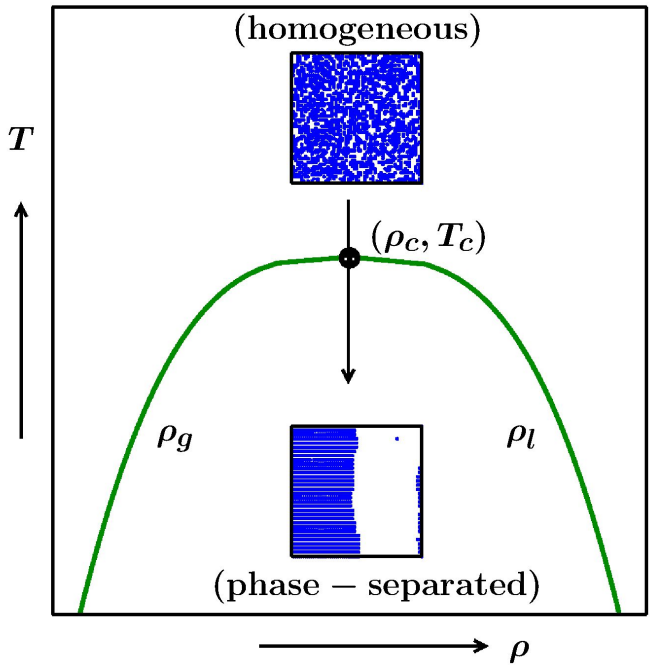

Figure 1.3: A schematic plot of phase-diagram in the density vs temperature plane for a vapor-liquid transition. T_c is known as the critical temperature and ρ_c the critical density. The curve represented by solid green line is known as the coexistence curve. The configuration plotted above is at $T > T_c$ and the one plotted below is for $T < T_c$. For the latter, the equilibrium state of the system is a phase separated one.

of the components, say A, x_A (concentration of A component being defined as $x_A = \frac{N_A}{N}$, where N_A is the number of A type of particles and N is the total number of particles). Though GGM remains always in nonequilibrium due to continuous dissipation of energy, the system reaches a clustered state where average domain size saturates and regions of particle-rich and particle-void resemble the liquid and vapor region. We will describe a corresponding phase-diagram-like plot in the second chapter [22].

Depending upon the kind of transition, the total value of the order-parameter (ψ_g) of the system may or may not be conserved [44,46,47] during

the evolution. In the case of nonconserved order-parameter (NCOP) dynamics, growth occurs via the curvature driven motion of the interface of the domains. While this picture is true in the conserved order-parameter (COP) scenario as well, depending upon the region to which the quench takes place inside the coexistence curve, coarsening scenario can be different in this case, viz., (a) spinodal decomposition [44, 46, 50] and (b) nucleation and growth [44, 46, 51, 55]. We will provide brief discussion on them.

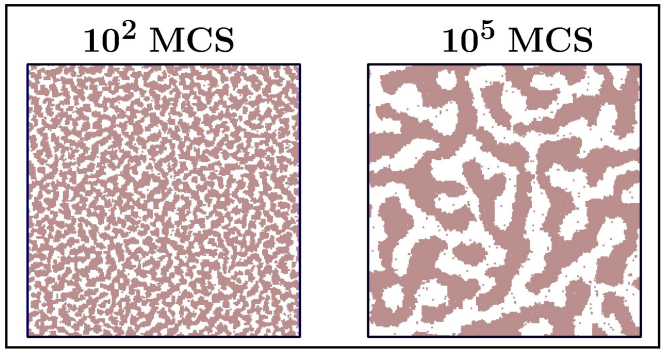

Figure 1.4: Snapshots showing the evolution of a COP system with critical composition (50% of A and 50% of B particles), obtained via Monte Carlo simulation of Kawasaki spin-exchange Ising model, after quenching to a temperature $T_f \simeq 0.5T_c$. The $+1$ spins (i.e., the A particles) are marked by brown dots and -1 spins (the B particles) are left unmarked. Percolating domains of like spins form and grow in the system.

Spinodal decomposition is the mechanism of domain coarsening when a system is quenched with overall density close to its critical value. The system falls out-of-equilibrium quite fast, i.e., the coarsening starts immediately after the quench. As an example, we mention about demixing transition of a binary mixture ($A+B$). Starting from a homogeneous mixture of $A+B$ with critical composition (i.e., 50 : 50) at $T > T_c$, when the system is quenched below the coexistence curve at $T < T_c$, it tries to evolve towards a new equilibrium

state, which is a phase-separated one [50], via the formation and growth of domains as shown in Fig. 1.4. From the snapshots, it is clear that the growing structures are percolating.

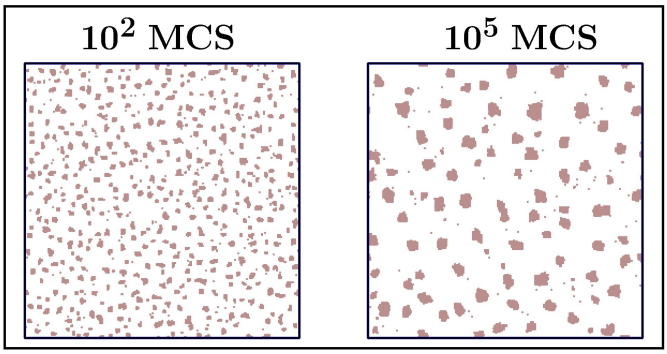

Figure 1.5: Evolution snapshots of a COP system with off-critical composition. The ratio of $+1$ and -1 spins is $10:90$. Simulation method and other parameters are same as in Fig. 1.4. Here, the $+1$ spins, marked by brown dots, form disconnected droplets which grow with time in the background of -1 spins.

Nucleation and growth picture applies when the quench is off-critical, i.e., very close to the coexistence curve. In this situation, long wavelength fluctuations are needed for the instability. In this case, it has been observed that the clusters are disconnected from each other [38, 51, 55]. Since the long wavelength fluctuations are rare, coarsening in this case doesn't start immediately after the quench. In Fig. 1.5 we present snapshots of an off-critical quench with 10% 'A' and 90% 'B' type of particles. As time progresses, we can see the droplet-like clusters of 'A' particles growing, in the background of 'B' type of particles.

1.5 Aspects related to structure and dynamics

1.5.1 Correlation function and structure factor

Typically a pattern is characterized by the two-point equal-time correlation function C, which is defined as [44, 46]

$$C(r,t) = \langle \psi(\vec{r},t)\psi(\vec{0},t)\rangle - \langle \psi(\vec{r},t)\rangle\langle \psi(\vec{0},t)\rangle \,, \tag{1.14}$$

where ψ is a space ($\vec{r}$) and time (t) dependent order parameter. In phase

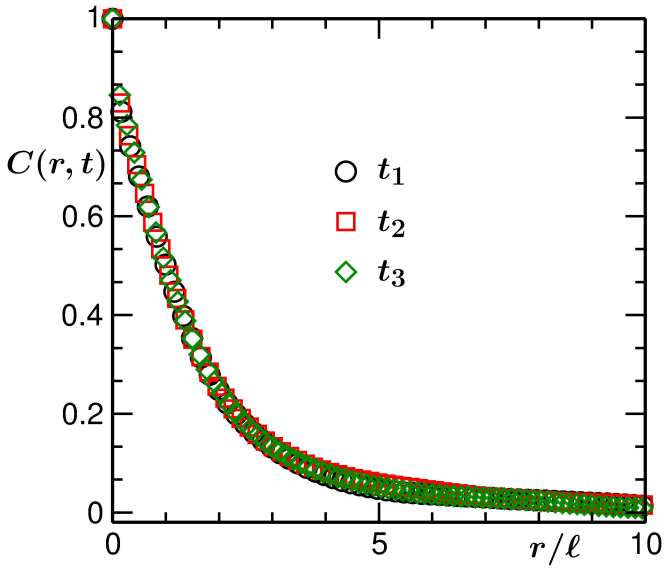

Figure 1.6: Plot of the scaled correlation function calculated at three different times. All of them follow a master curve when the abscissa is scaled by the corresponding average domain size ℓ at that particular time. These results are obtained from the simulations of a $2D$ granular system.

transition dynamics, where patterns at two different times are self-similar, $C(r,t)$, calculated at different times (say, t_1, t_2 and t_3, as shown in Fig. 1.6),

do overlap with each other, when scaled with the corresponding value of the time-dependent length-scale [46]. This implies the scaling form [44, 46]

$$C(r,t) \equiv \tilde{C}(r/\ell)\,, \tag{1.15}$$

where ℓ is the average domain size or characteristic length of the pattern at time t. In experimental situations measurement of C is difficult. There the quantity that is calculated is the structure factor ($S(k,t)$), which is the Fourier transform of the correlation function [44, 46]. It is defined as

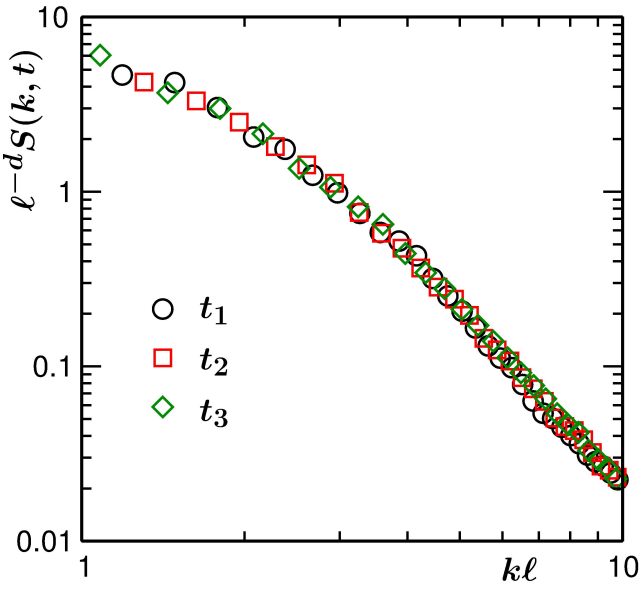

Figure 1.7: Scaling plot of the structure factor, $\ell^{-d}S(k,t)$ vs $k\ell$, calculated at three different times. All of them follow a master curve as shown in the figure. The presented results are obtained from the simulations of a $2D$ granular system.

$$S(\vec{k},t) = \int d\vec{r}\; e^{i\vec{k}\cdot\vec{r}}\; C(\vec{r},t)\,. \tag{1.16}$$

$S(k,t)$ also shows dynamical scaling (see Fig. 1.7), implying similarity among patterns at different times. The corresponding dynamical scaling has the form [46]

$$S(k,t) \equiv \ell^d \tilde{S}(k\ell)\,. \tag{1.17}$$

In Eqs. (1.15) and (1.17) $\tilde{C}$ and $\tilde{S}$ are the master functions independent of time. If the patterns are isotropic in nature, then only $\vec{r}$ and $\vec{k}$ can be replaced by its scalar counterparts. At large k-limit, structure factor obeys the power-law

$$S(k,t) \sim k^{-(d+n)}\,, \tag{1.18}$$

where n is the dimension of the order-parameter. For example, for the density related order parameter n is equal to 1, since in that case, one deals with a scalar quantity. Eq. (1.18) is referred to as the Porod law [44, 46, 56], which can be observed for sharp boundaries between two domains. With rough interface boundaries, one can observe a slower decay than Eq. (1.18) [23], due to fractality in the interfacial structure. For $k \to 0$ limit, structure factor obeys another power-law $S(k,t) \sim k^{\beta}$, where the exponent β depends upon the system dimensionality and conservation of order-parameter in the system. Values of β, for different cases, are summarized below [44, 54] :

$$\beta \sim \begin{cases} 0 & (\text{NCOP, in all } d)\,, \\ 2 & (\text{COP, } d=1)\,, \\ 4 & (\text{COP, } d=2,3)\,. \end{cases} \tag{1.19}$$

As stated above, $\ell(t)$ is a measure of the average cluster size at a particular time. It can be calculated as the length at which $C(r,t)$ decays to a particular value, say, half of its maximum value [44, 46]. In general, $\ell(t)$ grows in a power-law fashion with time [44]. In the next section we will discuss about the values of the power-law exponent, depending upon the mechanism of growth and the conservation of order-parameter.

1.5.2 Growth of clusters

Growth in solid systems

First, we will discuss about the cluster or domain growth in solid systems for both NCOP and COP models [44, 46]. In both the cases, the average domain size increases in a power-law fashion, $\ell(t) \sim t^{\alpha}$, as stated above.

In NCOP dynamics, e.g., in para-to-ferromagnetic transition, starting with an initial state with total order parameter of the system being zero, the system ends up with a global non-zero value of the order parameter. The average domain size in this case increases with time as $\ell(t) \sim t^{1/2}$, known as Cahn-Allen (CA) law [44, 57]. The domains grow via the curvature driven motion of the interface boundaries or walls between two domains. Thus one can write

$$\frac{d\ell(t)}{dt} \sim \frac{1}{\ell}\,. \tag{1.20}$$

Solution of this equation gives, $\ell(t) \sim t^{1/2}$.

In COP dynamics, due to the constraint of conservation of the order parameter, the growth is slower [44, 46]. The rate of change of $\ell(t)$ there can

be written as the gradient of the chemical potential (μ) as

$$\frac{d\ell(t)}{dt} \sim \frac{\mu}{\ell(t)} = \frac{\gamma}{\ell(t)^2}\,, \tag{1.21}$$

where γ is the interfacial tension. Solution of Eq.(1.21) gives $\ell(t) \sim t^{1/3}$, which is known as Lifshitz- Slyozov (LS) growth law [46, 58]. In Fig. 1.8, we have plotted $\ell(t)$ as a function of time for both the dynamics from the simulations done via the numerical solution of dynamical equations, namely, time dependent Ginzburg-Landau (TDGL) equation and Cahn-Hilliard (CH) equation, imitating NCOP and COP dynamics respectively [43, 46].

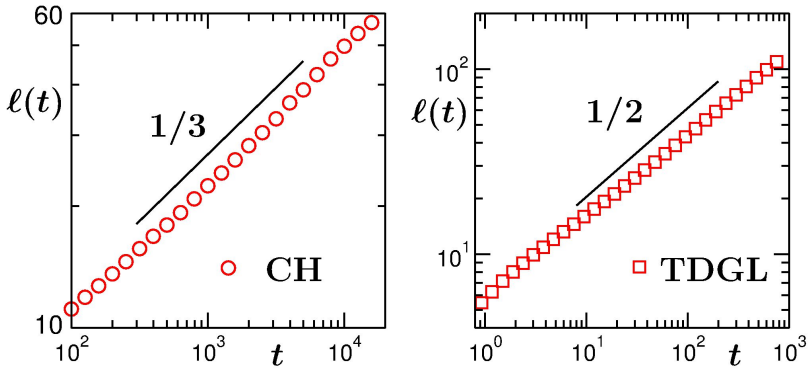

Figure 1.8: Plot of ℓ vs. t for COP and NCOP dynamics. The solid lines in the plots show the expected power-law behavior mentioned in the text, for the evolution of CH and TDGL equations. Values of $\ell(t)$ were obtained from the first moment of the domain size distribution function.

Before categorizing the granular gas into NCOP or COP, we mention below the governing dynamical mean-field equations for the evolution of the order-parameter ($\psi(\vec{r}, t)$) for the above mentioned models of phase transitions. The dynamical equations, in general, can be written as [43, 46]

$$\frac{\partial\psi(\vec{r},t)}{\partial t} = (-\nabla^2)^m[\psi(\vec{r},t) - \psi(\vec{r},t)^3 + \nabla^2\psi(\vec{r},t)]\,. \tag{1.22}$$

In Eq. (1.22) $m = 0$ corresponds to the TDGL equation and $m = 1$ corresponds to the CH equation. These equations can be derived phenomenologically by relating the time evolution of the order parameter to the functional derivative of the Ginzburg-Landau free energy which can be written as

$$F[\psi] = k_B T \int d\vec{r}\Big[-\frac{1}{2}\Big(\frac{T_c}{T} - 1\Big)\psi^2 + \frac{1}{12}\Big(\frac{T_c}{T}\Big)^3\psi^4 + \frac{T_c}{2qT}a^2\big(\vec{\nabla}\psi\big)^2\Big]\,, \tag{1.23}$$

where q is the coordination number and T_c is the critical temperature. For patterns formed during the evolution in these models see Figs. 1.9 and 1.10.

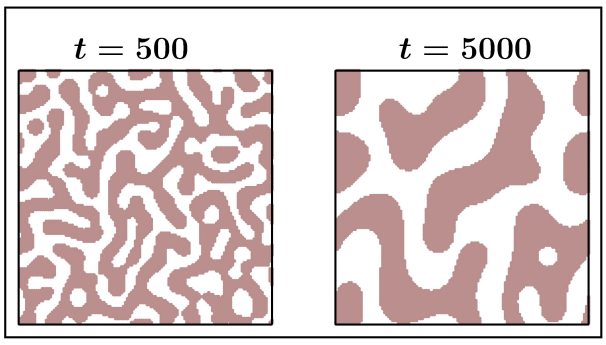

Figure 1.9: Evolution snapshots from the simulation of CH equation for critical quench. Brown dots mark the lattice points at which the value of order parameter $\psi > 0$.

Now, except the aforementioned two models, attention has also been given to the studies in which $m \to 0^+$, which is known as globally conserved (GC) TDGL equation [9,21]. The extra constraint here is that the total value of the

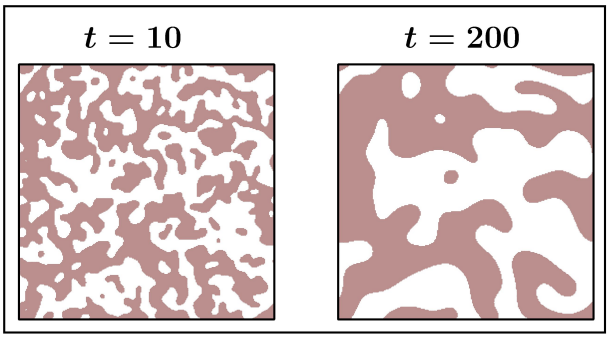

Figure 1.10: Evolution snapshots, from two different times, from the simulation of the TDGL equation for critical quench. Brown dots represent the lattice points in which the order-parameter $\psi > 0$.

order parameter of the system is preserved, but there is lack of conservation at the local level. The granular gas system, the total number of particles in the system being conserved and also having similarity of the patterns formed with that of the TDGL equations, it can be categorized as GC-TDGL model. Studies by Das and Puri [21] demonstrated that the evolution of the density field in GGM is consistent with that of GC-TDGL model. van Noije *et al.* [17] tried to develop Cahn-Hilliard type theory for unstable granular flows. Luding *et al.* [7] showed the exponent of the cluster growth in GGM to be consistent with CH type, though their results were not very much convincing. We will address this issue in more detail in the next chapter and also accurately quantify the exponent for the growth of clusters.

Growth in presence of hydrodynamics

In fluid systems, hydrodynamics plays crucial role in kinetics [47]. Thus, the growth exponent, at late time, crosses over to higher values than from the LS value (1/3), for COP dynamics. Hydrodynamic effects may as well

be expected in granular fluids [17]. Thus, it is relevant to discuss the growth laws in presence of hydrodynamics.

Here we will discuss growth exponent for percolating clusters. The growth exponent at early time shows consistency with diffusive (LS) 1/3 behavior [58]. At late stage, when there is a balance between surface energy density ($\gamma/\ell(t)$) and the viscous stress ($6\pi\eta v_\ell/\ell(t)$, v_ℓ being the interfacial velocity and η the viscosity), one can write down the following equation for an interconnected domain structures

$$\frac{d\ell(t)}{dt} = v_\ell = \frac{\gamma}{\eta}\,. \tag{1.24}$$

Solution of Eq. (1.24) gives the value of the exponent α to be 1, referred to as the viscous hydrodynamic exponent. At even later time, when $\ell(t) \gg \ell_{in}(\equiv \eta^2/\rho\gamma)$ (the inertial length), the surface energy density is balanced by kinetic energy density ρv_ℓ^2, which leads to the equation

$$\frac{d\ell(t)}{dt} \sim \frac{1}{\ell(t)^{1/2}}\,. \tag{1.25}$$

Solution of Eq. (1.25) provides $\ell(t) \sim t^{2/3}$, which is the exponent for inertial hydrodynamic growth. In molecular dynamics simulations, though the viscous hydrodynamic growth can be observed, it is very difficult to probe the inertial hydrodynamic regime. The latter has been observed in various lattice-Boltzmann simulations [46].

Values of the growth exponents in different regimes are summarized

below [44, 59]

$$\ell(t) \sim \begin{cases} t^{1/3} & \text{(Diffusive)}\,, \\ t & \text{(Viscous hydrodynamic)}\,, \\ t^{2/3} & \text{(Inertial hydrodynamic)}\,. \end{cases} \tag{1.26}$$

1.5.3 Aging in nonequilibrium systems

In nonequilibrium systems, study of aging is important to understand the relaxation dynamics [49, 54, 60]. This is studied via two-time quantities. This phenomena has been studied extensively in various systems, viz., glass transitions, phase transition in solid binary mixtures, para-to-ferro magnetic transitions, etc. [49, 52, 60]. For this purpose, usually one considers the two-time autocorrelation function ($C_{\rm ag}(t, t_w)$) [46], defined as

$$C_{\rm ag}(t, t_w) = \langle \psi(\vec{r}, t)\psi(\vec{r}, t_w)\rangle - \langle \psi(\vec{r}, t)\rangle\langle \psi(\vec{r}, t_w)\rangle\,, \tag{1.27}$$

where t is the observation time and t_w is called the waiting time or the age of the system. In equilibrium systems, always there exists time-translational invariance of $C_{\rm ag}(t, t_w)$ for different choices of t_w values. But, in nonequilibrium systems, $C_{\rm ag}(t, t_w)$ does not scale with the translated time $(t - t_w)$, which has been shown schematically in Fig. 1.11. It also depicts that with the increase of t_w the decay of $C_{\rm ag}(t, t_w)$ becomes slower, i.e., the relaxation time of the system increases.

In studies of aging phenomena, typically one is interested in extraction and understanding of scaling property exhibited by $C_{\rm ag}(t, t_w)$. Seminal work by Fisher and Huse (FH) showed the existence of scaling of $C_{\rm ag}(t, t_w)$ with

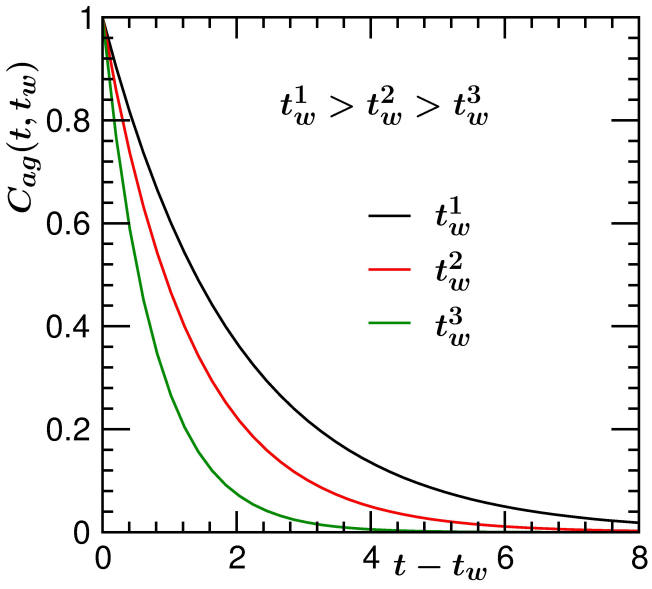

Figure 1.11: Schematic plot of $C_{\rm ag}(t, t_w)$ as a function of translated time $(t - t_w)$, for different values of t_w. This plot shows that the decay of the autocorrelation function becomes slower with the increase of t_w, the age of the system.

respect to t/t_w and a power law decay of the corresponding scaling function [49], i.e.,

$$\tilde{C}_{\rm ag}(t, t_w) = \left(\frac{\ell(t)}{\ell_w}\right)^{-\lambda} \sim \left(\frac{t}{t_w}\right)^{-\alpha\lambda}, \tag{1.28}$$

where λ is the aging exponent and ℓ_w is the average domain size at time t_w. FH also provided bounds on the value of λ as $d/2 \leq \lambda \leq d$ [49], d being the space dimension. Modifications on the lower bound by Yeung, Rao and Desai (YRD) requires an additional term β and predicts the lower bound to be $\lambda \geq (\beta + d)/2$ [54]. Discussions about β have already been provided in subsection 1.5.1.

Granular systems being inherently non-equilibrium, study of aging phenomena is important. We studied the aging dynamics in this system in space dimension $d = 1$, as well as for the BAM in $d = 2$ [61], and checked for the validity of YRD bound.

Next we discuss a few technical details for calculating various quantities.

1.6 Some Technical aspects

1.6.1 Calculation of centre of mass under periodic boundary condition

The centre of mass (CM) of a system of particles can be defined as the point in which all the masses are considered to be concentrated. The general formula used to calculate CM for a N-particle system is [29]

$$\vec{r}_{\rm CM} = \frac{\sum_{i=1}^{N} m_i \vec{r}_i}{\sum_{i=1}^{N} m_i}; \qquad \vec{r}_{\rm CM} = \frac{1}{N}\sum_{i=1}^{N} \vec{r}_i \;\text{ if } m_i = m \;\forall i\,. \tag{1.29}$$

In computer simulations, often we use periodic boundary conditions (PBC) to avoid the presence of the surface effects, which may lead to some differences in the expected results. In presence of PBC, parts of a particular cluster can lie on two different sides of the system. In this situation, one way to calculate CM is by appropriately shifting the particles from one side of the system to other. But this is a tidious procedure. To avoid this, the following method, which automatically takes care of the PBC imposed on the clusters, can be implemented [62]. For this, we need to define a quantity (θ_i), related to each particle i, as

$$\theta_i = 2\pi \frac{x_i}{L}\,, \tag{1.30}$$

where x_i is the x-component of the position vector $\vec{r}_i$ of the i-th particle, and L is the system size along x-direction, and $x_i \in [0, L]$. From this angle θ_i, two new points (α_i, β_i) can be generated as

$$\alpha_i = \cos(\theta_i), \quad \beta_i = \sin(\theta_i)\,. \tag{1.31}$$

Now, in (α, β) plane the coordinates lie on a circle of radius 1. From collection of α_is and β_is for all the particles in the cluster, average quantities, $\bar{\alpha}$ and $\bar{\beta}$, can be calculated. These values can be mapped back to the new angle $\bar{\theta}$ as

$$\bar{\theta} = \text{atan2}(-\bar{\beta}, -\bar{\alpha}) + \pi\,. \tag{1.32}$$

Here, the function atan2 computes angles between $-\pi$ to π, taking care of the signs of $\bar{\alpha}$ and $\bar{\beta}$. Then $\bar{\theta}$ is the correct value of the CM in polar coordinate system. It can be converted to Cartesian coordinate system, using the relation

$$x_{\text{CM}} = L \frac{\bar{\theta}}{2\pi}\,. \tag{1.33}$$

This process can be repeated for all dimensions of the system to obtain the complete set of coordinates for the CM.

1.6.2 Radius of gyration

Radius of gyration (R_g) of an object is related to the distribution of its mass around the axis of rotation. For an object, consisting of N particles of same mass each, R_g can be defined as [29]

$$R_g = \Big[\frac{1}{N}\sum_{i=1}^{N}(\vec{r}_i - \vec{r}_{CM})^2\Big]^{1/2} = \Big[\frac{1}{N(N-1)}\sum_{i=1}^{N-1}\sum_{j=i+1}^{N}(\vec{r}_i - \vec{r}_j)^2\Big]^{1/2}, \quad (1.34)$$

where $\vec{r}_{\rm CM}$ is the centre of mass of the object, and $\vec{r}_i$ the position of the i-th particle. Mass of the object, M, is related to R_g as $M \sim R_g^{d_f}$ [61], where d_f ($< d$) is the fractal dimension of the object. To understand the structure of an object, calculation of d_f is necessary.

1.6.3 Mean-squared displacement

The mean squared displacement (MSD) of a particle is defined as [63]

$$\text{MSD(t)} = \big\langle \big(\triangle \vec{r}_i(t)\big)^2\big\rangle = \big\langle \big(\vec{r}_i(t) - \vec{r}_i(0)\big)^2\big\rangle\,. \quad (1.35)$$

In Eq. (1.35), $\vec{r}_i(t) - \vec{r}_i(0)$ is the vector distance travelled by the particle over the time interval t. Angular brackets refer to the average over many such intervals. Often, this averaging is also done over the particles present in the system. For the latter one, the equation will be of the form

$$\text{MSD(t)} = \frac{1}{N}\sum_{i=1}^{N}\big(\vec{r}_i(t) - \vec{r}_i(0)\big)^2\,, \quad (1.36)$$

where N is the number of particles in the system.

If a particle does not encounter any collision with other particles, then the distance travelled by it will be equal to the velocity multiplied with time. Thus MSD will increase quadratically with time (MSD $\sim t^2$), referred to as the ballistic motion. But, when particles undergo several collisions with others, then their motion will be Brownian-like or diffusive. In this case, MSD increases linearly with time (MSD $\sim t$).

1.7 Computational methods

Computer simulations became an important tool in statistical mechanics as well as in other branches of physics [63, 64]. Monte carlo and molecular dynamics simulations are routinely used to study the properties of various complex systems ranging from materials to biological systems. Various nonequilibrium systems in this thesis have been studied via numerical simulations. Here, we will give a brief overview of the molecular dynamics (MD) technique [63]. Let us consider an N-particle system, where the positions ($\vec{r}_i$) and velocities ($\vec{v}_i$) of all the particles are known. In general, the equation of motion of the i-th particle of mass m_i can be written as [29, 63]

$$m_i \frac{d^2\vec{r}_i}{dt^2} = \vec{F}_i(\vec{r}_i, \vec{v}_i, t), \qquad i = 1, 2, ..., N\,, \tag{1.37}$$

where $\vec{F}_i$ is the total force acting on the i-th particle. Two types of molecular dynamics technique are commonly used in the literature. The first one is very conventional technique, which is known as time-step-driven MD (TDMD)

and the second one is event-driven MD (EDMD) [64]. Here, we will discuss both the techniques briefly. In our simulations of granular systems (i.e., for hard-core potential), we have used only EDMD. On the other hand, for active matter simulations we have used the TDMD method.

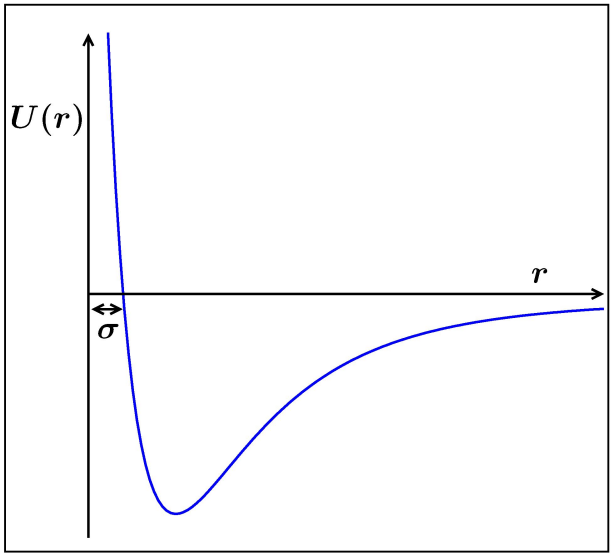

Figure 1.12: Figure shows schematic plot of a short-ranged soft-core potential $U(r)$, r being the measure of the inter-particle distance and σ the particle diameter.

1.7.1 Time-step-driven molecular dynamics

In TDMD [63], equations of motions of particles are solved in an interval of a small discrete time step (Δt). Thus if we know the system (i.e., positions and velocities of the particles) at time t and the force acting on the particles, then we can exactly determine the system at time $t + \Delta t$. In Fig. 1.12, we plot a typical short-ranged soft-core potential in which some overlap is allowed between the particles. $U(r)$ is the measure of the potential energy as a function of the interparticle separation (r) and σ is the diameter of

the particles. Thus when $r < \sigma$, the particles exert high repulsive force on each other. Various algorithms are generally used in TDMD. Steps generally followed, while performing TDMD, are pointed below [63].

- Initial positions ($\vec{r}_i(0)$) and velocities ($\vec{v}_i(0)$) of all the particles are generated.
- The forces (i.e., acceleration) acting on all the particles are calculated.
- From the above information positions and velocities of the particles at next instant of time are calculated. In each step, time increases by an amount Δt.
- These three steps are repeated to calculate the trajectories of the particles upto the desired time. One can also calculate various quantities of interest during the course of evolution.

Below we will discuss the velocity-Verlet (VV) integration scheme for position ($\vec{r}(t)$) and velocity ($\vec{v}(t)$) updates.

Velocity-Verlet algorithm

In the VV algorithm, the positions and velocities of the i-th particle at time $t + \Delta t$ can be obtained from their values at t as [63]

$$x_i(t + \Delta t) = x_i(t) + v_i^x(t)\Delta t + \frac{f_i^x(t)}{2m}\Delta t^2 \,, \tag{1.38}$$

$$v_i^x(t + \Delta t) = v_i^x(t) + \frac{f_i^x(t + \Delta t) + f_i^x(t)}{2m}\Delta t \,, \tag{1.39}$$

where x_i and v_i^x are the x-components of the position ($\vec{r}$) and velocity ($\vec{v}$) of the i-th particle, respectively, and f_i^x is the x-component of the force $\vec{f_i}$ ($\vec{f_i} = -\vec{\nabla} U_i$) acting on i-th particle at time t. To calculate the velocity at $t+\Delta t$, one needs to calculate the forces apriori (at $t+\Delta t$) from the knowledge of $\vec{r}(t + \Delta t)$.

The most time consuming part in MD simulation is the calculation of pair-wise forces. Thus several methods have been proposed to increase the efficiency of the force calculation. For example, for short-ranged forces (viz., truncated Lennard-Jones potential) one can use neighbor-list algorithm [63], in which one considers only the neighbors of a particle within a certain range, details of which will be discussed later.

In this thesis, we have performed TDMD simulations for Lennard-Jones potential in a canonical ensemble (i.e., NVT ensemble), where, the number of particles (N), the volume (V) and the temperature (T) are fixed at certain values. Updation of the positions and velocities of the particles have been done using VV algorithm. To keep the temperature of the system constant, one needs to apply a thermostat. Various thermostats can be used, viz., Andersen thermostat(AT), Langevin thermostat (LT), Nosé-Hoover thermostat(NHT), etc. [63,65]. In case of fluid, as hydrodynamics plays an essential role in the dynamics, choice of NHT, a hydrodynamic preserving thermostat, is a proper one. In case of active matter systems, which will be discussed in detail in chapter 6, we will use LT. Equations of motions solved during MD simulation related to NHT and LT are explained below.

(a) Nosé-Hoover thermostat

NHT follows a deterministic algorithm [63]. It was originally developed by Nosé [66] and further improvement was made by Hoover. The idea of using a thermostat is to attach the system to a heat reservoir, which tries to control the temperature of the given system. Actually, the thermal interaction between the heat reservoir and the system results in exchange of kinetic energy between them. In simulations often a reservoir is used in a different way than in experiments. Nosé introduced an additional degree of freedom, say, 's', as the position of the heat reservoir, along with its conjugate momenta 'p_s'. Here, one needs to introduce an effective mass, $Q = \frac{p_s}{\dot{s}}$, related to the additional degree of freedom. Q is often referred to as the coupling constant between the system and reservoir. Now, the Hamiltonian for the combined system can be written as [63]

$$H = \sum_{i=1}^{N} \frac{p_i^2}{2m_i s^2} + U + \frac{p_s^2}{2Q} + (3N+1)k_B T \ln s \,, \tag{1.40}$$

where U is the total potential energy and $(3N+1)$ is the total number of degrees of freedom in the system. Here, one needs to introduce a fictitious parameter, whose physical significance is that of friction, ζ, which essentially accelerates or slows down the particles, until the temperature reaches the

desired value. Now, the equations of motion for NHT will be as follows [63]

$$\frac{d\vec{r}_i}{dt} = \vec{v}_i\,, \tag{1.41}$$

$$\frac{d\vec{v}_i}{dt} = -\frac{1}{m_i}\frac{\partial U}{\partial t} - \zeta\vec{v}_i\,, \tag{1.42}$$

$$\frac{d\zeta}{dt} = \Big(\sum_{i=1}^{N} m_i\vec{v}_i^{\,2} - 3Nk_BT\Big)/Q\,, \tag{1.43}$$

$$\frac{d\ \mathrm{lns}}{dt} = \zeta\,. \tag{1.44}$$

Thus, from the above equations it is clear that ζ influences the velocities of the particles. Thus, if the instantaneous temperature increases or decreases, effect of ζ tries to bring it back to the desired value. This way the temperature always fluctuates around its assigned value. The strength of the fluctuation can be changed by varying the value of the coupling parameter Q. The equations for position and velocity updates (for the x-component) for NHT are given below [63]

$$x_i(t+\Delta t) = x_i(t) + v_i^x(t)\Delta t + \frac{\Delta t^2}{2}\Big[f_i^x(t) - \zeta(t)v_i^x(t)\Big]\,, \tag{1.45}$$

and,

$$\begin{aligned} v_i^x(t+\Delta t) = v_i^x(t) &+ \frac{\Delta t}{2}\Big[f_i^x(t) + f_i^x(t+\Delta t) - 2\zeta(t)v_i^x(t)\Big] \\ &-\frac{\Delta t^2}{2}\Big[\frac{\zeta(t)}{2}\Big(f_i^x(t) + f_i^x(t+\Delta t) - 2\zeta(t)v_i^x(t)\Big) + \\ &\qquad v_i^x(t)\Big(\sum_{j=1}^{N} v_j^x(t)^2 - 3NK_BT\Big)/Q\Big]\,. \end{aligned} \tag{1.46}$$

These equations for updation should be applied to each components of the positions and velocities to obtain the configurations at a later time from the earlier one.

(b) Langevin thermostat

This is a stochastic thermostat for simulations in NVT ensemble [65]. Unlike NHT, in which the hydrodynamics of the system is preserved, LT doesn't preserve hydrodynamics. In LT, at each step, all the particles receive a random force on it that compensates for a constant friction that tries to make their velocities lowered by an amount proportional to its velocity. The average magnitude of the random forces and friction are related via the 'fluctuation-dissipation' theorem.

In this method, the equation of motion of the i-th particle essentially becomes

$$m\frac{d^2\vec{r}_i}{dt^2} = -\vec{\nabla}_i U - \gamma m\vec{v_i} + \sqrt{6\gamma k_B T m}\vec{R}_i(t)\,. \tag{1.47}$$

Here, γ is the friction coefficient and $\vec{R}_i(t)$ is a delta-correlated random force which satisfies,

$$\langle R_i^x(t)\rangle = 0\,, \tag{1.48}$$

$$\langle R_i^x(t)R_j^x(t')\rangle = \delta(t-t')\delta_{ij}\,. \tag{1.49}$$

Verlet neighbor list

The improvement of the computational time during force calculation in MD simulations can be made by the use of Verlet neighbor list (VNL) [63].

For pair-wise force calculations, using VNL, the computational time will be much lesser than $\mathcal{O}(N^2)$, where N is the number of particles in the system. The construction and application of VNL can be illustrated by the following points (see also Fig. 1.13):

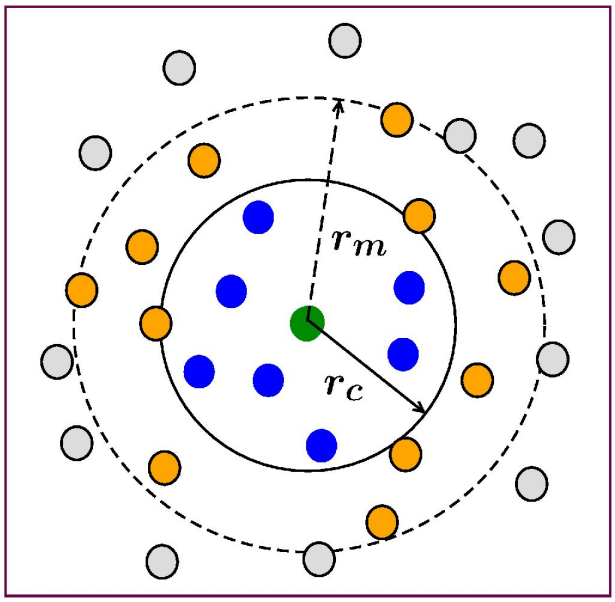

Figure 1.13: Schematic representation of the Verlet neighbor list, details of which is mentioned in the text.

- One needs to construct a list which contains, for each particle i (particle marked by green), the positions of other particles j (particles marked by blue and orange), whose distances from i are less than some choice of r_m, which should be chosen such that $r_m > r_c$, where r_c is a cut-off distance. Particle i interacts only with the particles (marked by blue) which are within r_c.

- The list for the particles needs to be updated in an interval of t_m steps. The scheme of updating the list is imperative when particles

from outside r_m start interacting with the particle i.

- t_m and r_m should be chosen such that, $(\vec{r}_m - \vec{r}_c) > t_m \vec{v}_a \Delta t$, where $\vec{v}_a$ is the typical velocity of a particle.

- Only the particles inside VNL are taken into account for the calculation of pairwise short range forces. Thus the computational time will be minimized. Here note that for short range interactions the potential is truncated at a distance r_c.

1.7.2 Event-driven MD for hard particles

For hard particles [25,64], one uses event driven molecular dynamics (EDMD). In Fig. 1.14 we have schematically shown the hard sphere potential. 'PE' stands for potential energy.

In this case, there is no interaction among the particles except for their exclusion over each other. Thus all the particles move in a force-free environment till they collide with other particles. A change in velocities of the colliding particles occur at those instants of time. So calculation of the forces on the particles are not needed. Instead of that, keeping track of collision events is required. This scheme is known as EDMD [25]. In EDMD, a natural way to measure time is to count the average number of collisions per particle in the system. But sometimes keeping track of actual time (t) is also necessary. The steps, which EDMD follows, are summarized below [25].

- Initialize the system as in TDMD, with positions and velocities of all particles.

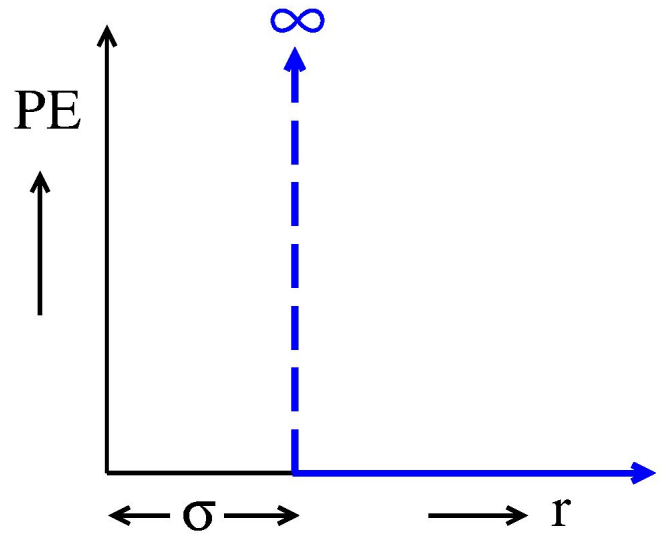

Figure 1.14: Figure shows a schematic plot of hard-sphere potential. There is no interaction between particles when $r > \sigma$. At $r \leq \sigma$ the potential is repulsively infinite and thus the minimum value of interparticle separation will be σ.

- Then identify collision partners and corresponding collision times according to Eq. (1.52).
- Find out the minimum time of collision ($t_{ij}^{\min}$) for the entire system.
- Advance all the particles upto $t_{ij}^{\min}$ with their corresponding velocities.
- Change the velocities of the colliding particles according to Eqs. (1.4) and (1.5).
- Recalculate collision times and partners only for the colliding particles, which undergo velocity changes.
- Then repeat all the above steps. In the meantime, one can calculate the necessary statistical quantities at regular intervals.

Calculation of collision time

Here we will briefly describe the calculation of collision time for the collision between two hard particles [25, 64]. Let us consider two particles i and j, each of diameter σ, whose positions are $\vec{r_i}$ and $\vec{r_j}$ and velocities are $\vec{v_i}$ and $\vec{v_j}$, respectively, at time t. If they collide at time $t + t_{ij}$, then the following equation needs to be satisfied [64]:

$$|\vec{r}_{ij}(t + t_{ij})| = |\vec{r}_{ij}(t) + \vec{v}_{ij}(t)t_{ij}| = \sigma\,, \tag{1.50}$$

where $\vec{r}_{ij}(t) = \vec{r}_i - \vec{r}_j$ and $\vec{v}_{ij}(t) = \vec{v}_i - \vec{v}_j$. Now if we define a quantity $b_{ij} = \vec{r}_{ij} \cdot \vec{v}_{ij}$, then the above equation reads

$$v_{ij}^2 t_{ij}^2 + 2b_{ij}t_{ij} + r_{ij}^2 - \sigma^2 = 0\,. \tag{1.51}$$

This is a quadratic equation in t_{ij}. The case $b_{ij} > 0$ mimics the fact that the particles are going away from each other and a collision between them is not possible. On the other hand, $b_{ij} < 0$ suggests that the particles are approaching each other. Now, if $\mathrm{D_r}\big(= [b_{ij}^2 - v_{ij}^2(r_{ij}^2 - \sigma^2)]\big) < 0$, then the equation has complex roots and again no collision is possible. If $\mathrm{D_r} > 0$, then two positive roots arise, smaller of which corresponds to the time of impact

$$t_{ij} = \frac{-b_{ij} - (b_{ij}^2 - v_{ij}^2(r_{ij}^2 - \sigma^2))^{1/2}}{v_{ij}^2}\,. \tag{1.52}$$

For granular gases, where only binary collisions occur, this algorithm works quite nicely.

Inelastic collapse

One drawback that EDMD suffers during simulation is the divergence of collision number in an infinitesimal time if we use a constant value for the coefficient of restitution (e). This is known as inelastic collapse (IC) [25, 67]. Possibility of IC increases with the reduction of dimensionality as well as with that of the value of e during a simulation. In $d = 1$, it is quite well understood and possible to calculate the requirements of IC with the change of e values. If $0 < e < (7 - 4\sqrt{3})$, three particles are required for IC to happen. If $(7 - 4\sqrt{3}) < e < (3 - 2\sqrt{2})$ then the collapse requires at least four particles. In higher dimensions, analytic arguments cannot calculate or predict IC exactly. There are several ways to get rid of this technical difficulty [68]. We have opted one of them, which will be discussed in detail in Chapter 3.

1.8 Finite-size scaling analysis

In computer simulations, we deal with finite sized systems which may not lead to the expected thermodynamic behavior of observables of interest [42]. This is essentially known as the finite-size effect (FSE). Thus, as a result, conclusions from the obtained data can sometimes be wrong. In particular, FSE has a strong influence on the data when one expects a diverging length-scale in the system. One way to eliminate the FSE is to make the system larger and larger. This method is not too graceful and not definitely an effective one in the presence of diverging length-scale. One well-known

example can be given in the context of critical phenomena, where equilibrium correlation length (ξ) diverges in a power-law fashion as [42] $\xi = \xi_0 \epsilon^{-\nu}$, where $\epsilon = |T - T_c|$ is a measure of the deviation of the temperature from the critical value T_c and ν is a critical exponent. When $T \to T_c$, $\xi \to \infty$. In Fig. 1.15, ξ, which is essentially the length over which the particles are correlated, is demonstrated schematically. Now, the maximum value of ξ can not exceed L. Thus, $\xi < \infty$, for $L < \infty$.

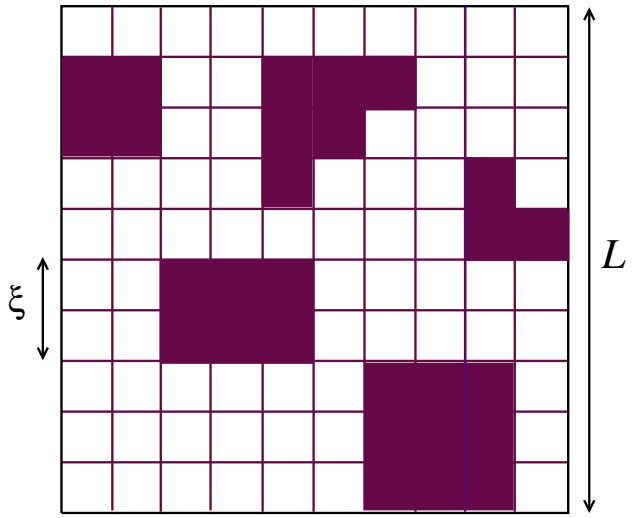

Figure 1.15: Schematic representation of the static correlation length ξ in a system of size L. ξ is the average length of the regions where correlations have build up. Here, maximum value of ξ will be equal to L.

This fact is also true in problems of domain coarsening, where quantities analogous to ξ and ϵ are ℓ and $1/t$. In this thesis, a significant part is dedicated to the coarsening and scaling of the growth of clusters in ICS in granular and active matters. Thus, we should mention about finite-size effect during domain coarsening. Let us consider the phase separation of a binary mixture with 50%-A and 50%-B kind of particles. Now, for a system of size L, the behavior of average domain size $\ell(t)$ growing with time deviates from

the expected divergence as $\ell \to L$. Thus, when L is relatively small it is very difficult to draw a correct conclusion about the growth exponent. If we use larger systems to obtain the correct value of the exponent, it will take longer times for simulation.

One way to overcome this difficulty is to analyze data via the finite-size scaling technique, which was first introduced by M. E. Fisher to accurately quantify various exponents related to equilibrium critical phenomena [42,48]. We will briefly discuss how it is used in equilibrium critical phenomena.

Let us consider a quantity Q, which shows singularity as $Q \sim \epsilon^{-q} \sim \xi^{q/\nu}$, where ξ, ϵ and ν are already defined. Due to restriction of $\xi = L$ at T_c, for a system of size L, one has $Q \sim L^{q/\nu}$. Away from T_c, one can introduce a L-independent scaling function $Y(y = (L/\xi)^{1/\nu})$ such that $Q = Y(y)L^{q/\nu}$. This is possible only when the parameter y is a dimensionless quantity, defined as a ratio of two length-scales. Far away from criticality, $Y \sim y^{-q}$, so the expected form at thermodynamic limit can be achieved. Thus, a plot of $QL^{-q/\nu}$ vs y, in the finite size unaffected region provide an exponent $-q$, when plotted in the log-log scale. The finite-size scaling analysis, to estimate the power-law exponent during the nonequilibrium evolution for the growth of average domain size in the scaling regime in ICS, will be discussed in the next chapter.

Bibliography

[1] Kerson Huang, *Statistical Mechanics* 2nd Edition (Wiley, 2012).

[2] M.C. Cross and P.C. Hohenberg, Rev. Mod. Phys. **65**, (1993).

[3] H.M. Jaeger, S.R. Nagel and R.P. Behringer, Rev. Mod. Phys. **68**, 1259 (1996).

[4] P.K. haff, J. Fluid Mech. **134**, 401 (1983).

[5] I. Goldhirsch and G. Zannetti, Phys. Rev. Lett. **70**, 1619 (1993).

[6] R. Brito and M.H. Ernst, Europhys. Lett. **43**, 497 (1998).

[7] S. Luding and H.J. Herrmann, Chaos **9**, 673 (1999).

[8] E. Ben-Naim, S.Y. Chen, G.D. Doolan and S. Redner, Phys. Rev. Lett. **83**, 4069 (1999).

[9] I.S. Aranson and C.S. Tsimring, Rev. Mod. Phys. **78**, 641 (2006).

[10] H.M. Jaeger and S.R. Nagel, Science **255**, 1523-1531 (1992).

[11] J.A.C. Gallas and H.J. Herrmann and S. Sokolowski, Phys. Rev. Lett. **69**, 1371 (1992).

[12] J.B. Knight, H.M. Jaeger and S.R. Nagel, Phys. Rev. Lett. **70**, 3728 (1993).

[13] R. Khosropour, J. Zirinsky, H. Pak and R.P. Behringer, Phys. Rev. E **56**, 4467 (1997).

[14] S. Luding, E. Clément, J. Rajchenbach and J. Duran, Europhys. Lett. **36**, 247 (1996).

[15] T. Pöschel, T. Schwager and C. Salueña, Phys. Rev. E **62**, 1361 (2000).

[16] I.H. Ansari and M. Alam, Phys. Rev. E **93**, 052901 (2016).

[17] TPC van Noije, M.H. Ernst, R. Brito and J.A.G. Orza, Phys. Rev. Lett. **79**, 411 (1997).

[18] J.J. Brey, J.W. Dufty, C.S. Kim and A. Santos, Phys. Rev. E **58**, 4638 (1998).

[19] T. Pöschel and N.V. Brilliantov, *Granular Gas Dynamics* (Springer, 2003).

[20] N.V. Brilliantov and T. Pöschel, *Kinetic Theory of Granular Gases* (Oxford University Press, Oxford, 2004).

[21] S.K. Das and S. Puri, Phys. Rev. E **68**, 011302 (2003).

[22] S. Paul and S.K. Das, Europhys. Lett. **108**, 66001 (2014).

[23] M. Shinde, D. Das and R. Rajesh, Phys. Rev. Lett. **99**, 234505 (2007).

[24] A. Snezhko, I.S. Aranson and W.-K. Kwok, Phys. Rev. Lett. **94**, 108002 (2005).

[25] T. Pöschel, T. Schwager, *Computational Granular Dynamics: Models and Algorithms* (Springer, 2005).

[26] G.F. Carnevale, Y. Pomeau and W.R. Young, Phys. Rev. Lett. **64**, 2913 (1990).

[27] C.V. Raman, Phys. Rev. **12**, 442 (1918).

[28] R. Ramírez, T. Pöschel, N.V. Brilliantov and T. Schwager, Phys. Rev. E **60**, 4465 (1999).

[29] H. Goldstein, C.P. Poole, and J.F. Safko, *Classical Mechanics* 3rd Ed. (Addison-Wesley, 2001).

[30] S.K. Das and S. Puri, Europhys. Lett. **61**, 749 (2003).

[31] M. Shinde, D. Das and R. Rajesh, Phys. Rev. E **84**, 031310 (2011).

[32] M. Shinde, D. Das and R. Rajesh, Phys. Rev. E **79**, 021303 (2009).

[33] X. Nie, E. Ben-Naim and S.Y. Chen, Phys. Rev. Lett. **89**, 204301 (2002).

[34] S.R. Ahmad and S. Puri, **75**, 031302 (2007).

[35] T. Schwager and T. Pöschel, Phys. Rev. E **57**, 650 (1998).

[36] S. Miller and S. Luding, Phys. Rev. E **69**, 031305 (2004).

[37] S.N. Pathak, Z. Jabeen, D. Das and R. Rajesh, Phys. Rev. Lett. **112**, 038001 (2014).

[38] S. Roy and S.K. Das, J. Chem. Phys. **139**, 044911 (2013).

[39] T. Vicsek, A. Czirók, E. Ben-Jacob, I. Cohen and O. Shochet, Phys. Rev. Lett. **75**, 1226 (1995).

[40] S. Ramaswamy, Annu. Rev. Condens. Matter Phys. **1**, 323 (2010).

[41] S.K. Das, J. Chem. Phys. **146**, 044902 (2017).

[42] H.E. Stanley, *Introduction to Phase Transitions and Critical Phenomena* (Oxford University Press, Oxford, 1971).

[43] A. Onuki, *Phase Transition Dynamics* (Cambridge University Press, Cambridge, 2002).

[44] A.J. Bray, Adv. Phys. **51**, 481 (2002).

[45] R.A.L. Jones, *Soft Condensed Matter* (Oxford University Press, Oxford, 2008).

[46] S. Puri and V. Wadhawan (eds.), *Kinetics of Phase transitions* (CRC Press, Boca Raton, 2009).

[47] P.C. Hohenberg and B.I. Halperin, Rev. Mod. Phys. **49**, 435 (1977).

[48] M.E. Fisher, in *Critical Phenomena*, edited by M.S. Green (Academic, London) p1 (1971).

[49] D.S. Fisher and D.A. Huse, Phys. Rev. B, **38**, 373 (1989).

[50] S. Majumder and S.K. Das, Phys. Rev. E **81**, 050102 (R) 2010.

[51] S. Roy and S.K. Das, Soft Matter **9**, 4178 (2013).

[52] J. Midya, S. Majumder and S.K. Das, Phys. Rev. E **92**, 022124 (2015).

[53] S. Chakraborty and S.K. Das, Eur. Phys. J. B **88**, 160 (2015).

[54] C. Yeung, M. Rao and R.C. Desai, Phys. Rev. E **53**, 3073 (1996).

[55] S. Roy and S.K. Das, Phys. Rev. E **85**, 050602(R) (2012).

[56] G. Porod, Small-Angle X-Ray Scattering, eds. O. Glater and O. Kratky (New York: Academic Press, 1982).

[57] S.E. Allen and J.W. Cahn, Acta. Metall. **27**, 1085 (1979).

[58] I.M. Lifshitz and V.V. Slyozov, J. Phys. Chem. Solids **19**, 35 (1961).

[59] E.D. Siggia, Phys Rev. A **20**, 595 (1979).

[60] S. Majumder and S.K. Das, Phys. Rev. Lett. **111**, 055503 (2013).

[61] S. Paul and S.K. Das, (to appear in Phys. Rev. E, 2017).

[62] L. Bai and D. Breen, J. Graphics, GPU, Game Tools **13**, 53 (2008).

[63] D. Frenkel and B. Smit, *Understanding Molecular Simulation* 2nd Ed. (Academic Press, California, 2002).

[64] M.P. Allen and D.J. Tildesley, *Computer Simulation of Liquids* (Clarendon, Oxford, 1987).

[65] T. Schlick, *Molecular Modeling and Simulation* (Springer, 2010).

[66] S. Nosé, J. Chem. Phys. **81**, 511 (1984).

[67] S. McNamara and W.R. Young, Phys. Rev. E **50**, 28(R) (1994).

[68] S. Luding and S. McNamara, Gran. Matter **GM9802.7** (1998).

Chapter 2

Dynamics of clustering in freely cooling granular fluid in space dimension $d = 2$

2.1 Introduction

Due to friction and inelastic nature of collisions, granular matters [1, 2] continuously dissipate energy, often leading to the formation of interesting patterns which are ideal testing ground for many important concepts of nonequilibrium statistical mechanics [2]. In this work, we are interested in the dynamics of a cooling granular gas model (GGM) where hard discs, of equal size and mass, collide inelastically and the velocities of particle i before and after ($'$) a collision with another particle j are related to each other via

the coefficient of restitution e as [3]

$$\overrightarrow{v}'_i = \overrightarrow{v}_i - \frac{1+e}{2}[\hat{n} \cdot (\overrightarrow{v}_i - \overrightarrow{v}_j)]\hat{n}, \tag{2.1}$$

$\hat{n}$ being the unit vector along the relative position of i and j particles.

This system exhibits interesting pattern formation [3–5], resembling the kinetics in a vapor-liquid transition [6], where domains, rich and poor in particles, grow with time (τ). It is believed that in such athermal systems, decay of the kinetic energy determines various properties [7,8], e.g., a crossover from uniform density to inhomogeneous density is determined by the fraction of the residual kinetic energy with respect to its value at the beginning. A broad objective of this work is to quantify the growth of the above mentioned pattern and understand if there is any connection of it with the energy decay. Elegant scaling arguments connecting the cluster size and energy decay have been used in the literature [7, 9–11] for sticky gas ($e = 0$). Further, in $d = 1$, an equivalence between perfectly and partially inelastic cases has been established [10, 11]. In this work we intend to persue the case for $e > 0$ in $d = 2$ and check for such scaling connection. To avoid technical problems, to be discussed later, we confine ourselves to $e \geq 0.75$. We investigate differences of the kinetics with the standard phase transition dynamics as well. For the quantification of the growth in this model, there exist only preliminary studies [12–14] and so an appropriate conclusion is not reached yet. For an accurate quantification of the dynamics, here we apply the finite-size scaling technique [15], rather than relying on the simulations of very large systems. In fact, choices of system sizes smaller than the standard practice turned out

to be beneficial in uncovering very interesting finite-size effects.

The characteristic length scale or the average domain size, ℓ, in a pattern forming system, with the structure exhibiting statistical self-similarity, typically grows as [16]

$$\ell(\tau) \sim \tau^{\alpha}. \tag{2.2}$$

The value of the exponent α depends upon [16] conservation of the order parameter, hydrodynamic effects, dimension of the system and the number of order-parameter components. In the present problem, of course, the "order-parameter" (the density) is a conserved scalar quantity, but it is unclear what and how important role a transport mechanism of particular type will play. Further, different mechanisms may become applicable depending upon the domain structure, e.g., whether the particle clusters are tube (stripe in $d = 2$) or droplet like [17–20].

In Ising like systems [6], after the saturation of the domain magnetization, the average domain size can be connected to the energy, since the latter is directly related to the interfacial area. This is because the difference in energy of a nonequilibrium configuration from that of an equilibrium one comes from the penalty of energy contributed by the interfaces. Thus, if the time dependence of the energy is known, the growth law can be derived from simple dimensional arguments. Such type of scaling concepts in granular cases, though exists, as stated above, needs verification, particularly in cases like the present problem where the growth is driven by the decay of kinetic energy. There may exist important differences between the present model and

standard phase separating systems. E.g., in Ising systems, the coarsening continues until ℓ reaches the equilibrium limit which scales linearly with the system size L. However, for the granular systems of such type, it is unclear whether the growth will continue till ℓ reaches maximum geometrically possible value, and if not, whether a linear scaling of the maximum domain size, $\ell_{\max}$, with L, still holds. The answers are interesting which we obtain via event driven molecular dynamics (EDMD) simulations [21, 22] of the model described above.

The rest of the chapter is planned as follows. In Section 2.2 we describe the methods. Results are presented in Section 2.3. Finally, we close the chapter with a brief summary in Section 2.4.

2.2 Methods

For the sake of brevity, we do not describe the standard EDMD method here, other than mentioning that in this technique, between two collisions particles move in straight lines, the velocities of colliding particles after a collision event being given in Eq. (3.1). In this work, to avoid an inelastic collapse [23] (divergence of number of collisions in a finite time interval), we stick to $e \geq 0.75$. (We provided more elaborate discussion on inelastic collapse in the next chapter.) Indeed, for such high values of e, we do not encounter inelastic collapse within the time scales of our simulations. Since friction is ignored in our work, these choices of e, for which we have only binary collisions, is further justified. Inelastic collapse is usually avoided [10] by making the collisions elastic for the relative velocities of colliding particles

smaller than a cut-off value. However, here we intend to stick to the basic model to avoid any undesirable changes in the outcomes.

We start with random initial configurations, in periodic square boxes of linear dimension L, where the density (ρ) is homogeneous throughout and the velocities have zero mean with Maxwellian distributions. We measure τ as the overall density of collisions (per particle) whose connection with the actual time (t) will be discussed later. For the calculation of ℓ, the domain boundaries are identified as the lines dividing regions of number densities higher and lower than a certain value, for which we stick to $\bar{\rho} = 0.37$, the overall density. The density at a point was calculated from the number of particles in a small grid around it. Following this, we obtained ℓ from the first moment of domain size distribution function as $\ell = \int d\ell_d \ell_d P(\ell_d, t)$, where ℓ_d was calculated as the distance between two successive boundaries in any direction. Note here that all the lengths are expressed in units of the diameter of the particles a. The choice of a higher threshold density than the number quoted above leads to a smaller value for the average cluster size. However, the scaling property remains same. This exercise is equivalent to a standard practice followed in the literature [12]. There, if the distance between two particles is below a cut-off distance, they are taken to be the parts of the same cluster. The length of a cluster then depends upon the choice of the cut-off.

2.3 Results

Let us begin by showing the evolution snapshots in Fig. 2.1, for $e = 0.9$. Up to a significant time the density remains homogeneous, referred to as the homogeneous cooling state (HCS) [3, 24]. At late time, the system becomes unstable to fluctuations, leading to the formation and growth of tube-like structures, the regime being termed as the inhomogeneous cooling state (ICS) [3, 24]. The crossover from the HCS to ICS is determined by the choice of $\bar{\rho}$ and e. In Fig. 2.2 we show a nonequilibrium phase diagram, in $e - \rho$ plane. This may have resemblance with the coexistence curve of a phase separating system but does not bear the same meaning which we will discuss soon. The left branch of this curve represents the density, as a function of e, in the vapor or particle-poor region, whereas, the right one is for the liquid region. For each value of e, these densities were obtained from the snapshots at times when the domain "magnetization" have saturated. Further clarification is provided in the caption.

Unlike a true vapor-liquid transition where, with the variation of overall density the pattern changes between droplet and percolating domains, here the domains are always "essentially" interconnected. This is due to the fact that, as opposed to standard phase separation, the kinetics here is not driven by the interfacial energy minimization. (Understanding the role of a kinetically driven interfacial tension, if exists [25], in the coarsening of the present model, is not very straight forward.) From here on, unless otherwise mentioned, we stick to $e = 0.9$ only, a value low enough to avoid strong density variation within a domain of particular type. For this particular

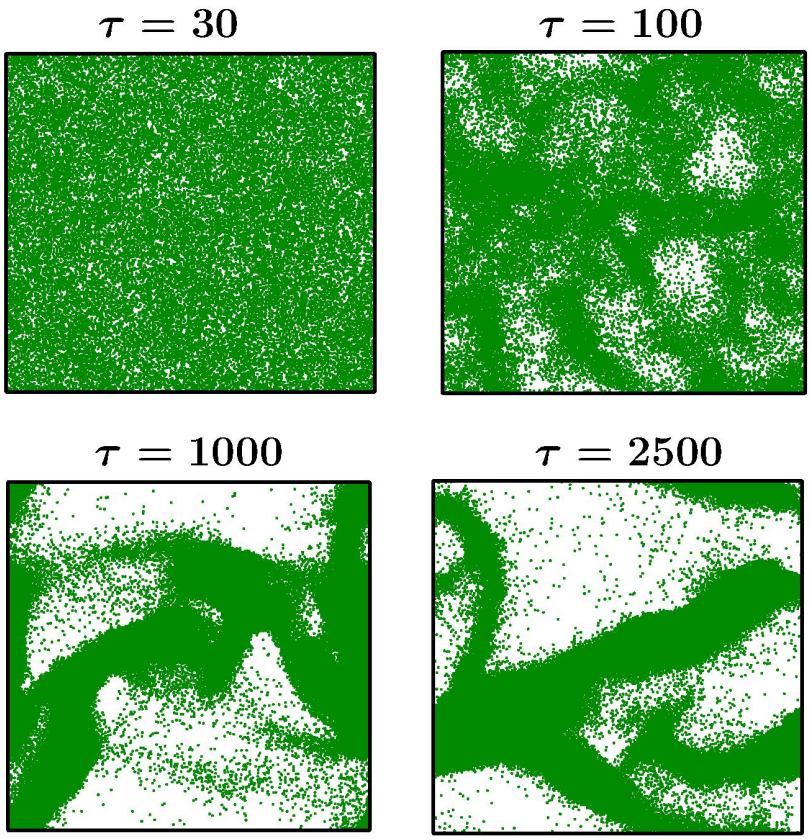

Figure 2.1: Snapshots from different times, green dots representing the particles, during the evolutions of a granular system with $\bar{\rho} = 0.37$, $e = 0.9$ and $L = 256$.

choice of e, the ratio of order-parameter probability density at the peak value of liquid density and that at the overall density is approximately 4. This number decreases with the increase of e, being less than 2 for $e = 0.95$. Such strong variation is due to the broad interfaces that prevents [4] observation of the Porod tail [16] in the structure factor which comes from the sharp interfaces and is seen in the true phase-separating systems. In the latter systems, say for a vapor-liquid transition, approximately 10% below the critical points, the probability at the overall density is zero to a good

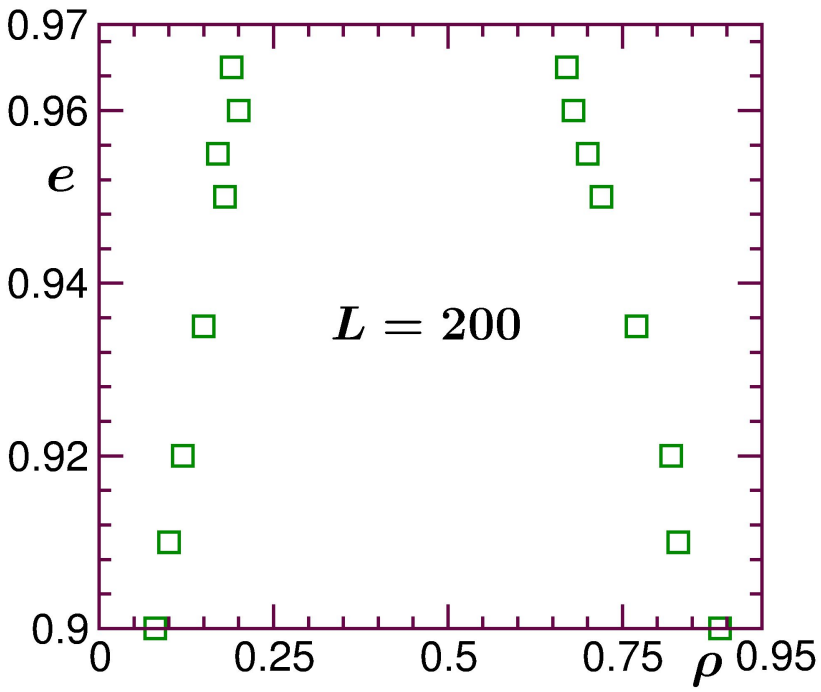

Figure 2.2: Nonequilibrium phase diagram with $L = 200$ and $\bar{\rho} = 0.37$. Points at different branches are average densities in the loose and dense regions of the structurally saturated configurations.

approximation.

In Fig. 2.3 we present a plot of ℓ as a function of τ, for $L = 256$. For $\tau \gtrsim 1000$, it appears that the structure stopped growing, possibly due to the finite-size effects. Noting that the time for the last snapshot in Fig. 2.1 falls in this regime, it is clear, unlike the standard separation related to phase transitions, this model does not exhibit complete phase separation, the possible reasons of which we discuss below.

The coarsening occurs following the parallelization of velocities due to the reduction of the normal relative velocities. In the ideal situation when the clustered particles move "perfectly" parallel to each other, the condition of momentum conservation prevents formation of a single big cluster. In such

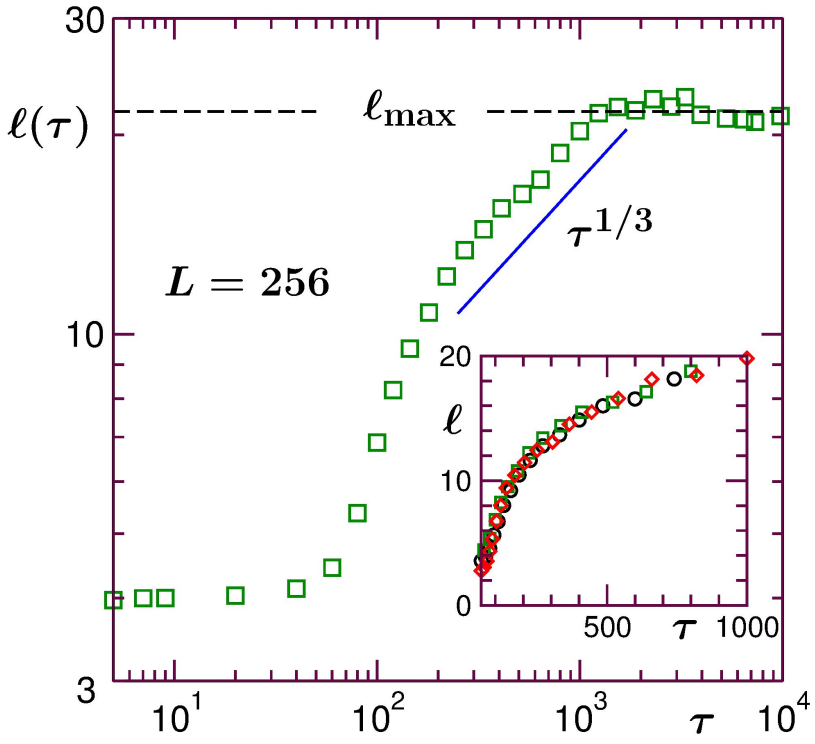

Figure 2.3: Plot of average cluster size as a function of τ, for $L = 256$. The solid line there represents the power-law $\tau^{1/3}$. The dashed line corresponds to $\ell_{\max}$. Inset shows qualitative equivalence of ℓ when local density is calculated using different grid sizes. Various data sets, corresponding to two square grids of area $4a^2$ and $16a^2$ as well as a circular grid of area $4\pi a^2$, are scaled to superimpose on top of each other. For analysis purpose we have chosen the circular grid.

a situation, there may be a competition between the growth and break up, the latter happening when two oppositely moving clusters collide with each other. This restricts the value of $\ell_{\max}$, calculation of which is demonstrated in this figure, significantly below L. However, the break-up scenario need not be the only possibility. This is because of the fact that there does exist dispersion in the particle velocities within a cluster such that the momentum conservation may be satisfied even if a single cluster exists. In that case

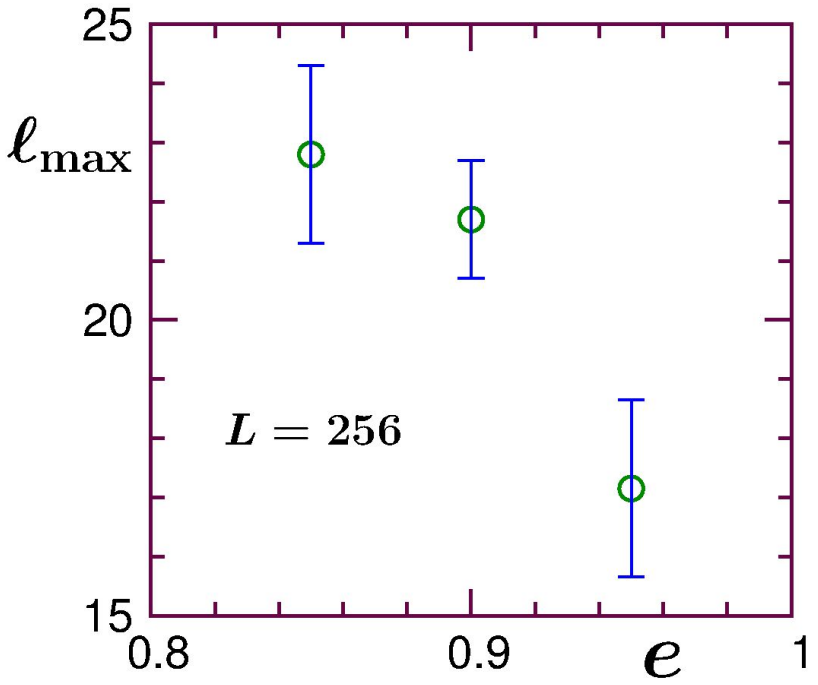

Figure 2.4: Figure shows a plot of $\ell_{\max}$ vs e.

the saturation of the length at a value much smaller than the maximum geometrically allowed value can be due to the following reason. Unlike the standard phase separating systems, minimum interfacial region at the end is not a requirement in this case. Thus, a single cluster with branching can exist, leading to a smaller value of $\ell_{\max}$. For lower values of e, break-up, if at all happens, is a lesser possibility, leading to a higher number for $\ell_{\max}$. A plot of $\ell_{\max}$ vs e is presented in Fig. 2.4. This trend of $\ell_{\max}$ decreasing with increasing e is due to a combined effect of lesser break-up and weaker density fluctuation for smaller e. Here note that the saturation in the domain growth does not come with any special morphological characteristics. This we have checked via the scaling property of the two-point equal time correlation functions. The saturation in the cluster size, however, is related to that in

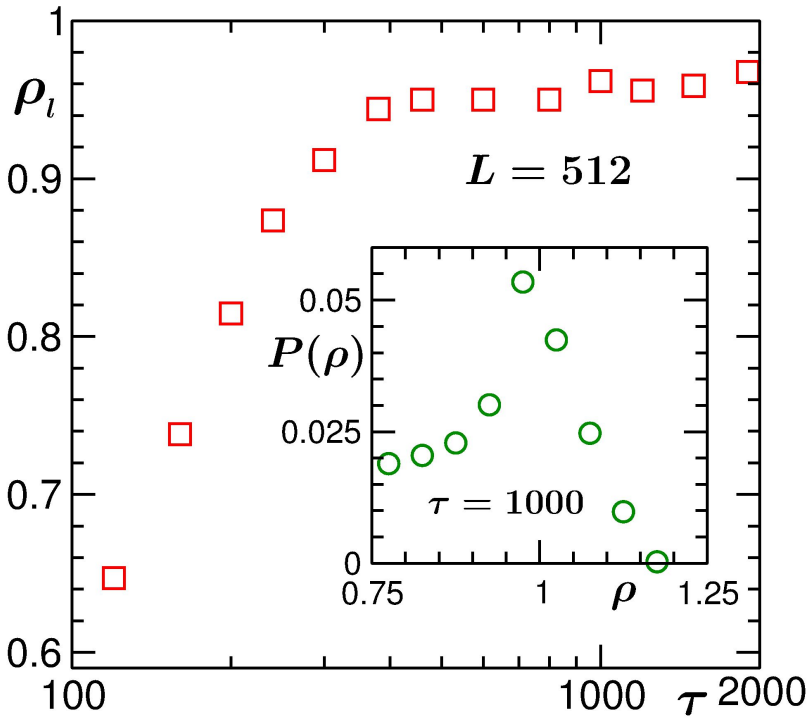

Figure 2.5: Variation of density, obtained from the locations of the peaks of density distributions in the liquid region, as a function of τ, for $L = 512$. Inset shows the probability distribution of density for the liquid regions, at $\tau = 1000$. Nonzero values at $\rho > 1$ are obtained due to counting of disc centres inside the grids.

the ordering in velocity pattern.

As explained, estimation of the length scale requires calculation of the local density. The results depend upon the choice of grid size. However, the qualitative behavior remains unchanged, if the grid size is not too big, as demonstrated in the inset of Fig. 2.3. There, results from different grid sizes are scaled by appropriate factors to obtain a data collapse. See caption for further details.

The early flat part in Fig. 2.3, for $\tau \leq 50$, corresponds to the HCS. A fast rise of ℓ marks the crossover from HCS to ICS. In the ICS, a nice

power-law behavior is observed for a rather extended period of time and the data show consistency with an exponent 1/3. In Fig. 2.5 we show how the density at the location of the peaks of the density distribution functions in the liquid region, ρ_l, varies as a function of τ. It increases dramatically when a crossover from HCS to ICS occurs, thus, any effort to extract a functional form of the growth of ℓ during this period may not be meaningful. On the other hand, ρ_l remains reasonably flat when the $\tau^{1/3}$ scaling behavior of ℓ is observed. The inset of Fig. 2.5 refers to the density distribution, calculated from the number of disc centres in suitably chosen bins, size being mentioned in the caption of Fig. 2.3, for the liquid region, at $\tau = 1000$.

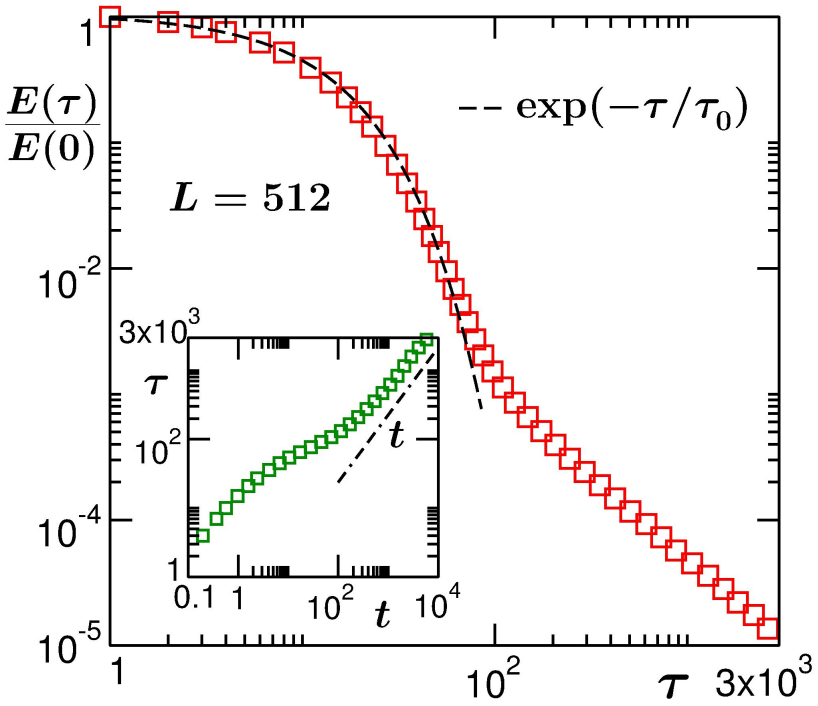

Figure 2.6: Log-log plot of the decay of kinetic energy $E(\tau)$ for system size $L = 512$. The dashed line corresponds to Haff's law in HCS. The inset shows relationship between τ and t, for $L = 512$. The dashed-dotted line there has a linear behavior.

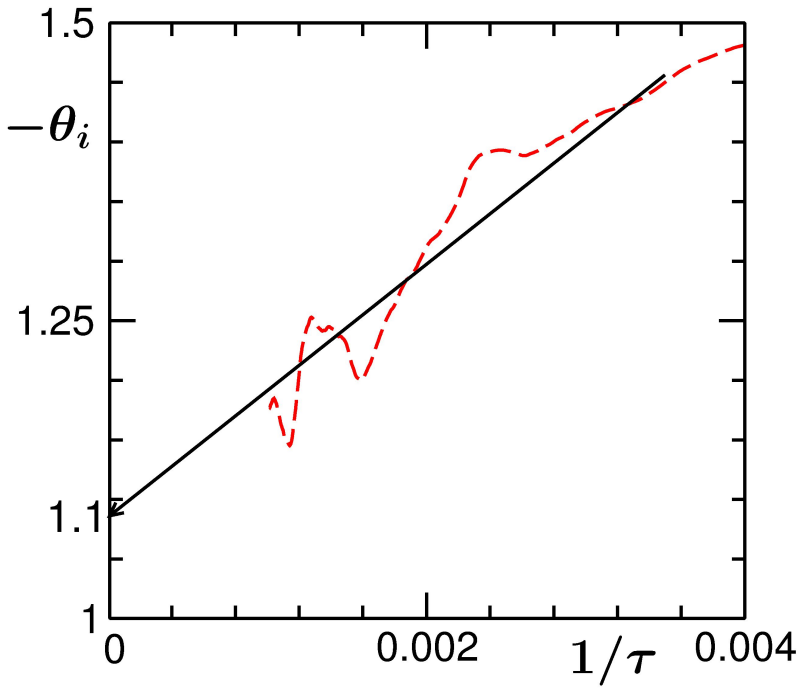

Figure 2.7: Plot of the instantaneous exponent θ_i, vs. $1/\tau$, for the energy decay in ICS, the solid line being a guide to the eyes. The data were running averaged.

After the preliminary indication that $\alpha = 1/3$, we take a look at the decay of the kinetic energy E in Fig. 2.6. There $E(\tau)/E(0)$ is plotted versus τ for $L = 512$. It is clearly seen that there is a difference in the forms of decay in the HCS and ICS. The dashed line in this figure represents an exponential decay $e^{-\tau/\tau_0}$, predicted by Haff [26], τ_0 being an $e-$dependent time constant, which is in good agreement with the simulation data in HCS. On the other hand, in the ICS, the data are reasonably consistent with a power-law [8], $E \sim \tau^{-\theta}$. An analysis via the computation of instantaneous exponent, $\theta_i = d(\ln E)/d(\ln \tau)$, by taking data in the range $\tau \in [250, 1000]$ for $L = 512$ (see Fig. 2.7), provides $\theta \simeq 1.1$. In that case, the scaling

hypothesis [7, 9] predicts $\alpha \simeq 1/2$ (mentioned in the introduction and will be further elaborated in the next chapters – here we just mention that the prediction is: $E \sim 1/m \sim 1/\ell^d \sim t^{-\frac{2d}{d+2}}$), which is significantly higher than our observation. To this end, to bring a connection of E and ℓ with t, in inset of Fig. 2.6 we have plotted τ vs. t, for $L = 512$, that shows a reasonably linear relationship between these two times, in ICS. This indicates that our observation of the decay of E in ICS is consistent with $E \sim t^{-1}$, as reported previously [8]. Thus, even though the energy decay follows the prediction, growth of mass does not.

Such scaling argument, we feel, will work if the dissipation were primarily due to the collisions in the boundary regions which is true in a sticky gas where particles from the vapor region collide with the droplet boundary and literally stick to the cluster for ever, providing a ballistic aggregation. In the present case, we have checked that most of the collisions occur inside the clusters, having no role in the growth, which contribute primarily to the observed decay of energy. Further, the decay continues even after $\ell_{\max}$ is reached, as expected.

Here it needs to be mentioned that there can be different measures for quantifying the growth. Traditionally, in the area of granular matter, average mass of clusters has been calculated. In $d = 1$, this is equivalent to ℓ. For $d > 1$, in addition to differing dimensionally, these quantities may have other technical differences. E.g., if the morphology is not taken care of, which is automatically included in our calculation, for a percolating structure the average mass will not provide an information on the growth of the pattern. In

that case, the growth will stop once the structure has percolated. Nevertheless, this measure also provides important information, though of different type. In the present problem, its relevance stems from the facts that a perfect bicontinuous structure does not exist from the beginning and there is a possibility of breaking of domains due to the collisions, during the course of the evolution. Interestingly, the growth of the average mass also provides an exponent [12] approximately same as that we obtained for ℓ. However, this was an outcome of a preliminary study and the authors warned about the seriousness of their conclusions. Along this line, another study [13, 14] also suffered from statistical inaccuracy, to our understanding.

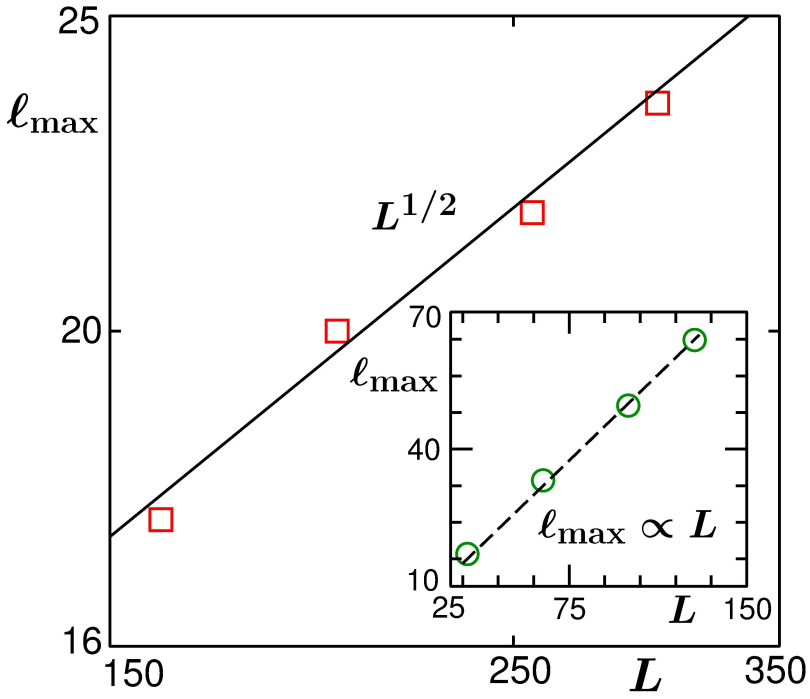

Figure 2.8: Log-log plot of $\ell_{\max}$ vs system size L. The solid-line is a power-law fit to the data providing an exponent ~ 0.5. Inset shows the same plot for Ising model in linear scales, for a 50 : 50 composition of up and down spins, at $T = 0.6T_c$.

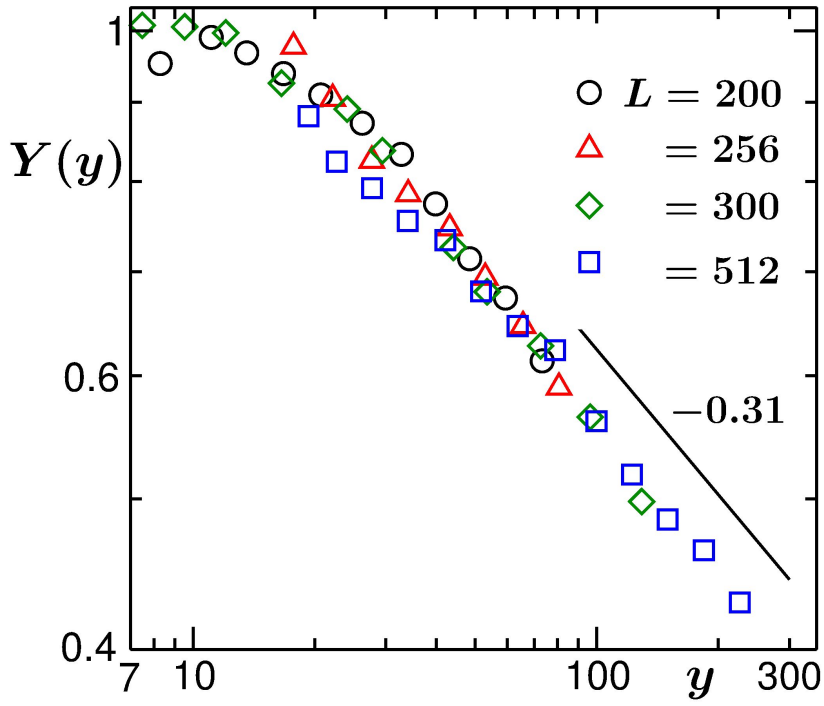

Figure 2.9: Finite-size scaling plot of length-scale data of granular systems of different sizes. The solid line corresponds to a power-law with exponent −0.31.

We now move onto accurate quantification of the growth via the finite-size scaling (FSS) analysis [15,27]. This is because, often, due to the presence of off-sets, fluctuations in the data and finite-size effects, a conclusion about a power-law exponent from log-log plot can be misleading. Let us consider a problem with diverging length scale, e.g., the equilibrium critical phenomena, where a quantity (Q) shows singularity as $Q \sim \epsilon^{-q} \sim \xi^{q/\nu}$, ξ being the diverging correlation length with the critical exponent ν and ϵ the temperature (T) deviation from the critical value (T_c). Due to the restriction of ξ equaling L at the criticality, one has $Q \sim L^{q/\nu}$. Away from the critical point, one introduces a L-independent scaling function $Y(y = (L/\xi)^{1/\nu})$ such that

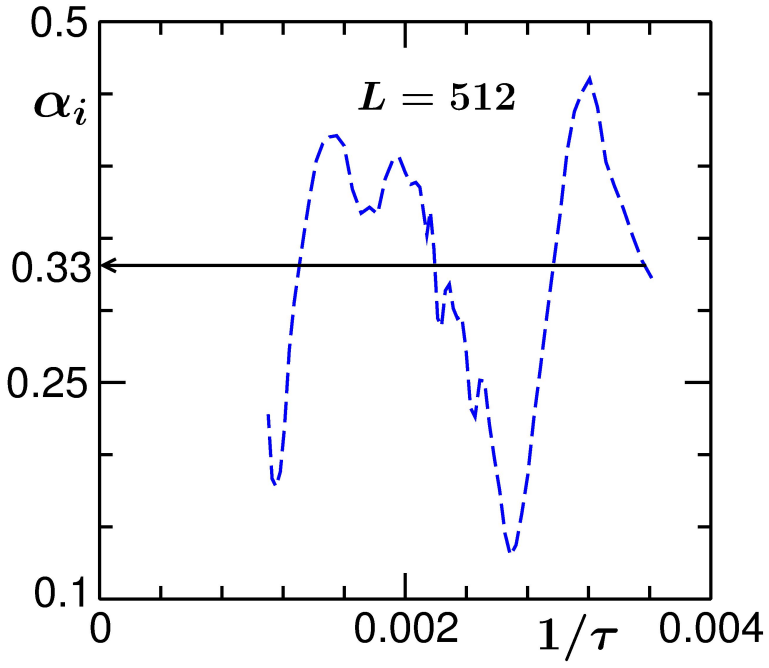

Figure 2.10: Figure shows the plot of instantaneous exponent α_i, vs. $1/\tau$, calculated using $L = 512$ data in ICS.

$Q = Y(y)L^{q/\nu}$. Far away from the criticality $Y \sim y^{-q}$, so that the expected thermodynamic limit form of the singularity is recovered. Thus, a plot of $QL^{-q/\nu}$, vs y, in the finite-size unaffected region, will provide a power law with the exponent $-q$. A deviation from it will mark the onset of the finite-size effects. In the present problem Q and ξ both should be identified with ℓ, ϵ with $1/\tau$ and α with q. Here, as we have observed in Fig. 2.1 and Fig. 2.3, the saturation length does not reach L, so $\ell_{\max}$ should replace L. Thus, for the present problem one writes the FSS equation as

$$\ell(\tau) = \ell_{\max} Y(y); \qquad y = (\ell_{\max}/\ell)^{1/\alpha}. \tag{2.3}$$

Then, a plot of $\ell/\ell_{\rm max}$, vs $y = \ell_{\rm max}^{1/\alpha}/\tau$, should provide a slope of $-\alpha$ in double-log scale, with data from all system sizes collapsed onto each other, for correct choice of α, of course. Before moving on to that exercise, we take a look at the relation between $\ell_{\rm max}$ and L in Fig. 2.8. It appears that they do not scale linearly, rather $\ell_{\rm max} \sim L^{1/2}$, thus the saturation of growth is sudden. This, of course, is a striking observation and should be compared with a linear behavior exhibited by corresponding data from the Monte Carlo simulations [28] of conserved Ising model with the Kawasaki exchange kinetics [28], shown in the inset. In the granular model, the exponent 1/2 for the scaling of $\ell_{\rm max}$ with L, is extremely disadvantageous that drastically restricts the utility of the brute force method of simulating bigger systems and collecting data for decades in time and length.

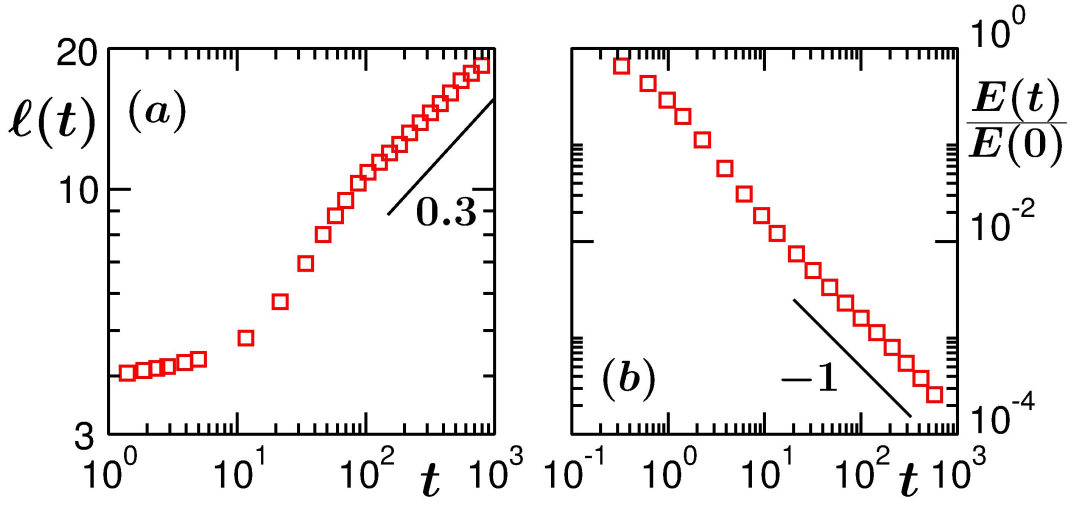

Figure 2.11: (a) Plot of ℓ as a function of t. The solid line there represents the power-law $t^{0.3}$. (b) Log-log plot of the decay of E vs t. The solid line corresponds to a t^{-1} decay. Results in both (a) and (b) correspond to $e = 0.75$, $\bar{\rho} = 0.37$ and $L = 256$.

In Fig. 2.9 we show the finite-size optimum data collapse, obtained for

$\alpha = 0.31$. In Fig. 2.10 we have shown a plot of the instantaneous exponent, $\alpha_i = d(\ln \ell)/d(\ln \tau)$, as a function of $1/\tau$, which also shows consistency with the exponent observed in finite size scaling.

In fluid phase separation, there are two mechanisms for the growth of tube like domains [16]. Simple diffusion mechanism provides an exponent 1/3. On the other hand, in the hydrodynamics dominated case, fast flow of material due to pressure gradient [18], caused by interfacial tension, across the tubes, provides a much higher exponent. Here, the exponent being rather small, it appears, this latter picture does not apply. In fact, interfacial tension plays crucial role in both these mechanisms. However, from the discussion of the phase behavior and the structure, it is apparent that interfacial tension, as expected, is irrelevant for the evolution here.

Even though we presented results only for one combination of e and $\bar{\rho}$, we have checked that the conclusions are valid for a rather significant range of these parameters, all providing very similar fractal structure which we have checked via application of an algorithm by Grassberger and Procaccia [29]. In Fig. 2.11, for another representative value of e, viz., $e = 0.75$, we have demonstrated that a connection between E and ℓ is indeed not strong. In this case, we have presented the results as functions of t.

2.4 Conclusion

In conclusion, we have presented results from extensive event driven molecular dynamics simulations of a cooling granular fluid in $d = 2$, with particular emphasis on the understanding of the growth of pattern. Via application of

the finite-size scaling theory, we have quantified the growth of the average domain size. It is shown that the scaling argument [7] relating the decay of energy with growth of ℓ does not work, at least for high value of restitution coefficient, in this dimension. A striking difference of the present model with the standard phase separation models is on the finite-size effects. While in latter models, the maximum length, $\ell_{\max}$, scales linearly with L, the system size, in the granular case we observe $\ell_{\max} \sim L^{1/2}$, indicating that the growth ceases rather suddenly.

In future, in addition to taking up the case of $d = 3$, we intend to study the aging phenomena [30] in this inherently nonequilibrium system. To understand the cluster growth, various different quantities, e.g., average length of domains, average mass of clusters, maximum cluster size, total number of particles in the clustered regions, etc., are important and will be looked at. In higher dimension, there have been only preliminary studies on the behavior of some of these quantities.

In this work, we have treated e same for all collisions. In reality, value of e depends upon the relative velocities [4,5] of the colliding particles, providing fluctuation in e. In such a situation also, following a homogeneous regime, clustering occurs which, however, departs towards homogeneity again. Thus, this is a much more complex scenario, understanding of which requires appropriate knowledge from the studies of fixed e case. Further, Casimir like effects [31, 32] can be studied in granular systems as well. Such phenomena has in fact been studied in driven granular systems [33, 34]. It will be interesting to compare the findings of the latter studies with nondriven systems.

Bibliography

[1] N.V. Brilliantov and T. Poeschel, *Kinetic Theory of Granular Gases* (Oxford University press, Oxford, 2004).

[2] I.S. Aranson and L.S. Tsimring, Rev. Mod. Phys. **78**, 641 (2006).

[3] I. Goldhirsch and G. Zanetti, Phys. Rev. Lett. **70**, 1619 (1993).

[4] M. Shinde, D. Das and R. Rajesh, Phys. Rev. Lett. **99**, 234505 (2007).

[5] A. Bodrova, A.K. Dubey, S. Puri and N.V. Brilliantov, Phys. Rev. Lett. **109**, 178001 (2012).

[6] A. Onuki, *Phase Transition Dynamics* (Cambridge University Press, UK, 2002).

[7] G.F. Carnevale, Y. Pomeau and W.R. Young, Phys. Rev. Lett. **64**, 2913 (1990).

[8] X. Nie, E. Ben-Naim, and S. Chen, Phys. Rev. Lett. **89**, 204301 (2002).

[9] Z. Jabeen, R. Rajesh and P. Ray, Europhys. Lett. **80**, 34001 (2010).

[10] E. Ben-Naim, S.Y. Chen, G.D. Doolan and S. Redner, Phys. Rev. Lett. **83**, 4069 (1999).

[11] M. Shinde, D. Das and R. Rajesh, Phys. Rev. E **84**, 031310 (2011).

[12] S. Luding and H.J. Herrmann, Chaos **9**, 673 (1999).

[13] S.K. Das and S. Puri, Europhys. Lett., **61**, 749 (2003).

[14] S.K. Das and S. Puri, Phys. Rev. E. **68**, 011302 (2003).

[15] M.E. Fisher, in *Critical Phenomena*, edited by M.S. Green (Academic Press, London, 1971).

[16] A.J. Bray, Adv. Phys. **51**, 481 (2002).

[17] K. Binder and D. Stauffer, Phys. Rev. Lett. **33**, 1006 (1974).

[18] E.D. Siggia, Phys. Rev. A. **20**, 595 (1977).

[19] S. Majumder and S.K. Das, Europhys. Lett. **95**, 46002 (2011).

[20] S. Roy and S.K. Das, Phys. Rev. E **85**, 050602 (2012).

[21] M.P. Allen and D.J. Tildesley, *Computer Simulations of Liquids* (Clavendon, Oxford, 1987).

[22] D.C. Rapaport, *The Art of Molecular Dynamics Simulations* (Cambridge University Press, Cambridge, England, 2004).

[23] S. McNamara and W.R. Young, Phys. Rev. E. **50**, R28 (1994).

[24] R. Brito and M.H. Ernst, Europhys. Lett. **43**, 497 (1998).

[25] S.R. Ahmad and S. Puri, Europhys. Lett. **75**, 56 (2006).

[26] P.K. Haff, J. Fluid Mech. **134**, 401 (1983).

[27] S.K. Das, S. Roy, S. Majumder and S. Ahmad, Europhys. Lett. **97**, 66006 (2012).

[28] D.P. Landau and K. Binder, *A guide to Monte Carlo Simulations in Statistical Physics* (Cambridge University Press, Cambridge, 2009).

[29] P. Grassberger and I. Procaccia, Phys. Rev. Lett. **50**, 346 (1983).

[30] M. Zannetti, in *Kinetics of Phase Transitions*, edited by S. Puri and V. Wadhawan (CRC Press, Boca Raton, 2009).

[31] H.B.G. Casimir, Proc. Kon. Nederlandse Akad. Wetenschappen **B51**, 793 (1948).

[32] M.E. Fisher and P.G. de Gennes, C. R. Acad. Sci. Paris **B287**, 207 (1978).

[33] C. Cattuto, R. Brito, U.M.B. Marconi, F. Nori and R. Soto, Phys. Rev. Lett. **96**, 178001 (2006).

[34] M. Reza Shaebani, J. Sarabadani and D.E. Wolf, Phys. Rev. Lett. **108**, 198001 (2012).

Chapter 3

Ballistic aggregation in systems of inelastic particles: Cluster growth, structure and aging in one dimension

3.1 Introduction

Structure and dynamics during cooling in systems of inelastically colliding particles have been of much research interest [1–22]. An importance of this topic stems from the relevance of it in the agglomeration of cosmic dust [21]. Two models in this context have been of significant importance, viz., the granular gas model (GGM) and ballistic aggregation model (BAM). In the BAM, following a collision between two freely moving clusters, the colliding partners form a single larger object. In one dimension this corresponds to

the sticky gas. While collisions trigger clustering immediately in the case of BAM, for the GGM (with coefficient of restitution $0 < e < 1$) the system remains in a homogeneous density state during an initial period, referred to as the homogeneous cooling state (HCS) [3,18]. The dynamics in the latter then crosses over to an inhomogeneous cooling state (ICS) [3], where particle-poor and particle-rich domains emerge. Time scale for such a crossover gets shorter with the decrease of e. These domains or clusters may grow for indefinite period of time if the system size is thermodynamically large [22]. Thus, even if not a phase transition, it is quite natural to study clustering phenomena in these models from the perspectives of phase transition kinetics [23–25].

In problems of phase transitions [23], having been quenched from a homogeneous state to a state inside the miscibility gap, as a system proceeds towards the new equilibrium, one is interested in understanding the domain pattern [23], its growth [23] and aging [25]. Typically, a pattern is characterized via the two-point equal-time correlation function [23] C, which, in an isotropic situation, is calculated as [23] (r being the scalar distance between two points)

$$C(r,t) = \langle \psi(\vec{r},t)\psi(\vec{0},t)\rangle - \langle \psi(\vec{r},t)\rangle\langle \psi(\vec{0},t)\rangle, \tag{3.1}$$

where ψ is a space ($\vec{r}$) and time (t) dependent order parameter. For a vapor-liquid transition, which granular systems have resemblance with, ψ is related to the local density. For a self-similar pattern, $C(r,t)$ and its Fourier transform, $S(k,t)$ (k being the magnitude of the wave vector), the structure factor,

obey the scaling properties [23]

$$C(r,t) \equiv \tilde{C}(r/\ell),\ S(k,t) \equiv \ell^d \tilde{S}(k\ell), \tag{3.2}$$

where $\tilde{C}$ and $\tilde{S}$ are time-independent master functions [23]. These dynamic scalings reflect the fact that structures at two different times are similar, apart from a change in length scale ℓ, the average size of domains, that grows with time as [23]

$$\ell \sim t^{\alpha}. \tag{3.3}$$

For the study of aging property, one considers a two-time autocorrelation function [26, 27]

$$C_{\rm ag}(t,t_w) = \langle \psi(\vec{r},t)\psi(\vec{r},t_w)\rangle - \langle \psi(\vec{r},t)\rangle\langle \psi(\vec{r},t_w)\rangle, \tag{3.4}$$

where t_w ($\leq t$) is referred to as the waiting time or age of the system [25]. Unlike the equilibrium situation, the decay of $C_{\rm ag}(t,t_w)$ gets slower with the increase of t_w, when plotted vs $t - t_w$, since there is no time translation invariance in an evolving system. In kinetics of phase transitions, $C_{\rm ag}(t,t_w)$ follows a scaling relation [25, 26]

$$C_{\rm ag}(t,t_w) \equiv \tilde{C}_{\rm ag}(\ell/\ell_w), \tag{3.5}$$

where ℓ_w is the domain size at t_w and $\tilde{C}_{\rm ag}$ is a master function [25] that typically exhibits power-law decay as a function of ℓ/ℓ_w. Examination of these facts for systems as nontrivial as those consisting of inelastic particles

should be of genuine interest, to gain an universal picture of the concepts of nonequilibrium statistical mechanics, since these systems continuously dissipate kinetic energy.

Like in phase transitions, in the case of inelastic particles also, considered to be hard spheres in many theoretical studies, power-law growths have been observed [5, 8–11, 13]. In phase transitions, ℓ can be connected to the interfacial energy. Even though a connection with interfacial energy does not exist here, for the BAM the average cluster mass (m) has been related with the average kinetic energy (E) [21]. In many problems of coarsening, the growth exponent α depends upon the transport mechanism and system dimensions [23]. In the case of BAM also time-dependence of m has been predicted to have strong influence from dimension [21]. Despite these advancements, many questions remain open, including the issue related to the equivalence between BAM and GGM.

For the growth of m ($\sim \ell^d$, d being the system dimension) via the ballistic aggregation mechanism, a scaling theory predicts [21]

$$m \sim \frac{1}{E} \sim t^{\frac{2d}{d+2}}. \tag{3.6}$$

In $d = 1$, this has been confirmed via simulations, for both BAM and GGM cases [6, 7, 10, 11, 21]. In higher dimensions, on the other hand, the status is not satisfactory with respect to the equivalence between the two models. Even though the time-dependence of E is reported to be consistent with Eq. (3.6), for the growth of m in GGM there exists evidence for dimension independence [13]. This raises question whether the complete validity of Eq.

(3.6) in $d = 1$, for both BAM and GGM cases, is accidental. Thus, even in this dimension, direct confirmation of the mechanism for GGM is essential, to draw a conclusion on the equivalence [6] between the two models.

Furthermore, while some aspects of kinetics have been studied, aging property [25–32] of the density field and its connection to pattern and growth did not receive attention for these models, though important [33]. To the best of our knowledge, there exists only one study [34] that addresses scaling property of the two-time correlation function in the granular-matter context. This, however, considers aging in a different quantity, for a model different from the one considered here.

Here note that various scaling properties that have been established with respect to aging are related to approach of a far-from-equilibrium system to an equilibrium state, like in phase transitions. Given that systems of inelastically colliding particles are always out of equilibrium, examination of the validity of these properties in such systems should be of fundamental importance. If scaling exists, it is of interest then to compare the scaling functions associated with GGM and BAM cases, to establish a more complete equivalence.

In this chapter, our primary objective is to identify the scaling property related to aging in ballistic aggregation in one dimension. For this purpose, it has been shown, via a state-of-the-art dynamic renormalization group theoretical method of analysis [35], that the growth law for one-dimensional GGM in ICS is same as that for the BAM. In this dimension, we also directly show that the mechanism of aggregation in GGM is indeed ballistic. These, along with our results on aging, establish a more complete equivalence between

GGM and BAM in $d = 1$. We show that, the above scaling property of the autocorrelation function holds for both the models as long as the growth occurs via ballistic aggregation. These results are discussed with reference to the picture in standard phase transitions. The functional forms of $\tilde{C}_{\rm ag}$ have been estimated and understood via analyses of the structure [28].

We organize the rest of the chapter as follows. We provide details of the models and methods in Section 3.2. Results are presented in Section 3.3. Finally, Section 3.4 concludes the chapter.

3.2 Model and Methods

For the GGM we use the following update rule for (hard) particle velocities. The post and pre-collisional velocities of the particles are related via [3,36,37]

$$\vec{v}_i{}' = \vec{v}_i - \Big(\frac{1+e}{2}\Big)[\hat{n}\cdot(\vec{v}_i - \vec{v}_j)]\hat{n}, \tag{3.7}$$

$$\vec{v}_j{}' = \vec{v}_j - \Big(\frac{1+e}{2}\Big)[\hat{n}\cdot(\vec{v}_j - \vec{v}_i)]\hat{n}, \tag{3.8}$$

where $(')$ stands for the post event, $\vec{v}_i$ and $\vec{v}_j$ are velocities of particles i and j, respectively, and $\hat{n}$ is the unit vector in the direction of the relative position of the particles i and j. With this model, we perform event driven [36, 37] molecular dynamics simulations where an event is a collision. In this method, between two collisions, since there are no inter-particle interaction or external potential, particles move with constant velocities till the next collision, which is appropriately identified after every event.

For the BAM case [21], following every collision, mass of the product

particle increases, which was appropriately incorporated in the collision rule (see next chapter for details). Typically, in such event driven simulations, time is specified in two different ways, viz., by using the number of collisions per particle (τ) and actual time (t), the latter being calculated by keeping track of the free time between successive collisions. In this work, we will use the latter.

A serious problem faced in event driven simulations of the GGM is the inelastic collapse [38]. This phenomenon is related to the fact that for very low values of the relative velocity collisions keep happening only among a small group of neighboring particles, thereby essentially providing no progress in time. The problem is more severe in lower dimension, since fewer particles are needed to satisfy the corresponding condition. There can be two ways to avoid such singularity in collision numbers, viz., setting the value of e, for the collision partners with relative velocities less than a threshold value δ, to either 0 or 1. We adopt the latter [6, 38–40] given that in the experimental situation value of e increases with the decrease of the relative velocity [10–12, 41].

All our results will be presented from simulations with periodic boundary conditions and density of particles starting with $\rho = N/L = 0.30$, N being the number of particles and L the linear dimension of the system.

In the case of GGM, clusters were appropriately identified as regions with density above a critical value ρ_c ($= 0.5$). Higher values of ρ_c also provide similar results, deviating from each other only by a multiplicative factor. The end to end distance for a cluster along any direction provides a cluster length (ℓ_c). In $d = 1$, the number of particles within these boundaries is the

mass (m_c) of that cluster. For the BAM case, information on the cluster length and mass are contained in the particle radius. The average values of the above mentioned quantities were obtained from the first moments of the corresponding distributions. Ideally, ℓ should equal m in $d = 1$, but in the case of GGM it takes time for a cluster to settle down to a particular density value. Thus, equality holds only at late time. For the calculation of the correlation functions and structure factors [8, 9], the order-parameter ψ at a point was assigned a value $+1$ if the density (calculated by counting the number of nearest neighbors) there was higher than ρ_c, else -1. The average length can be calculated from the scaling property of $C(r, t)$ or $S(k, t)$ as well.

3.3 Results

As mentioned above, in this dimension, via accurate analyses, we first confirm an equivalence between the BAM and GGM, with respect to the energy decay, growth law and mechanism. These results are followed by those for aging property. As we will see, the latter, in addition to being of separate importance, will make the above mentioned equivalence more complete.

In Fig. 3.1 we show the decay of energy, for both GGM and BAM, as a function of time, on a log-log scale. The BAM results, for energy and mass (see Fig. 3.2(a)), are already understood. However, we present these for the sake of completeness, as well as to facilitate the discussion that follows. For the GGM, results for a few different cut-off values of the relative velocity

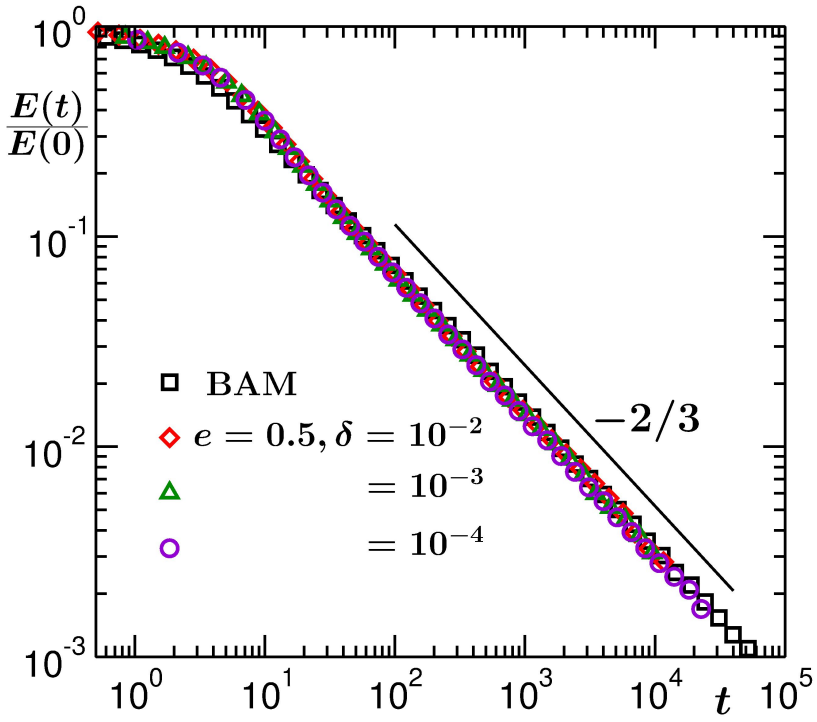

Figure 3.1: Plots of energy decay as a function of time, for BAM and GGM cases in $d = 1$. For the GGM case, value of e has been fixed to 0.5 and results for several choices of δ are presented. The starting number of particles for BAM and GGM are respectively 160000 and 10000. The solid line is a power-law with exponent $-2/3$.

are shown. For this case, in this dimension, all our results correspond to $e = 0.5$. After a minor disagreement over brief initial period (corresponding to HCS in the GGM), all the results are consistent with each other, exhibiting power-law behavior over several decades in time, with the expected exponent $-2/3$.

In Fig. 3.2(a) we plot m as a function of t, on a log-log scale, for the BAM case. This shows a power-law growth with exponent $2/3$, validating Eq. (3.6). The m vs t results for the GGM are shown in Fig. 3.2(b), for the same values of δ as in Fig. 3.1. An interesting observation here is

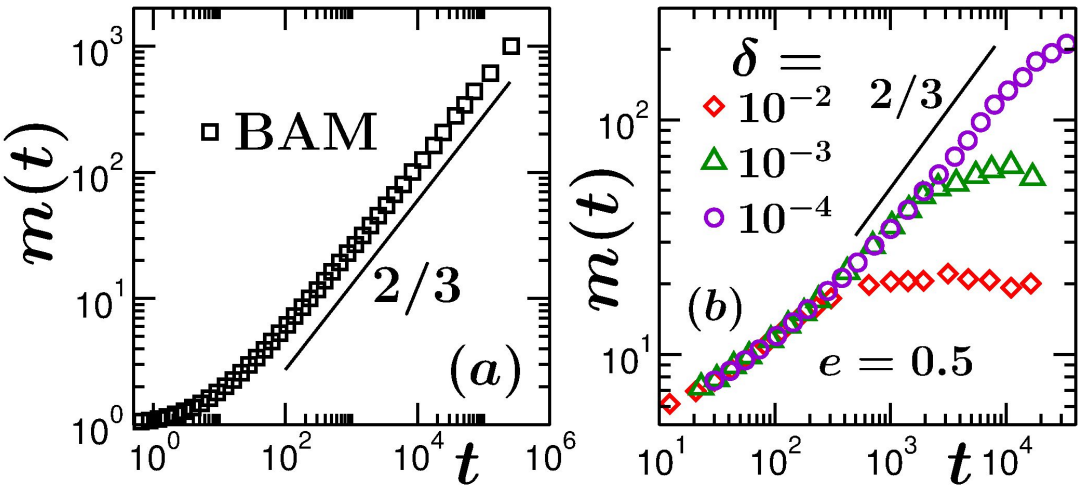

Figure 3.2: (a) Average cluster mass, m, is plotted vs time, for BAM. (b) Same as (a) but for GGM with multiple values of δ as in Fig. 3.1. The solid lines in these figures correspond to power-laws, exponents being mentioned. The starting number of particles for BAM and GGM are same as the previous figure. Rest of the simulations for GGM are done with 20000 particles and $\delta = 5 \times 10^{-5}$. All results are for $d = 1$.

that, for the GGM, even though the energy decay follows $t^{-2/3}$ behavior till late for all values of δ, the picture is different for the growth of mass. The growth stops earlier for larger value of δ, even though energy decay continues with the predicted functional form. This should not be a finite-size effect, since the saturation is δ dependent. Rather, this has connection with late time declusterization phenomena [10, 11] that has been observed for relative velocity dependent e. Furthermore, the m vs t data, particularly for larger values of δ, do not appear consistent with the exponent 2/3. This discrepancy can possibly be due to the presence of substantial length at the beginning of the scaling regime. In such a situation, confirmation of an exponent from a log-log plot requires data over several decades in time [42]. In absence of that, alternative accurate method of analysis is needed to obtain correct value of

the exponent [35, 42, 43]. In any case, the observations above, with respect to the saturation of m, further justify the need for direct identification of the growth mechanism. Before moving to that we will accurately quantify the growth law. For this purpose, in the following we will work with the length rather than the mass, since for the aging property we will need this latter quantity. Unless otherwise mentioned, all our results for the GGM, from here on, will be presented for $\delta = 5 \times 10^{-5}$.

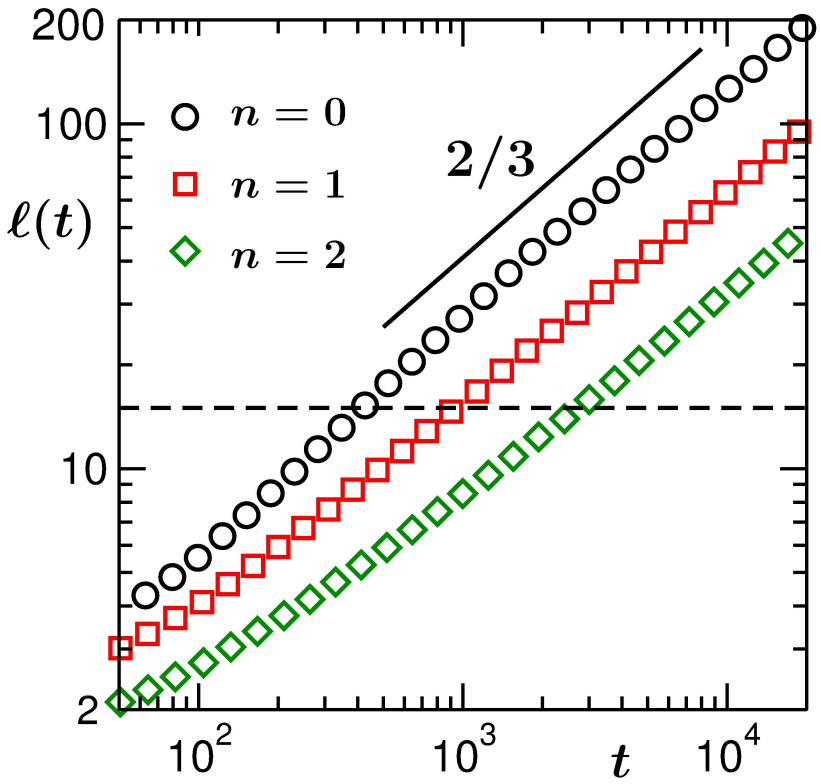

Figure 3.3: Plots of ℓ vs t for three different stages of renormalization. The dashed horizontal line is for the extraction of times for the same length at different levels of renormalization. The solid line represents a power-law with exponent 2/3. All results correspond to the GGM in $d = 1$.

We use a renormalization-group method of analysis [35] for the accurate

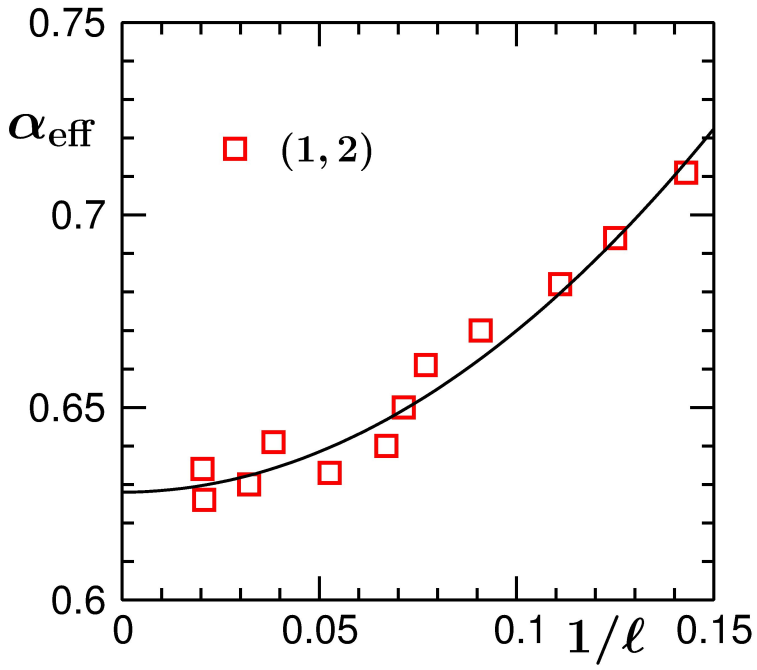

Figure 3.4: Plot of the effective exponent, obtained via the renormalization-group analysis using the combination $n = 1$ and 2, vs the inverse of the original length. The solid line is a quadratic fit to the simulation data. All results correspond to the GGM in $d = 1$.

quantification of the growth for the GGM. We consider a Kadanoff type block transformation [44] of the order parameter. For this purpose, as mentioned in the context of calculation of the correlation functions, we have mapped the density field to $\psi = \pm 1$. The blocking exercise then becomes similar to that for the Ising model [23]. At successive iterations of the transformation, order parameter over a length of b particle diameters is averaged over and represented by a single point, reducing the system size by a factor b, for which we choose the value 2. Thus, a particular value of ℓ in different levels (n) of renormalization will be obtained at different times, viz., for $n = p$ and

$p+1$ one writes [35]

$$\ell(p,t) = \ell(p+1, b^{1/\alpha}t). \tag{3.9}$$

This is demonstrated in Fig. 3.3, where, in addition to the original data ($n = 0$), we have presented length vs time plots for renormalizations with $n = 1$ and 2. The horizontal line in this figure is related to the estimation of times for the same length scale for different values of n. From the shifting or scaling of time, due to the scaling in length, the growth exponent can be estimated. However, because of technical reasons the true exponent will be realized only in the limit $\ell \to \infty$ and for finite time we will denote it by $\alpha_{\rm eff}$.

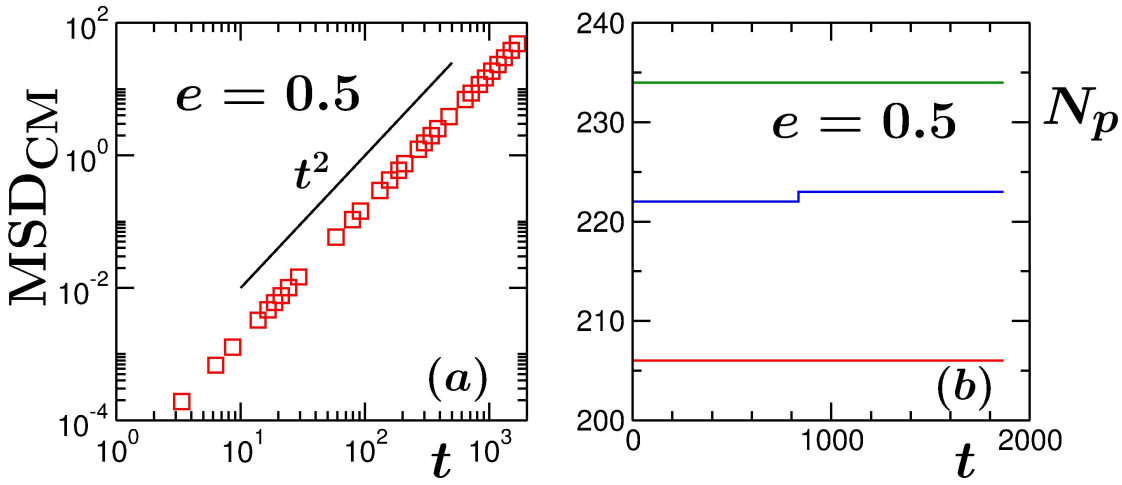

Figure 3.5: (a) Mean-squared-displacement of the centre of mass of a typical cluster, for GGM, is plotted vs time, on a log-log scale. The solid line corresponds to ballistic motion. (b) Number of particles in a few different clusters, for GGM, are plotted vs translated time, before they undergo collisions. All results are from $d = 1$.

Estimated values of $\alpha_{\rm eff}$, from the combination involving $n = 1$ and 2, are presented in Fig. 3.4, vs $1/\ell$, which indeed have time dependence [45]. The time dependence is due to the nonscaling early time transient and presence

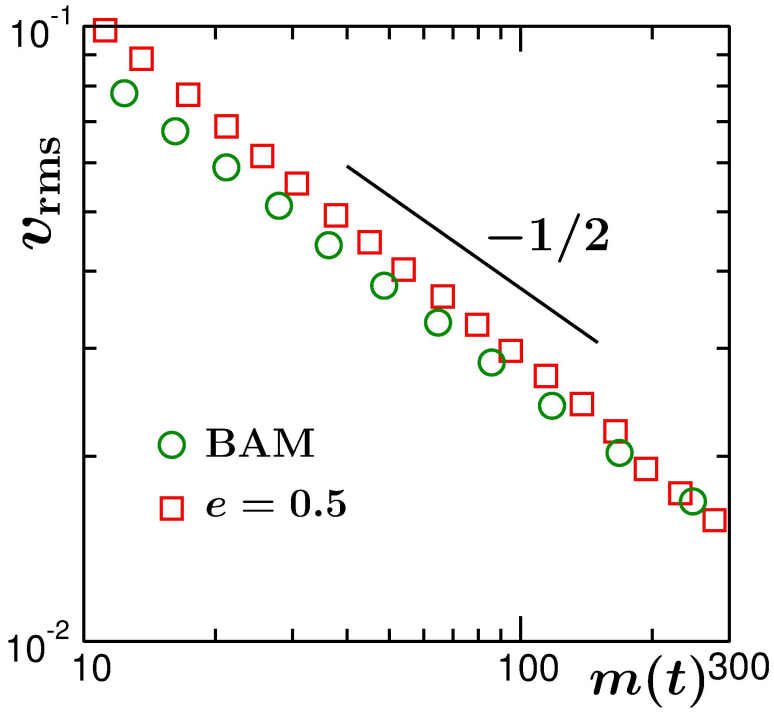

Figure 3.6: Root-mean-squared velocity of the clusters are plotted vs m, for both BAM and GGM. The solid line is a power-law decay, exponent being mentioned. All results are from $d = 1$.

of a large off-set when scaling is reached. When such time dependence exits, as already stated, α should be estimated from the convergence of the data in the $\ell \to \infty$ limit. By looking at the trend of the data set, we have fitted it to the form $\alpha_{\rm eff} = \alpha + a/\ell^2$, that provides convergence to $\alpha \simeq 0.63$. This is very close to the ballistic aggregation [21] value 2/3. To check, whether this minor deviation of the simulation data from the theoretical expectation is a true fact, one needs to study other values of e as well. Such a systematic study we leave out for a future work. The deviation could be due to the finite-size effects and δ-dependent saturation.

Having identified the growth exponent for the GGM, we, in Fig. 3.5,

identify the mechanism. The growth exponent 2/3 can be obtained from a (nonequilibrium) kinetic theory for ballistic aggregation [21, 46, 47]. As the name suggests, the growth occurs in this mechanism due to collisions among clusters and between collisions the clusters move with constant velocities. Since the particles in our models are noninteracting, it is understandable that the clusters in the BAM will move ballistically between collisions. In the GGM case also, following more and more collisions, particles within a cluster may move parallel to each other, providing collective directed motion. However, when a cluster moves through a vapor region, growth in this case may occur due to random deposition of particles on them. It is then necessary to check if at late enough time the motion of the clusters, during the interval between two big mass enhancing collisions, are ballistic and during that period the growth of the clusters is negligible.

In part (a) of Fig. 3.5 we show the mean-squared-displacement of the centre of mass (CM), $\mathrm{MSD}_{\mathrm{CM}}$, of a cluster, calculated as [48]

$$\mathrm{MSD}_{\mathrm{CM}} = \langle |\vec{R}_{\mathrm{CM}}(t) - \vec{R}_{\mathrm{CM}}(0)|^2 \rangle, \tag{3.10}$$

$\vec{R}_{\mathrm{CM}}$ being the time-dependent location of the CM of the cluster, for GGM, over an extended period of time, before it undergoes a collision with another cluster. On the log-log scale, a very robust t^2 behavior is visible, confirming ballistic motion [48]. In Fig. 3.5(b) we show number of particles in a few clusters, as a function of translated time. The constant values over long time confirm that the mechanism of growth in the GGM is indeed ballistic aggregation.

The mass part of Eq. (3.6) can be derived from [21, 46, 47]

$$\frac{dn_c}{dt} = -\ell^{d-1} v_{\rm rms} n_c^2, \tag{3.11}$$

where n_c is the cluster density and $v_{\rm rms}$ is the root-mean-squared velocity of the clusters. An exponent 2/3 requires $v_{\rm rms} \sim m^{-1/2}$, an outcome for uncorrelated cluster motion [47], can be realized for Boltzmann distribution of cluster kinetic energies [15, 46]. In Fig. 3.6, we plot $v_{\rm rms}$ vs m, for BAM as well as GGM, both of which show reasonable consistency with the requirement. Here note that at low values of particle density, strong velocity correlation is expected to appear, since the collisions are less random, leading to deviation from such Boltzmann distribution picture. At high density, the collisions are random and such a picture is a good approximation. The reasonable validity of $v_{\rm rms}$ with the $m^{-1/2}$ form, that is observed, should, however, be checked for other values of e for the GGM to see if there exists complex density dependence. Any deviation, though does not invalidate the ballistic aggregation, can bring in change in the growth exponent. Here, as a passing remark, we mention that for the ballistic aggregation of fractal clusters (with fractal dimension d_f) in d dimensions, with $v_{\rm rms} \sim m^{-\gamma}$, the exponent for the time dependence of mass will have the form

$$\zeta = \frac{d_f}{1 - d + d_f(1+\gamma)}, \tag{3.12}$$

if Eq. (3.11) is a good starting point. Given that for the present problem $d_f = d = 1$ and our estimate of γ for the GGM is 0.55, $\zeta = 0.645$, in

agreement with the conclusion from Fig. 3.4. We obtain similar result for ζ via analysis of the instantaneous exponent. For $d = 2$, in the next chapter, we will adopt this method, instead of the renormalization group.

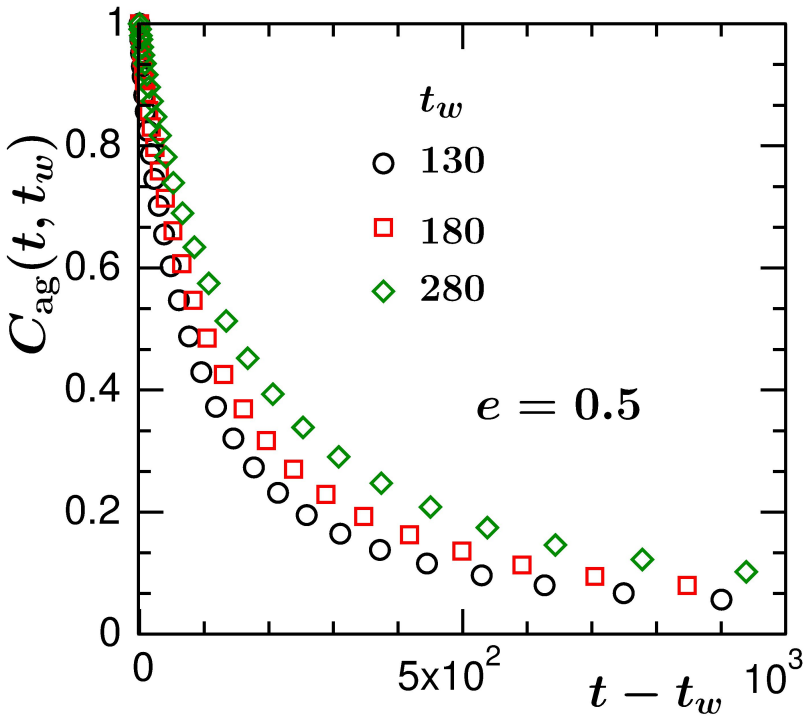

Figure 3.7: Plots of the autocorrelation function, vs $(t - t_w)$, for three different choices of t_w, as mentioned, for the $d = 1$ GGM.

Next we present results for the aging property [25, 26]. We stress again, not only in the granular matter context, to the best of our knowledge, aging has not been studied previously for ballistic aggregation in any other system. In Fig. 3.7 we plot $C_{\rm ag}(t, t_w)$ vs $t - t_w$, for a few different values of t_w, for the GGM. As expected, no time translation invariance is noticed which is an equilibrium [48] (or steady-state) property. Sticky gas (BAM) results are similar (not shown). In Fig. 3.8 we show $C_{\rm ag}(t, t_w)$ vs ℓ/ℓ_w, on a log-log scale, for the GGM. Nice collapse of data from all chosen values of t_w are seen, as

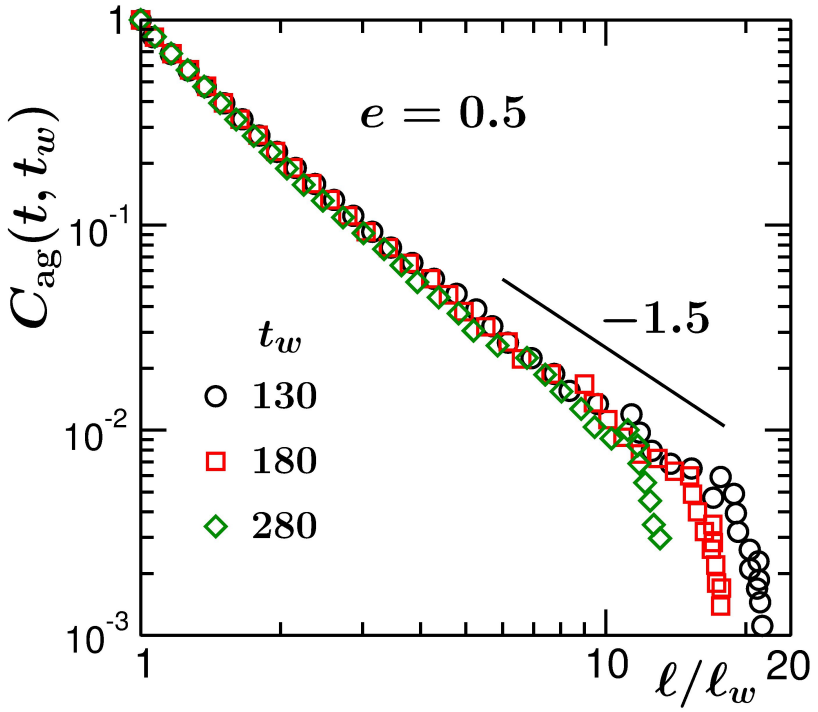

Figure 3.8: Log-log plots of $C_{\rm ag}(t, t_w)$ vs ℓ/ℓ_w, using the data sets in Fig. 3.7. The solid line shows a power-law decay with exponent $\lambda = 1.5$.

in kinetics of phase transition. Deviations of the data sets from the master curve, appearing earlier for larger values of t_w, are due to finite-size effects [49]. In phase transitions, the system moves towards an equilibrium state. Interestingly, similar scaling is observed in the present case, despite the fact that the system is continuously dissipating kinetic energy. Corresponding plots for the BAM are shown in Figure 3.9. Again, very good quality collapse is observed. In both the cases, power-law decays [26]

$$\tilde{C}_{\rm ag} \sim x^{-\lambda};\ x = \ell/\ell_w, \tag{3.13}$$

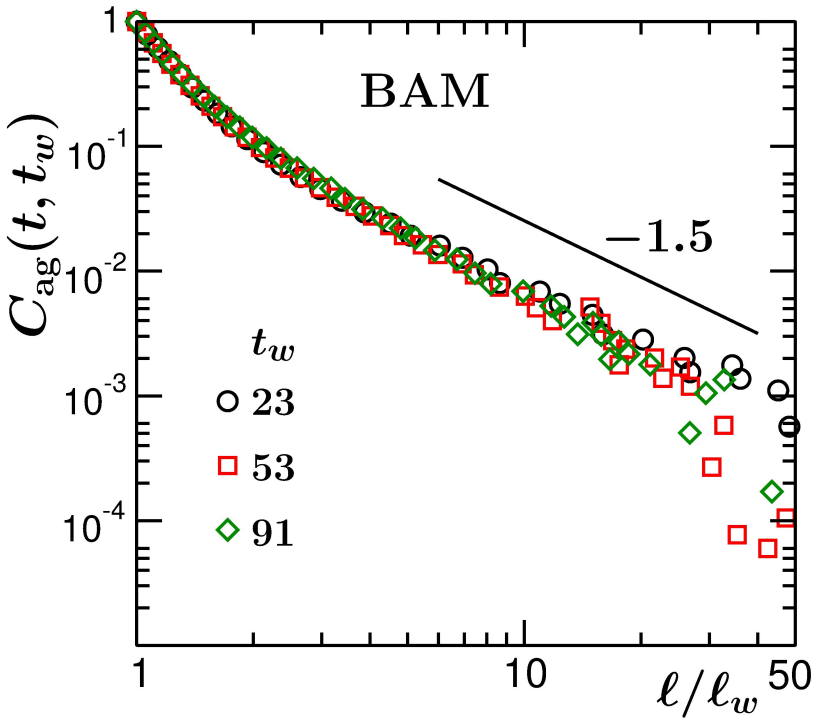

Figure 3.9: Same as Fig. 3.8 but for the $d = 1$ BAM case. The values of t_w are mentioned on the figure. The solid line represents power-law decay with an exponent $\lambda = 1.5$.

of the scaling function are observed for $x >> 1$, the exponent value, mentioned on the figures, being same (or close to each other) in the two cases. This further confirms the equivalence between the BAM and the GGM.

In phase transitions, there exists a lower bound [26, 28] for the value of λ, viz.,

$$\lambda \geq \frac{d+\beta}{2}, \tag{3.14}$$

where β is the exponent for the small wave number power-law behavior of the structure factor:

$$S(k,t) \sim k^{\beta}. \tag{3.15}$$

The bound in (3.14) was derived by Yeung, Rao and Desai (YRD) [28]. For this purpose, starting from the structure factors at times t and t_w, YRD obtained

$$C_{\rm ag}(t,t_w) \leq \ell^{d/2} \int_0^{2\pi/\ell} dk k^{d-1} [S(k,t_w)\tilde{S}(k\ell)]^{1/2}. \qquad (3.16)$$

The bound follows when Eq. (3.15), for the small k behavior of $S(k,t_w)$, is used in the above expression. To check whether λ in the present case also obeys the bound (3.14), we analyze the structure.

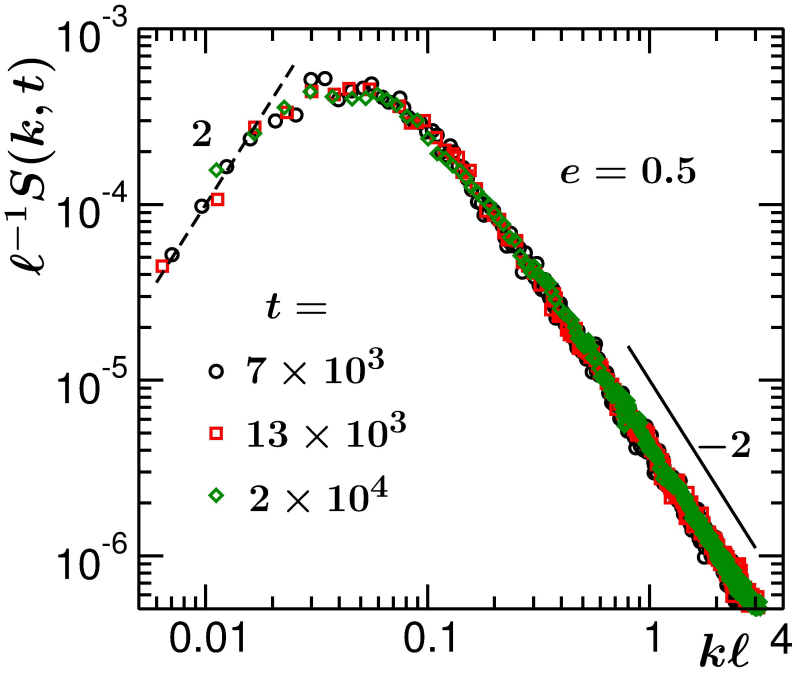

Figure 3.10: Scaling plot of the equal-time structure factors for the $d = 1$ GGM. Here we have shown collapse of $S(k,t)/\ell(t)$, when plotted as a function of $y = k\ell(t)$, using data from three different times. The dashed and the solid lines correspond to $\sim y^2$ and $\sim y^{-2}$, respectively.

In Fig. 3.10 we show the scaling plot of the structure factors, viz., we plot $\ell^{-1}S(k,t)$ vs $k\ell$, for the GGM. Nice collapse of data from all different times imply structural self-similarity [23]. The consistency of the long wave-vector

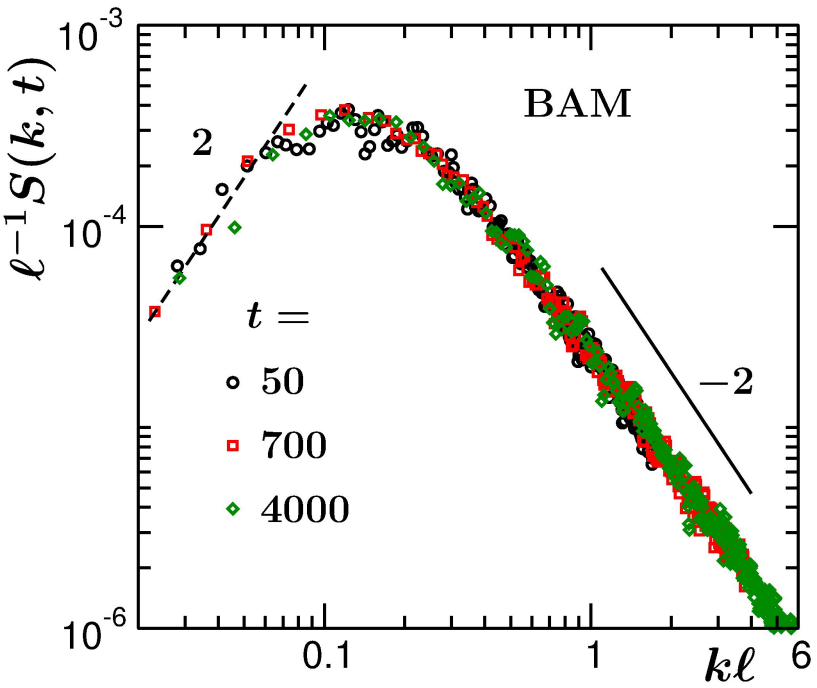

Figure 3.11: Scaling plot of the equal-time structure factors for the $d = 1$ BAM. Here we have shown collapse of $S(k,t)/\ell(t)$, when plotted as a function of $y = k\ell(t)$, using data from three different times. The dashed and the solid lines correspond to $\sim y^2$ and $\sim y^{-2}$, respectively.

data with k^{-2} imply validity of the Porod law [23, 50, 51]

$$S(k,t) \sim k^{-(d+1)}, \tag{3.17}$$

a consequence of short-distance singularity in $C(r,t)$, due to scattering from sharp interfaces. The small k behavior appears consistent with $\beta = 2$. The behavior for the BAM structure factor, shown in the inset of Fig. 3.11, is very similar. This value of β was predicted [52] for coarsening in Ising-like systems in $d = 1$. The number is different for higher dimensions [53]. The dimension dependent values of β can be obtained [54] from dynamical equation of structure factor (starting from the Cahn-Hilliard equation [54])

in k space, by arguing that for $d = 1$ thermal energy is dominant, whereas for $d > 1$ interfacial free energy takes over. Agreement of our results with such prediction is very interesting. The information on the consistency, for both short and long range structures, between GGM and BAM, that these data sets convey, is further supportive of the presence of sharp interfaces, compact clusters and ballistic aggregation in the GGM.

The observed value of β sets the lower bound for λ at 1.5. Thus, this bound is obeyed in both the cases and the actual values of the aging exponent in fact are very close to this lower bound. Here note that recently violation of such power-law decay of the autocorrelation function was demonstrated [31,32] for advective transport in fluid phase separations. Even for conserved order parameter with diffusive dynamics, though power-law, the decays in $d > 1$ are observed [55] to be significantly faster than the ones provided by the the (lower) bound (3.14). However, in the latter example, agreement with the bound gets better as the dimension decreases [55]. With the lowering of d, particularly for Ising kinetics, motion of the boundaries of domains (during no growth periods) gets restricted. However, since the mechanism is ballistic in the present problem, boundary movement does exist even during no growth period, though decreases with the increase of mass, thus time. Nevertheless, the agreement with the lower bound is rather close.

3.4 Conclusion

We have studied the kinetics of cluster growth in an one-dimensional granular gas (GGM) [3]. The results are compared with those from the ballistic

aggregation model (BAM) [21]. It is shown that the average size of the clusters grows as power-law with time. Via a dynamic renormalization group theoretical method of analysis [35], the exponent has been identified to be approximately 2/3, in agreement with that for the BAM. The growth is inversely proportional to the energy decay, showing consistency with the scaling predictions of Carnevale et al. [21] for ballistic aggregation. The mechanism has been identified to be indeed ballistic, by calculating the mean-squared-displacements [48] of the centres of mass of clusters before they undergo collisions.

To avoid the inelastic collapse, for the granular gas we have used a cut-off δ. For relative velocities $< \delta$, the value of e was set to unity for the colliding partners [6]. We observed saturation in the growth of mass, earlier for larger values of δ. Interestingly, in such saturation regime also the energy decay continued to follow the theoretical scaling form $t^{-2/3}$. This calls for further investigation.

This is a first study for the aging property [25,26] in ballistic aggregation. It is shown, like in kinetics of phase transitions, the order-parameter autocorrelation function scales with ℓ/ℓ_w. The scaling function has been identified to be a power-law. The corresponding exponent has been estimated and discussed in the context of structural property. It is shown that the exponent obeys a lower bound [28] predicted for kinetics of phase transition where systems move towards a new equilibrium. The similar values of the exponent obtained for the granular and the BAM, further suggests close equivalence between the dynamics in the two cases, in this dimension.

Bibliography

[1] I. S. Aranson and L. S. Tsimring Rev. Mod. Phys. **78**, 641 (2006).

[2] N.V. Brilliantov and T. Poeschel *Kinetic Theory of Granular Gases* (Oxford University Press, Oxford, 2004).

[3] I. Goldhirsch and G. Zanetti, Phys. Rev. Lett. **70**, 1619 (1993).

[4] R. Brito and M. H. Ernst, Europhys. Lett. **43**, 497 (1998).

[5] S. Luding and H.J. Herrmann, Chaos **9**, 673 (1999).

[6] E. Ben-Naim, S.Y. Chen, G.D. Doolan and S. Render, Phys. Rev. Lett. **83**, 4069 (1999).

[7] X. Nie, E. Ben-Naim and S. Chen, Phys. Rev. Lett. **89**, 204301 (2002).

[8] S.K. Das and S. Puri, Europhys. Lett. **61**, 749 (2003).

[9] S.K. Das and S. Puri, Phys. Rev. E **68**, 011302 (2003).

[10] M. Shinde, D. Das and R. Rajesh, Phys. Rev. Lett. **99**, 234505 (2007).

[11] M. Shinde, D. Das and R. Rajesh, Phys. Rev. E **84**, 031310 (2011).

[12] A. Bodrova, A.K. Dubey, S. Puri and N.V. Brilliantov, Phys. Rev. Lett. **109**, 178001 (2012).

[13] S. Paul and S.K. Das, Europhys. Lett. **108**, 66001 (2014).

[14] E. Trizac and J.-P. Hansen, Phys. Rev. Lett. **74**, 4114 (1995).

[15] E. Trizac and J.-P. Hansen, J. Stat. Phys. **82**, 1345 (1996).

[16] E. Trizac and P.L. Krapivsky, Phys. Rev. Lett. **9**1, 218302 (2003).

[17] A. Lipowski, D. Lipowska and A. L. Ferreira, Phys. Rev. E **73**, 032102 (2006).

[18] P. K. Haff, J. Fluid Mech. **134**, 401 (1983).

[19] O. Herbst, R. Cafiero, A. Zippelius, H. J. Herrmann and S. Luding, Phys. of Fluids **17**, 107102 (2005).

[20] S. Ulrich and A. Zippelius, Phys. Rev. Lett. **109**, 16601 (2012).

[21] G.F. Carnevale, Y. Pomeau and W.R. Young, Phys. Rev. Lett. **64**, 2913 (1990).

[22] M. Hummel and M.G. Mazza, Phys. Rev. E **93**, 022905 (2016).

[23] A.J. Bray, Adv. Phys. **51:2**, 481 (2002).

[24] A. Onuki, *Phase Transition Dynamics* (Cambridge University Press, Cambridge, 2002).

[25] M. Zannetti, in *Kinetics of Phase Transitions*, ed. S. Puri S. and V. Wadhawan (Boca Raton: CRC Press, 2009).

[26] D.S. Fisher and D.A. Huse, Phys. Rev. B **38**, 373 (1988).

[27] F. Liu and G.F. Mazenko, Phys. Rev. B **44**, 9185 (1991).

[28] C. Yeung, M. Rao and R.C. Desai, Phys. Rev. E **53**, 3073 (1996).

[29] M. Henkel, A. Picone and M. Pleimling, Europhys. Lett. **68**, 191 (2004).

[30] F. Corberi, E. Lippiello, A. Mukherjee, S. Puri and M. Zannetti, Phys. Rev. E **85**, 021141 (2012).

[31] S. Ahmad, F. Corberi, S.K. Das, E. Lippiello, S. Puri and M. Zannetti, Phys. Rev. E **86**, 061129 (2012).

[32] S. Majumder and S.K. Das, Phys. Rev. Lett. **111**, 055503 (2013).

[33] M. Hummel, J.P.D. Clewett and M.G. Mazza, Europhys. Lett. **114**, 10002 (2016).

[34] A. Baldassari, U.M.B. Marconi and A. Puglisi,Phys. Rev. E **65**, 051301 (2002).

[35] C. Roland and M. Grant, Phys. Rev. B **41**, 4663 (1990).

[36] M.P. Allen and D.J. Tildesley, *Computer Simulation of Liquids* (Clarendon, Oxford, 1987).

[37] D.C. Rapaport, *The Art of Molecular Dynamics Simulations* (Cambridge University Press, Cambridge, England, 2004).

[38] S. McNamara and W.R. Young, Phys. Rev. E **50**, R28 (1994).

[39] C.S. Campbell, Annu. Rev. Fluid Mech. **22**, 57 (1990).

[40] S. Luding and S. McNamara, Gran. Matter **1**, 113 (1998).

[41] C.V. Raman, Phys. Rev. **12**, 442 (1918).

[42] S. Majumder and S.K. Das, Phys. Rev. E **81**, 050102 (2010).

[43] D.A. Huse, Phys. Rev. B **34**, 7845 (1986).

[44] N. Goldenfeld, *Lectures on Phase Transitions and the Renormalization Group* (Addison-Wesley, 1992).

[45] S.K. Das and S. Puri, Phys. Rev. E **65**, 26141 (2002).

[46] J. Midya and S.K. Das, Phys. Rev. Lett. **118**, 165701 (2017).

[47] S.N. Pathak, D. Das and R. Rajesh, Europhys. Lett. **107**, 44001 (2014).

[48] J.-P. Hansen and I.R. McDonald, *Theory of Simple Liquids* (Academic Press, London, 2008).

[49] J. Midya, S. Majumder and S.K. Das, J. Phys.: Condens. Matter **26**, 452202 (2014).

[50] G. Porod, Small-Angle X-Ray Scattering, eds. O. Glatter and O. Kratky (Academic Press, New York, 1982).

[51] Y. Oono and S. Puri, Mod. Phys. Lett. B **2**, 861 (1988).

[52] S.N. Majumdar, D.A. Huse and B.D. Lubachevsky, Phys. Rev. Lett. **73**, 182 (1994).

[53] C. Yeung, Phys. Rev. Lett. **61**, 1135 (1988).

[54] H. Furukawa, Phys. Rev. B **40**, 2341 (1989).

[55] J. Midya, S. Majumder and S.K. Das, Phys. Rev. E **92**, 022124 (2015).

Chapter 4

Cluster growth, structure and aging in ballistic aggregation of inelastic particles in two dimensions

4.1 Introduction

The models of freely cooling granular gas (GGM) and ballistic aggregation (BAM) are relevant in many physical situations, including clustering in cosmic dust [1–22]. In the GGM [6] the particles possess coefficient of restitution (e) falling in the range $(0, 1)$. Thus, due to inelastic collisions, the system keeps losing kinetic energy, even though the mass and momentum remains conserved. Due to reduction in normal relative velocity, following every collision, particles move more and more parallel to each other. This gives rise

to clustering in the model. On the other hand, in the BAM [2], following a collision the colliding partners merge to form a larger particle with same spherical shape. There has been significant interest in understanding the time (t) dependence of (kinetic) energy (E) and average mass (m) in these models.

For the BAM, Carnevale *et al.* [2] predicted an inverse relation between these two quantities in space dimension d as

$$m \sim \frac{1}{E} \sim t^{2d/d+2}. \tag{4.1}$$

In $d = 1$, this prediction has been verified via computer simulations [2]. On the other hand, the validity of Eq. (4.1) has been questioned in higher dimensions [7]. Here note that Eq. (4.1) can be obtained from the solution of the rate equation [7, 22, 23]

$$\frac{dn_c}{dt} = -\ell^{d-1} v_{\rm rms} n_c^2, \tag{4.2}$$

n_c being the number of clusters of average size ℓ and root mean squared velocity $v_{\rm rms}$, under the assumption that the clusters form disconnected pattern and are spherical. Another requirement, of course, is that the cluster momenta are uncorrelated and scales with m as [7] $v_{\rm rms} \sim m^{-1/2}$. In addition to verifying the validity of Eq. (4.1) in BAM, there has also been interest in understanding if there exists an equivalence between the GGM and BAM.

Given that the growth scenario in these models resembles that during kinetics of phase transitions [24, 25], it is important that aging properties

[26–28] in these models are also studied. We stress here that knowledge of aging is crucial to the understanding of growth kinetics and in the literature of phase transitions important scaling relations with respect to this have been established [26–28]. One of the quantities that is studied to understand aging in nonequilibrium systems is the two-time auto-correlation function, $C_{\rm ag}(t, t_w)$, defined as [26–28]

$$C_{\rm ag}(t, t_w) = \langle \psi(\vec{r}, t)\psi(\vec{r}, t_w)\rangle - \langle \psi(\vec{r}, t)\rangle\langle \psi(\vec{r}, t_w)\rangle, \tag{4.3}$$

where ψ is a space ($\vec{r}$) and time dependent order parameter, and t_w ($\leq t$) is the waiting time or age of the evolving system. With growing age, the decay of $C_{\rm ag}$, as a function of $t - t_w$, becomes slower. This reflects the fact that an younger system relaxes faster than an older one. In phase transition dynamics it has been demonstrated that $C_{\rm ag}$ obeys the scaling relation [26–28]

$$C_{\rm ag}(t, t_w) \equiv \tilde{C}_{\rm ag}(\ell/\ell_w), \tag{4.4}$$

where ℓ and ℓ_w are average domain or cluster sizes at times t and t_w, respectively. It has also been demonstrated that in absence of hydrodynamics $\tilde{C}_{\rm ag}$ exhibits power-law [26–31] as a function of ℓ/ℓ_w.

In this chapter, our primary objective is to identify the scaling related to aging in ballistic aggregation in two dimensions. For this purpose, first we have pointed out that there exist vast difference between the structure and dynamics of GGM and the corresponding theoretical expectations for the BAM. Thus, the growth mechanism in $2D$ GGM is not ballistic aggregation

and so, the equivalence between GGM and BAM does not hold. Thus, in this dimension, for the calculation of aging property we work only with the BAM. We show that, the scaling property of the autocorrelation function holds for the BAM in $d = 2$ as well. The functional forms of $\tilde{C}_{\rm ag}$ have also been estimated and understood via the calculation of the structure factor [32]. Here, via accurate analyses, we also check the validity of a hyperscaling relation involving the decay of energy and growth of clusters for the BAM.

Rest of the chapter is organized in the following sequence. Models and methods are described in Section 4.2. Section 4.3 contains the results. Section 4.4 concludes the chapter with brief summary.

4.2 Models and Methods

For the GGM, the post and pre-collisional velocities of the colliding particles i and j are related via the equations [6, 12, 33]

$$\vec{v}_i{}' = \vec{v}_i - \Big(\frac{1+e}{2}\Big)[\hat{n}\cdot(\vec{v}_i - \vec{v}_j)]\hat{n}, \tag{4.5}$$

$$\vec{v}_j{}' = \vec{v}_j - \Big(\frac{1+e}{2}\Big)[\hat{n}\cdot(\vec{v}_j - \vec{v}_i)]\hat{n}, \tag{4.6}$$

where different symbols have already been defined in the earlier chapter. With this model, for GGM, we perform event driven [33, 34] molecular dynamics (EDMD) simulations, details of which have been given in the previous chapters.

In the BAM [2], we again emphasize that the mass of the product particle increases in every collision. The mass $m^{'}$ of the product particle following

collision between particles of masses m_i and m_j can be written as

$$m^{'} = m_i + m_j. \tag{4.7}$$

The position and velocity of this newly formed particle of larger mass (larger diameter) can be obtained from the conservation equations of centre-of-mass and the momentum, respectively, as [35]

$$m^{'}\vec{r}^{'} = m_i\vec{r}_i + m_j\vec{r}_j, \tag{4.8}$$

$$m^{'}\vec{v}^{'} = m_i\vec{v}_i + m_j\vec{v}_j, \tag{4.9}$$

where $\vec{r}_i$ and $\vec{r}_j$ are the positions and $\vec{v}_i$ and $\vec{v}_j$ are the velocities of i and j particles, respectively, before the collision. For the BAM also we perform EDMD simulations, by appropriately taking care of the change in particle diameters.

Unlike the previous chapter, for the simulations of GGM, here in $d = 2$ we set δ (the cut-off value of relative velocity to avoid inelastic collapse) to zero as the problem of inelastic collapse is less severe in higher dimensions [36] and so, significantly large cluster sizes can be accessed without encountering such collapse [19].

All our results will be presented from simulations of particles located within a square box of linear dimension L, with periodic boundary conditions applied in both the directions. The density of particles ($\rho = N/L^2$) for the BAM is 0.30 and for the GGM it is 0.37, N being the total number of particles to start with. In GGM, N remains constant, but for the BAM

value of N decreases with time. L is defined in units of the initial choice of the diameter of the particles ($\sigma = 1$). In GGM, diameter of the particles remain unchanged, whereas, for the BAM this is not valid.

In the case of GGM, clusters have been appropriately identified as regions with density above a critical value ρ_c ($= 0.5$). Higher values of ρ_c also provide similar scaling exponents for the growth. The end to end distance for a cluster along any direction provides a cluster length (ℓ_c). For the BAM case, the average mass can be directly calculated from the particle diameters. In general, m is related to ℓ as ℓ^d. But in the case of GGM it takes time for the clusters to settle down to a particular density. Thus, the aforementioned equality holds only at late time in the GGM. For the calculation of the correlation functions and structure factors [14, 15, 19], the order-parameter ψ at a lattice point (the continuum configurations were mapped onto lattice systems for the purpose of analysis) was assigned a value $+1$ or -1, depending on whether the local density (calculated by counting the number of nearest neighbors) is greater or less than the value of ρ_c, respectively.

4.3 Results

First, we briefly discuss the case of GGM, to convince ourselves that the growth in this case does not occur via the ballistic aggregation mechanism. Unlike the simulations of GGM in $d = 1$, as mentioned above, we do not use any nonzero cut-off value (δ) for the relative velocity here. This is because, for high enough value of e, in this dimension, we are able to access relevant scaling regime without encountering an inelastic collapse [19].

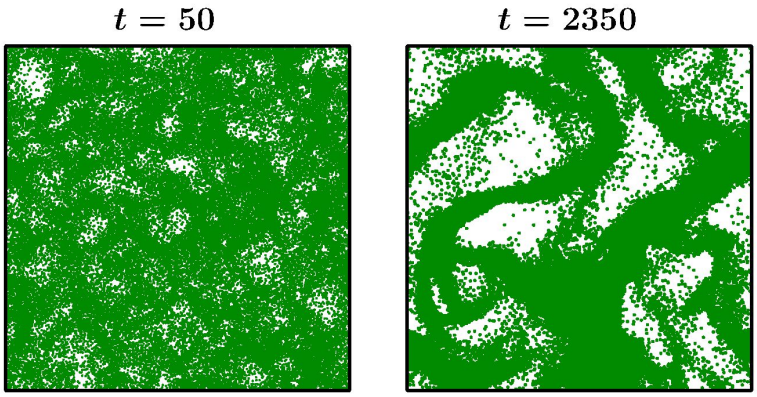

Figure 4.1: Snapshots from two different times, mentioned in the figure, during the evolution of GGM, with $e = 0.9$ in $d = 2$, are presented. The particles are marked by dots.

In Fig. 4.1 we show the evolution snapshots for the $d = 2$ GGM with $e = 0.9$. Interesting patterns, with coexisting high and low particle-density domains, are visible. A log-log plot of the decay of kinetic energy for the system, as a function of t, is presented in Fig. 4.2(a). The initial decay (corresponding to HCS) is consistent with the prediction of Haff [37], $E \sim e^{-a\tau}$ (a is a constant; analytical curve is not shown). The late time data follow a power-law in t, with exponent -1. This is, thus, consistent with the prediction of Eq. (4.1). In Fig. 4.2(b) we show a log-log plot of m vs t. The data in the late time scaling regime are seen to obey a power law, the exponent being $\lesssim 2/3$. Here we mention that in a previous work [19], via a finite-size scaling analysis, we had shown that the average domain length grows as t^{α} with $\alpha \simeq 1/3$. The conclusion from Fig. 4.2(b) is thus in agreement with this earlier study. Nevertheless, given that for the GGM there exists possibility of continuous change of density within the domains, it is instructive to calculate the average mass [19].

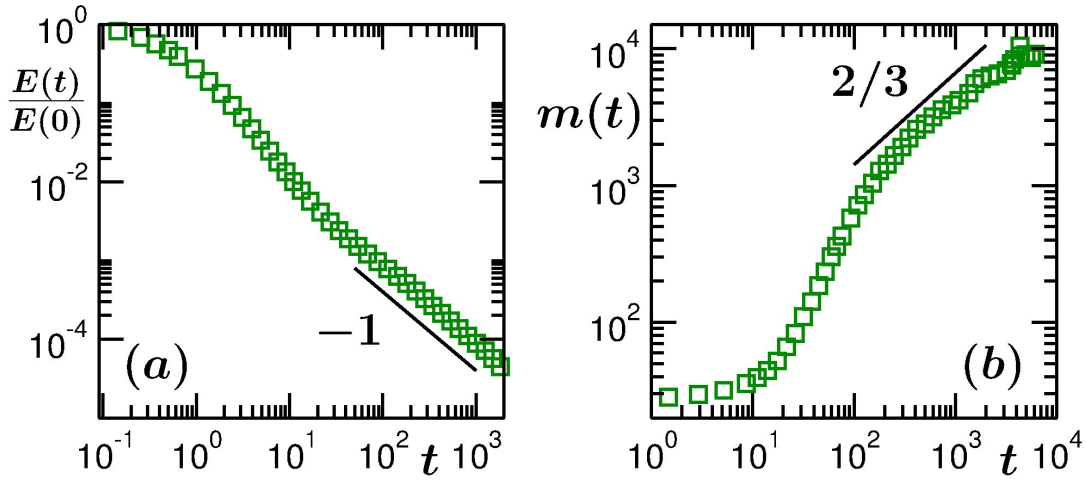

Figure 4.2: (a) Log-log plot of the energy as a function of t, for the system in Fig. 4.1. (b) Log-log plot of mass vs time, for the GGM in Fig. 4.1. All results are for $L = 512$. The solid lines in (a) and (b) represent power laws, exponents for which are mentioned.

Since Eq. (4.1) predicts inverse relationship between mass and energy, the kinetics of GGM is different from ballistic aggregation, particularly when the exponents do not follow even a hyperscaling relation [7,9] (see discussion below in the context of BAM). Matching of the exponent for energy decay (with Eq. (4.1)) is accidental. In the rest of the section, therefore, we focus only on the BAM. This is by keeping the primary objective of studying aging during ballistic aggregation in mind.

There are different variants of models dealing with ballistic aggregation. E.g. there exists interest in a model where ballistically moving particles from a source get deposited on a fixed substrate or seed. Such models are of relevance in situations like construction of vapor-deposited thin films and the corresponding structures are fractal [38]. In the present case, however, all the clusters move ballistically, between collisions. Simulation of such BAM in

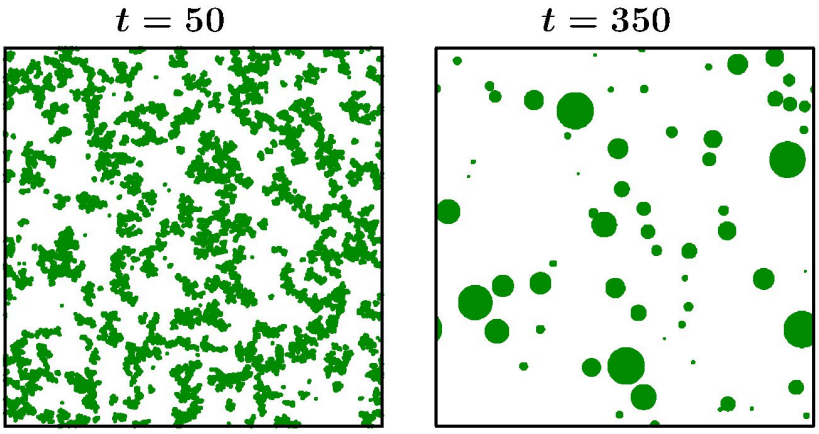

Figure 4.3: (Left frame) A snapshot during the evolution of the fractal BAM in $d = 2$ with $L = 512$. See text for details. (Right frame) Same as the left frame but with spherical structural approximation and for $L = 1024$. In both the frames only parts of the original systems are shown. Times are mentioned on top of the frames.

$d > 1$ is not straight forward. If no deformation of the clusters is considered, highly fractal structures are expected in this situation as well. In that case, one needs to keep track of the exact points of contact, when two clusters collide. This is a difficult task, particularly if the rotations of the clusters are considered. In the left frame of Fig. 4.3 we show a snapshot, obtained during an evolution for the BAM, without incorporating any deformation and considering only the translational motion of the clusters. Nice fractal pattern is seen. We have estimated the fractal dimension which we discuss later.

Because of the above mentioned difficulty in dealing with the actual physical scenario, researchers [7, 9, 22] have adopted a spherical structural approximation, as briefly mentioned above. In this method, after a collision between two spherical objects of diameters σ_1 and σ_2, the mass of the resulting cluster is (usually uniformly) distributed over the volume of a sphere or

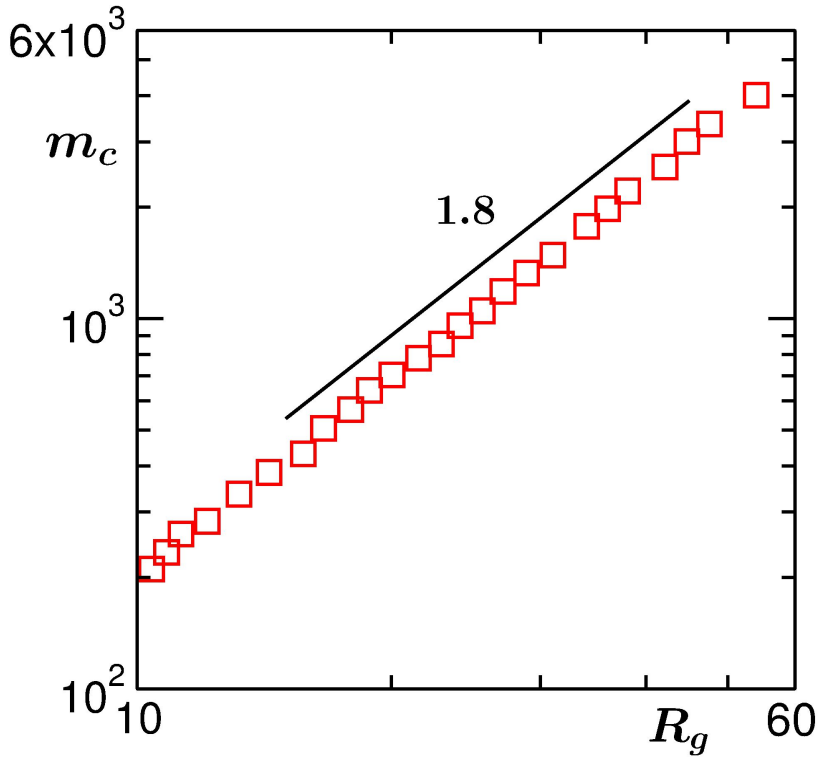

Figure 4.4: Cluster mass, from a typical snapshot, is shown as a function of the radius of gyration, R_g, for the fractal BAM case, on a log-log scale, with $L = 512$. The solid line there is a power-law with exponent 1.8. Rest of the results will be presented for $L = 1024$ and spherical BAM.

circle (depending upon the system dimension) of diameter

$$\sigma = (\sigma_1^d + \sigma_2^d)^{1/d}. \tag{4.10}$$

Many materials are prone to permanent deformation after high impact collisions. This is, thus, a reasonable approximation if the time scale of deformation is low, compared to the mean free time. In any case, given that fractality offers larger collision cross-section, the dynamics of the systems with such spherical structural approximation will be different from those

without the approximation. In the rest of the subsection, unless otherwise mentioned, by BAM we will refer to the ballistic aggregation model with circular approximation.

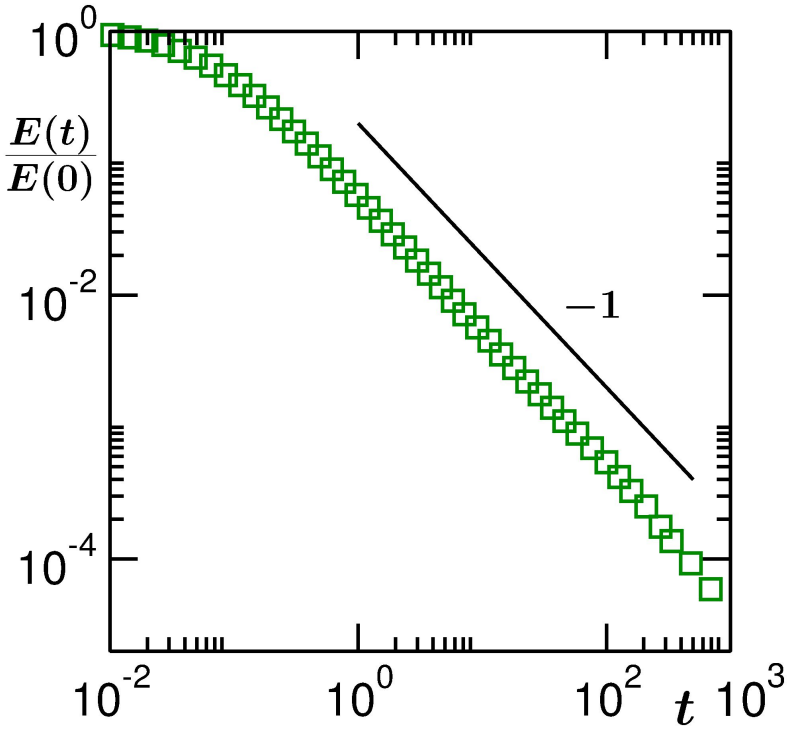

Figure 4.5: Log-log plot of the kinetic energy vs time for the $d = 2$ BAM. The solid line in the figure is power-law with exponent -1.

In the BAM, the post-collisional position and velocity of a new cluster can be obtained from the conservation equations related to centre of mass and linear momentum, as mentioned above. A snapshot during the evolution of a system with such rules is shown in the right frame of Fig. 4.3. Before presenting results on dynamics of this simplified model, in Fig. 4.4 we present result for the fractal dimension corresponding to the snapshot in the left frame of Fig. 4.3. Here we show mass of individual clusters as a

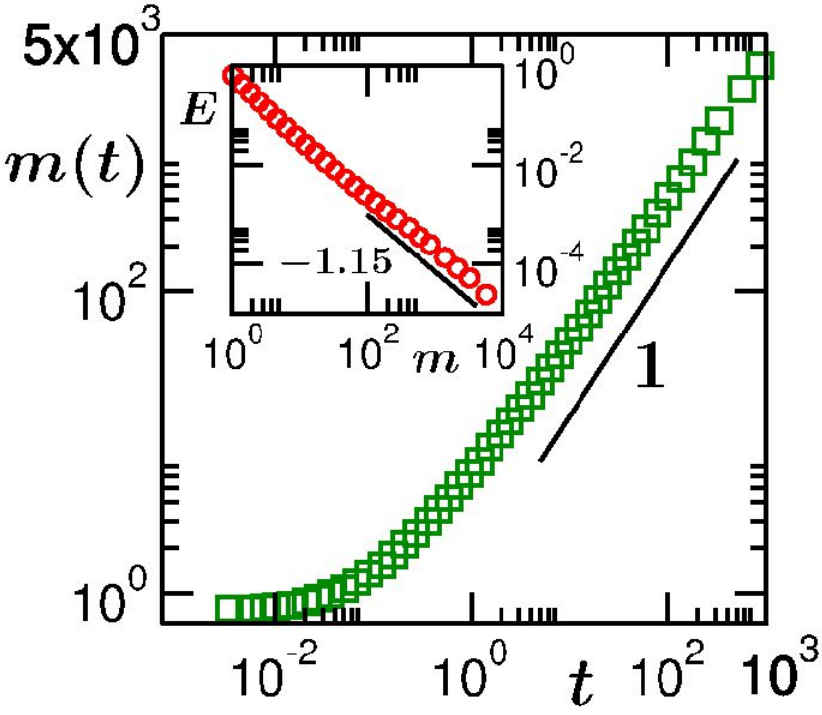

Figure 4.6: Log-log plot of mass vs time, for the $d = 2$ BAM. The solid line represents a power-law with exponent 1. In the inset we show a log-log plot of E vs m. The solid there is a power-law with exponent -1.15.

function of the radius of gyration (R_g), on a log-log scale. Nice power-law behavior is visible, providing (mass) fractal dimension $d_f \simeq 1.8$. As mentioned above, henceforth we will work with only the circular BAM. Even though the primary aim is to examine scaling property related to aging, in the following we present accurate results for energy decay and cluster growth as well, from appropriate analyses. To the best of our knowledge, such accurate analyses were not previously performed to draw conclusions on the behavior of these quantities.

In Fig. 4.5 we show a log-log plot of energy decay as a function of time. A plot for the growth of mass is shown in Fig. 4.6. Power laws in both the

cases can be identified. While from these log-log plots it appears that the energy and mass are inversely proportional to each other, as predicted in Eq. (4.1), the inset of Fig. 4.6, where we show kinetic energy as a function of mass, provides a different information. There the exponent of the power-law decay appears clearly higher than unity, approximately 1.15, over a significant range. For an accurate estimate we, thus, calculate the instantaneous exponents [39] for the time dependence of m and E as

$$\theta_i = -\frac{d\ \ln E}{d\ \ln t}, \qquad \zeta_i = \frac{d\ \ln m}{d\ \ln t}. \tag{4.11}$$

Such exercises were performed for the $d = 1$ BAM as well. However, we avoided presenting those results, since this aspect in $d = 1$ is better understood.

We have plotted θ_i, vs $1/t$, and ζ_i, vs $1/m$, in Figures 4.7 and 4.8, respectively. In the asymptotic limit we obtain $\theta \simeq 1.08$ and $\zeta \simeq 0.94$. Thus, the predictions of Eq. (4.1) are not obeyed. These numbers, however, appear consistent with a hyper-scaling relation [9] in $d = 2$ (for ballistic aggregation):

$$\theta + \zeta = 2. \tag{4.12}$$

The failure of Eq. (4.1) lies in the fact that at low packing fraction the assumption related to uncorrelated velocity, inherent in the derivation of Eq. (4.1), breaks down [40]. It is expected that at higher density, where the collision events are more frequent, this prediction will work [9, 22, 40]. The derivation of the exponent for the growth of mass can be realized from Eq.

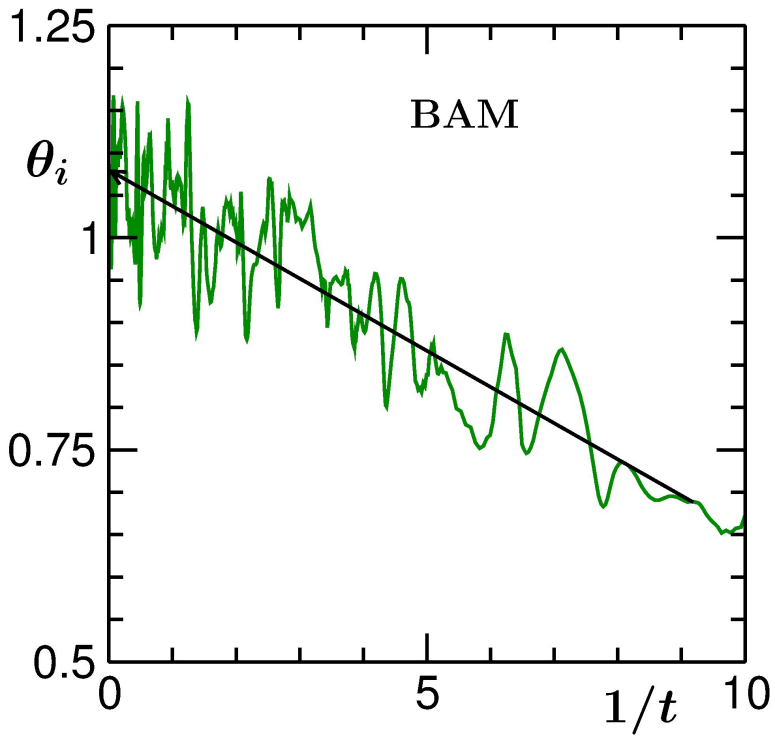

Figure 4.7: Plot of θ_i vs $1/t$, for the $2D$ BAM. The solid line is a guide to the eye.

(4.2), which describes the evolution of the density of clusters. An exponent $\xi = 1$ requires the fact that $v_{\rm rms} \sim m^{-1/2} \sim n_c^{1/2}$, an outcome of the uncorrelated momenta of clusters, which is true for the Boltzmann distribution of cluster energies. At higher densities this assumption is valid as the collisions are random, but fails at lower densities. In general, if the relation between $v_{\rm rms}$ and m can be written as $v_{\rm rms} \sim m^{-\gamma}$, the exponent for the growth of mass will be of the form

$$\zeta = \frac{d_f}{1 - d + d_f(1+\gamma)}, \tag{4.13}$$

taking Eq. (4.2) as the starting equation. Here we ask the question is it

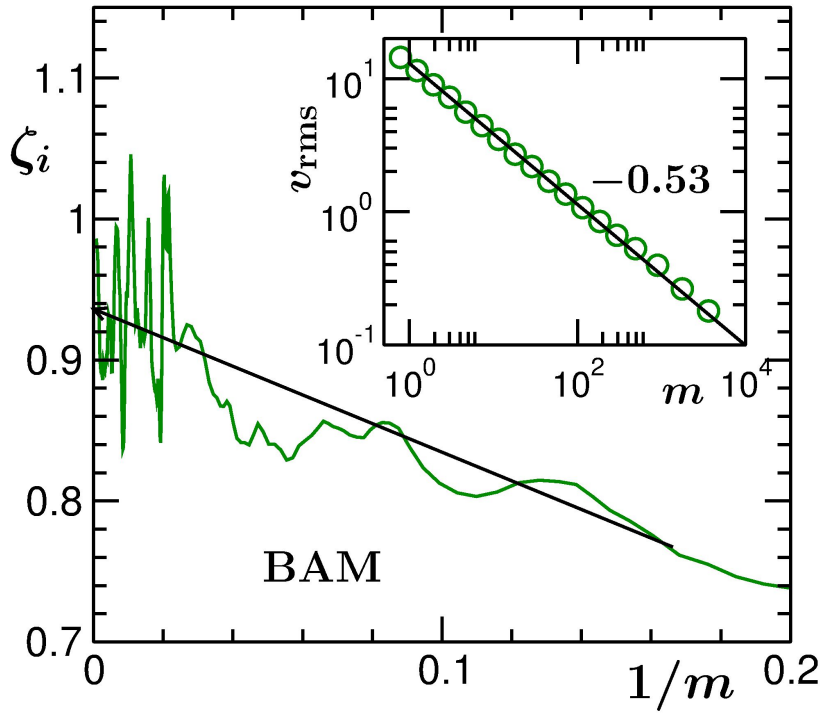

Figure 4.8: Plot of ζ_i vs $1/m$, for the BAM in $d = 2$. The solid line is a guide to the eye. Inset: Log-log plot of $v_{\rm rms}$ vs m, for the $2D$ BAM. The solid line there is a power-law, exponent for which is mentioned next to it.

not possible to obtain the above mentioned value of ζ from Eq. (4.2) or (4.13)? Note that under the spherical approximation $d_f = 2$. Thus, we need to estimate γ to find out the reason for deviation of ζ from unity (see Eq. (4.1)).

In the inset of Fig. 4.8 we plot $v_{\rm rms}$ as a function of m. A power-law behavior from the log-log plot can be appreciated. The corresponding exponent ($\gamma \simeq 0.53$) provides $\zeta \simeq 0.97$ (see Eq. (4.13)). Even though this number is smaller than 1, no conclusive remark should be made from such small deviation. Following Ref. [40], we state here the reason behind a deviation between θ and ζ. Via the introduction of a dissipation parameter

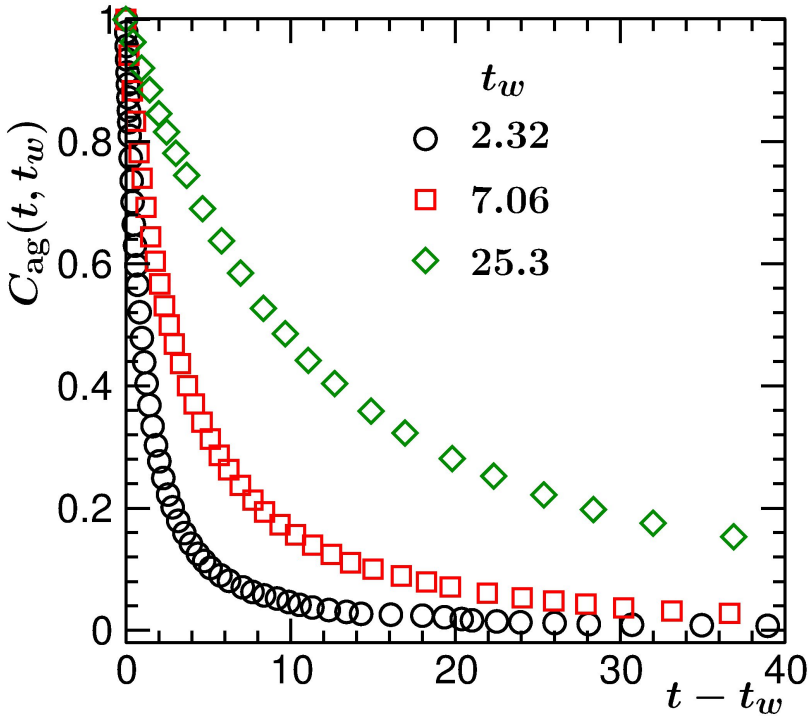

Figure 4.9: For the $2D$ BAM the autocorrelation function $C_{\rm ag}(t, t_w)$ is plotted vs $t - t_w$. Results from three different t_w values are included.

(α'), ratio between kinetic energy dissipation in a collision and mean kinetic energy per particle, these authors showed that $\alpha' = 1$ for high collision frequency. On the other hand, for low frequency, i.e., at low particle density, $\alpha' > 1$. In the latter scenario, the particles with larger kinetic energy than the mean undergo more frequent collisions, enhancing the dissipation. This leads to a value of θ higher than unity. This fact becomes more prominent at densities smaller than the one considered here. E.g., for $\rho = 0.005$, we find $\theta \simeq 1.15$ and $\zeta \simeq 0.85$. Similar fact is observed in $d = 3$. There, in future, we intend to verify how well the corresponding hyperscaling relation [9] holds. Next we present results for aging.

In Fig. 4.9 we show plots of $C_{\rm ag}(t, t_w)$, vs $t - t_w$, for a few different values

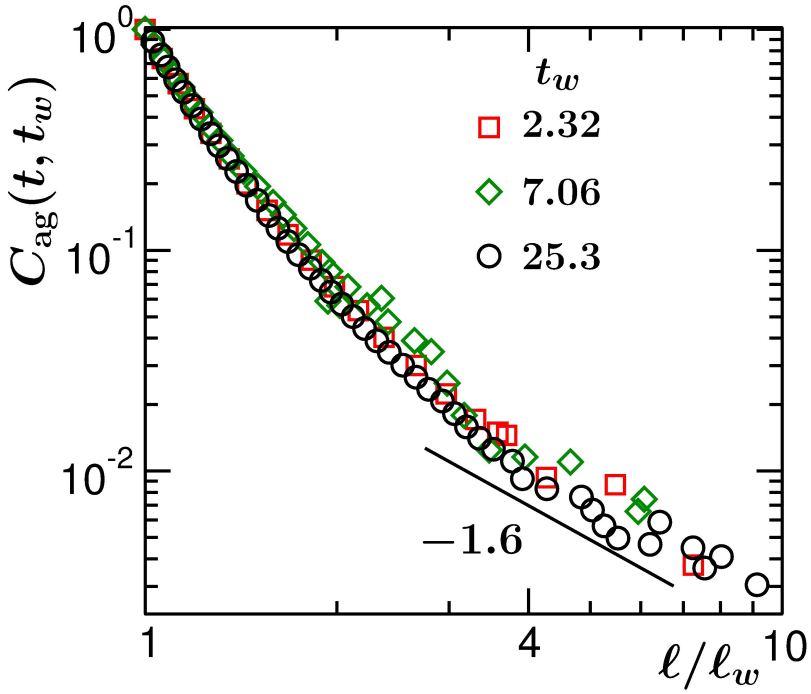

Figure 4.10: Log-log plot of $C_{\rm ag}(t, t_w)$ vs x $(= \ell/\ell_w)$, using data sets of Figure 4.9. The solid line represents a power-law with exponent $\lambda = 1.6$.

of t_w. Like in $d = 1$, in the previous chapter, here also, the time translational invariance is absent, as expected. It is clearly seen that with increasing age relaxation gets slower. In Fig. 4.10 we show the log-log plots of $C_{\rm ag}(t, t_w)$ as a function of $\ell/\ell_w (\equiv x)$. Very nice collapse of data on a master curve is visible. This confirms the scaling property of Eq. (4.4). For large values of ℓ/ℓ_w power-law decay becomes prominent. Continuous bending of the master curve for small abscissa variable implies early-time correction to the power-law. The large x data appear to be consistent with an exponent $\lambda \simeq 1.6$, the number being roughly the same as in the $d = 1$ case, as seen in the previous chapter. For aging in kinetics of phase transitions, on the other hand, one observes strong dimension dependence of λ [29,30]. There exists a dimension

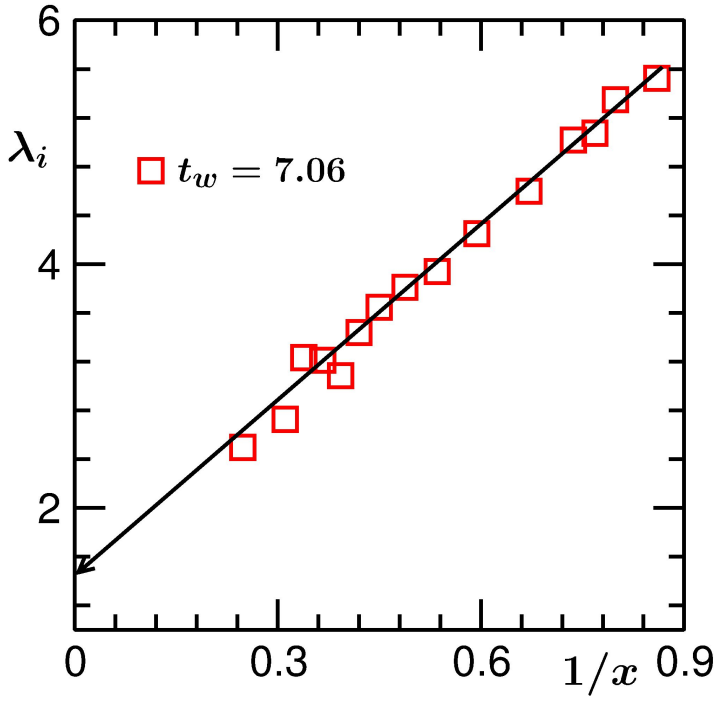

Figure 4.11: We show the instantaneous exponent λ_i as a function of $1/x$, for $2D$ BAM. The solid line there is a linear extrapolation to $x = \infty$.

dependent lower bound of λ, i.e.,

$$\lambda \geq \frac{d+\beta}{2}, \tag{4.14}$$

where β is the exponent for the increment of the structure factor $S(k,t)$ at small-k limit. This bound, which has been discussed in the previous chapter, has been obtained by Yeung, Rao and Desai. Here note that in $d = 2$ we expect [41] $\beta = 4$. Thus, the (lower) bound in (4.14) is 3. This calls for a look at the behavior of the equal-time structure factor for the present problem. While for bicontinuous domain structures ($d > 1$) the analytical prediction ($\beta = 4$) has been numerically confirmed [41,42], the cases of discrete domain morphology are less studied. Before taking a look at the equal time structure

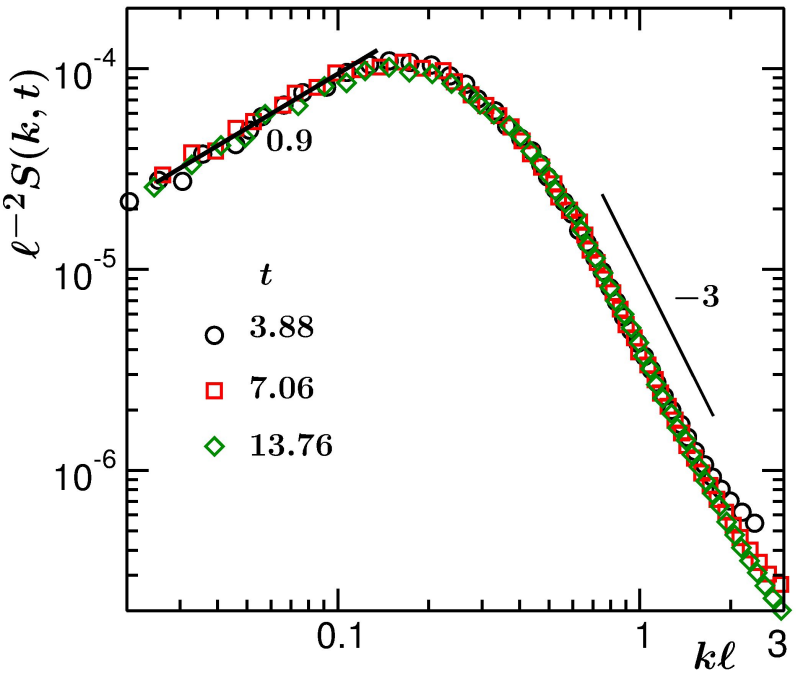

Figure 4.12: Log-log plot of $\ell^{-2}S(k,t)$ vs $k\ell$, for the BAM in $d = 2$. The solid lines are power laws, exponents for which are mentioned on the figure.

factor, since a violation of the bound appears to be a possibility, in Fig. 4.11 we plot the instantaneous exponent

$$\lambda_i = -\frac{d\ \ln C_{\rm ag}}{d\ \ln x}, \tag{4.15}$$

as a function of $1/x$, to accurately quantify λ. The data set provides an asymptotic value $\lambda \simeq 1.55$.

In Fig. 4.12 we present a scaling plot of $S(k,t)$, viz., we show $\ell^{-2}S(k,t)$ vs $k\ell$, on a log-log scale. At larger values of the wave vector k, for the smooth interfaces of the domains, $S(k,t)$ follows Porod law behavior, $S(k,t) \sim k^{-(d+1)}$, for scalar order parameter. Thus, in the BAM, the large k data are consistent with the power-law exponent -3, that corresponds to the Porod law [43]. In

the small k region, on the other hand, the enhancement is much weaker than k^4. In fact, in the relevant region, we observe $\beta \lesssim 1$. Similar number we have observed in recent studies of kinetics of phase transition with conserved off-critical composition as well, for which one naturally obtains circular or spherical domain structures. In that case we have the lower bound to be $\lesssim 1.5$, which is satisfied by the above estimated value of λ.

4.4 Conclusion

We have studied the kinetics of clustering in models of granular gas (GGM) and ballistic aggregation (BAM), in $d = 2$. For the GGM we have presented results for decay of energy and growth of mass. These results differ from those for the BAM.

For the BAM, the energy and mass do not appear to obey an inverse relationship, as predicted by Carnevale *et al.* [2]. However, the corresponding power-law exponents follow a hyperscaling relation [7]. This fact we have verified via a rather accurate method of analysis. The inverse relation may, however, be observed at higher packing fractions.

In addition, for the BAM we studied the aging property [26] of the density field. The order-parameter autocorrelation functions, calculated at different times, scale with ℓ/ℓ_w. The power-law exponent for the asymptotic form of the scaling function has been estimated via the calculation of a time-dependent exponent λ_i. It has been shown that the asymptotic value of the exponent follows a dimension dependent lower bound which has been derived by taking the structural property [32] of the clusters into account. Like in

$d = 1$, as shown in the previous chapter, here also, in $d = 2$, the asymptotic value of the exponent stays close to the lower bound.

With respect to the more realistic ballistic aggregation, the simulations are rather challenging for $d > 1$. This is because of the formation of fractal structures. Because of this reason, like in the existing simulation studies, spherical structural approximation has been used by us. It will be interesting to investigate the scaling properties related to aging and other aspects without such approximation.

Bibliography

[1] I.S. Aranson and L.S. Tsimring Rev. Mod. Phys. **78**, 641 (2006).

[2] G.F. Carnevale, Y. Pomeau and W.R. Young, Phys. Rev. Lett. **64**, 2913 (1990).

[3] E. Ben-Naim, S. Redner and F. Leyvraz, Phys. Rev. Lett. **70**, 1890 (1993).

[4] E. Ben-Naim, P.L. Krapivsky and S. Redner, Phys. Rev. E **50**, 822 (1994).

[5] L. Frachebourg, Phys. Rev. Lett. **82**, 1502 (1999).

[6] I. Goldhirsch and G. Zanetti, Phys. Rev. Lett. **70**, 1619 (1993).

[7] E. Trizac and J.-P. Hansen, Phys. Rev. Lett. **74**, 4114 (1995).

[8] F. Leyvraz, Phys. Rep. **383**, 95 (2003).

[9] E. Trizac and J.-P. Hansen, J. Stat. Phys. **82**, 1345 (1996).

[10] S.F. Shandarin and Y.B. Zeldovich, Rev. Mod. Phys. **61**, 185 (1989).

[11] R. Brito and M. H. Ernst, Europhys. Lett. **43**, 497 (1998).

[12] N.V. Brilliantov and T. Poeschel, *Kinetic Theory of Granular Gases* (Oxford University Press, Oxford, 2004).

[13] S. Luding and H.J. Herrmann, Chaos **9**, 673 (1999).

[14] S.K. Das and S. Puri, Europhys. Lett. **61**, 749 (2003).

[15] S.K. Das and S. Puri, Phys. Rev. E **68**, 011302 (2003).

[16] M. Shinde, D. Das and R. Rajesh, Phys. Rev. Lett. **99**, 234505 (2007).

[17] M. Shinde, D. Das and R. Rajesh, Phys. Rev. E **84**, 031310 (2011).

[18] A. Bodrova, A.K. Dubey, S. Puri and N.V. Brilliantov, Phys. Rev. Lett. **109**, 178001 (2012).

[19] S. Paul and S.K. Das, Europhys. Lett. **108**, 66001 (2014).

[20] E. Ben-Naim, S.Y. Chen, G.D. Doolan and S. Render, Phys. Rev. Lett. **83**, 4069 (1999).

[21] X. Nie, E. Ben-Naim and S. Chen, Phys. Rev. Lett. **89**, 204301 (2002).

[22] S.N. Pathak, Z. Jabeen, D. Das and R. Rajesh, Phys. Rev. Lett. **112**, 038001 (2014).

[23] J. Midya and S.K. Das, Phys. Rev. Lett. **118**, 165701 (2017).

[24] A.J. Bray, Adv. Phys. **51:2**, 481 (2002).

[25] A. Onuki, *Phase Transition Dynamics* (Cambridge University Press, Cambridge, England, 2002).

[26] M. Zannetti, in *Kinetics of Phase Transitions*, ed. S. Puri S. and V. Wadhawan (Boca Raton: CRC Press, 2009).

[27] D.S. Fisher and D.A. Huse, Phys. Rev. B **38**, 373 (1988).

[28] F. Liu and G.F. Mazenko, Phys. Rev. B **44**, 9185 (1991).

[29] J. Midya, S. Majumder and S.K. Das, J. Phys.: Condens. Matter **26**, 452202 (2014).

[30] J. Midya, S. Majumder and S.K. Das, Phys. Rev. E **92**, 022124 (2015).

[31] S. Majumder, J. Zierenberg and Wolfhard Janke, Soft Matter **13**, 1276 (2017).

[32] C. Yeung, M. Rao and R.C. Desai, Phys. Rev. E **53**, 3073 (1996).

[33] M.P. Allen and D.J. Tildesley, *Computer Simulation of Liquids* (Clarendon, Oxford, 1987).

[34] D.C. Rapaport, *The Art of Molecular Dynamics Simulations* (Cambridge University Press, Cambridge, England, 2004).

[35] H. Goldstein, C.P. Poole, and J.F. Safko, *Classical Mechanics* 3rd Ed. (Addison-Wesley, 2001).

[36] S. McNamara and W.R. Young, Phys. Rev. E **50**, R28 (1994).

[37] P. K. Haff, J. Fluid Mech. **134**, 401 (1983).

[38] P. Ramanlal and L.M. Saner, Phys. Rev. Lett. **54**, 1828 (1985).

[39] D.A. Huse, Phys. Rev. B **34**, 7845 (1986).

[40] E. Trizac and P.L. Krapivsky, Phys. Rev. Lett. **91**, 218302 (2003).

[41] C. Yeung, Phys. Rev. Lett. **61**, 1135 (1988).

[42] S. Ahmad, S.K. Das and S.Puri, Phys. Rev. E **85**, 031140 (2012).

[43] G. Porod, Small-Angle X-Ray Scattering, eds. O. Glatter and O. Kratky (Academic Press, New York, 1982).

Chapter 5

Density dependence of ballistic aggregation in 2- and 3-dimensions

5.1 Introduction

Ballistic aggregation is common in nature [1–6]. Examples [4, 7–11] include growth of liquid droplets and solid clusters in clouds, clustering in cosmic dust, among others. In this context, a simple model, referred to as the ballistic aggregation model (BAM) [1], has been of much theoretical interest. In this model, spherical particles merge upon collision and form a larger aggregate by keeping the shape unchanged. In this process, the mass and momentum of the system remains conserved, whereas the (kinetic) energy decays. Even though appears a bit unrealistic, this model has provided

important insights into the understanding of growth in many complex systems [1, 4–6, 12, 13]. It is, of course, understood that upon collision fractal structures will emerge [11] in space dimension $d > 1$. However, in many situations colliding objects undergo deformation and so, if the collision interval is long, the above mentioned spherical structural approximation is reasonably good.

Carnevale *et al.* [1], in a pioneering work, via scaling arguments, predicted the behavior of energy (E) decay and growth of average mass (m) of clusters in ballistic aggregation process. Specifically, this theory predicts

$$m \sim 1/E \sim t^{2d/d+2}, \tag{5.1}$$

in which an inherent assumption is that the particle momenta are uncorrelated. Even though the predictions in Eq. (5.1) are in agreement with the computer simulations in $d = 1$, discrepancies have been reported [4, 14] in $d > 1$. Another theory predicts the existence of a hyperscaling relation involving the energy decay and mass growth. If one writes

$$E \sim t^{-\theta} \tag{5.2}$$

and

$$m \sim t^{\zeta}, \tag{5.3}$$

then the (positive) power-law exponents θ and ζ are expected to be connected

to each other in d dimensions via [4]

$$2\zeta + d\theta = 2d. \tag{5.4}$$

Furthermore, there have been efforts to understand if the freely cooling granular gas model (GGM) is equivalent to the BAM. While in $d = 1$, equivalence, with respect to energy decay, mass growth and aging, between the two models has been established [14–17], in a recent work we have shown [14] that the equivalence does not exist in $d = 2$. Here note that in the case of GGM [18], the coefficient of restitution e lies in the range $0 < e < 1$. Thus, following inelastic collisions, particles do not stick to each other. Nevertheless, velocity parallelization occurs due to reduction in normal relative velocity, following the collisions. This gives rise to clustering phenomena in this model [13–15, 18–22].

The objective of this chapter is to investigate the correctness of the hyperscaling relation of Eq. (5.4), for the BAM in $d = 2$ and 3, and check for an analogous behavior in GGM. To verify the hyperscaling relation [4] in the BAM, we consider different packing fractions. We observe that the relation is valid irrespective of the dimension and packing fraction. In the high density limit, in addition, the prediction of Eq. (5.1) appears correct. This is because of the fact that the collisions are more random and thus velocities are uncorrelated in this density limit. On the other hand, the results for the GGM does not provide any hint for a hyperscaling relation of this type.

The rest of the chapter is organised as follows. In Section 5.2 we provide

more details on the theoretical predictions. Models and methods are discussed in Section 5.3. Results are presented in Section 5.4. Finally, Section 5.5 concludes the paper wth a brief summary and outlook.

5.2 Theoretical Background

While originally derived from a different approach, Eq. (5.1) can also be derived by starting from the kinetic equation [4, 11, 12, 14]

$$\frac{dn}{dt} = - \text{ “collision cross-section” } \times v_{\text{rms}} \times n^2, \tag{5.5}$$

where n is the particle or cluster density and v_{rms} is the root-mean-squared velocity of the particles. For spherical particles the collision cross-section is ℓ^{d-1}, where ℓ is the average diameter of the particles which scales with average mass as $m^{1/d}$. For uncorrelated velocity one can take [4] $v_{\text{rms}} \sim m^{-1/2}$. The particle density, given that total mass is conserved, scales inversely with the average mass. Incorporation of these facts in Eq. (5.5) leads to

$$\frac{dm}{dt} = m^{\frac{d-2}{2d}}. \tag{5.6}$$

Solution of Eq. (5.6) provides time dependence of mass in Eq. (5.1). Given that v_{rms} has above mentioned dependence on mass, kinetic energy will have inverse relation with m. A deviation from $v_{\text{rms}} \sim m^{-1/2}$, however, can invalidate the predictions in Eq. (5.1). In fact, for $v_{\text{rms}} \sim m^{-z}$, the growth exponent ζ becomes [14]

$$\zeta = \frac{d}{1 + dz}. \tag{5.7}$$

Starting from Eq. (5.5) and without substituting any mass dependence of $v_{\rm rms}$, one writes [4]

$$\frac{dm}{dt} = m^{\frac{d-1}{d}} v_{\rm rms}. \tag{5.8}$$

From Eq. (5.8), substituting the time dependence of energy from Eq. (5.2) and, that of mass from Eq. (5.3), after considering that $v_{\rm rms} \sim E^{1/2}$, one arrives at

$$\zeta t^{\zeta-1} = t^{\frac{2\zeta d - 2\zeta - \theta d}{2d}}. \tag{5.9}$$

Simple power counting provides the hyperscaling relation [4] of Eq. (5.4). Eq. (5.4) in $d = 2$ and 3 reads [4]

$$\theta + \zeta = 2. \tag{5.10}$$

and

$$3\theta + 2\zeta = 6, \tag{5.11}$$

respectively. We intend to verify these equations for the BAM.

5.3 Models and Methods

For both the models, hard spherical particles, mass being uniformly distributed over the volume or area of the particles, move freely between collisions [4, 18]. Mass and momentum remain conserved during collisions. For the BAM, even though the size of the new particle increases, its shape remains unchanged. For example, two initial spheres of masses and diameters

(m_i, σ_i) and (m_j, σ_j), respectively, coalesce into a single sphere of mass

$$m' = m_i + m_j, \tag{5.12}$$

with diameter [4]

$$\sigma' = (\sigma_i^d + \sigma_j^d)^{1/d}. \tag{5.13}$$

In this shape retaining process, if the new sphere overlaps with any other particle, then they are treated as another collision and same method of update is applied. The position ($\vec{r}\,'$) and velocity ($\vec{v}\,'$) of the new particle can be obtained from the following conservation equations [23]:

$$m\,'\vec{r}\,' = m_i\vec{r}_i + m_j\vec{r}_j, \tag{5.14}$$

$$m\,'\vec{v}\,' = m_i\vec{v}_i + m_j\vec{v}_j, \tag{5.15}$$

where $\vec{r}_i$ and $\vec{r}_j$ are the positions and $\vec{v}_i$ and $\vec{v}_j$ are the velocities of particles i and j, respectively, before the collision.

In the case of GGM, the particle velocities are updated as [18, 23]

$$\vec{v}_i{}' = \vec{v}_i - \Big(\frac{1+e}{2}\Big)[\hat{n}\cdot(\vec{v}_i - \vec{v}_j)]\hat{n}\,, \tag{5.16}$$

$$\vec{v}_j{}' = \vec{v}_j - \Big(\frac{1+e}{2}\Big)[\hat{n}\cdot(\vec{v}_j - \vec{v}_i)]\hat{n}\,, \tag{5.17}$$

where $\vec{v}_i{}'$ and $\vec{v}_j{}'$ are the post collisional velocities. In Eqs. (5.16) and (5.17) $\hat{n}$ represents the unit vector parallel to the relative position of the particles i and j. In this case, since the colliding particles do not undergo

coalescence, the particle mass remains unchanged throughout the evolution. In our simulations of the GGM all particles have same diameter and mass, both of which are set to unity.

We perform event driven molecular dynamics simulations with these models [24, 25], where an event is a collision. In this method, since there is no inter-particle interaction or external potential, particles move with constant velocities till the next collision. Time and partners for the collisions are appropriately identified [25].

All the results will be presented from simulations in periodic boxes of linear dimension L, in units of the starting particle diameter (see below). We start with random initial configurations for both positions and velocities, with $\sigma_i = 1$ for all particles. The density mentioned in this chapter corresponds to the starting number density $\rho = N/L^d$, N being the initial number of particles in a box. Values of N will be specified in appropriate places. Here note that in the case of BAM the number of particles decreases with time. So, for this model the number corresponds to the value at the beginning of the simulations.

For the calculation of the average mass, identification of the clusters is required. For the GGM it was appropriately done by identifying the closed cluster boundaries within which the density is higher than a cut-off number ρ_c [14], taken to be $\simeq 0.4$. On the other hand, in the case of BAM, the information on the mass of a cluster is carried by the size of the particles.

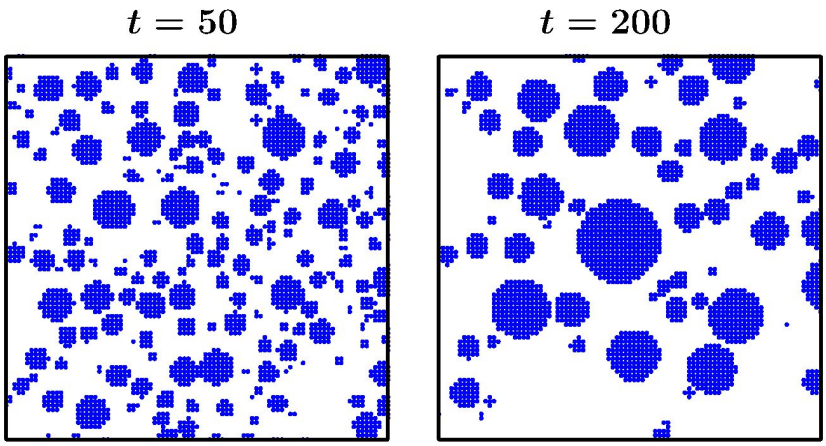

Figure 5.1: Snapshots during the evolution of the two-dimensional BAM, for the starting particle density $\rho = 0.1$. The times are mentioned on the top of the frames. The simulation box size is $L = 512$.

5.4 Results

We divide this section into three sub-sections. The BAM results for $d = 2$ and $d = 3$ will be presented in the first two sub-sections. The GGM results are presented in the last one.

5.4.1 BAM in d=2

In Fig. 5.1 we show the snapshots for the $2D$ BAM from two different times. The snapshots presented here are from late enough times when the clusters are reasonably well grown. The smaller droplets do not appear circular. This is because of a technical difficulty – we have discretized the whole space into a discrete lattice and marked the lattice sites that fall within one or the other droplet. From the two snapshots, it is clear that the number of clusters is decreasing and thus, the average mass of the system is increasing with time.

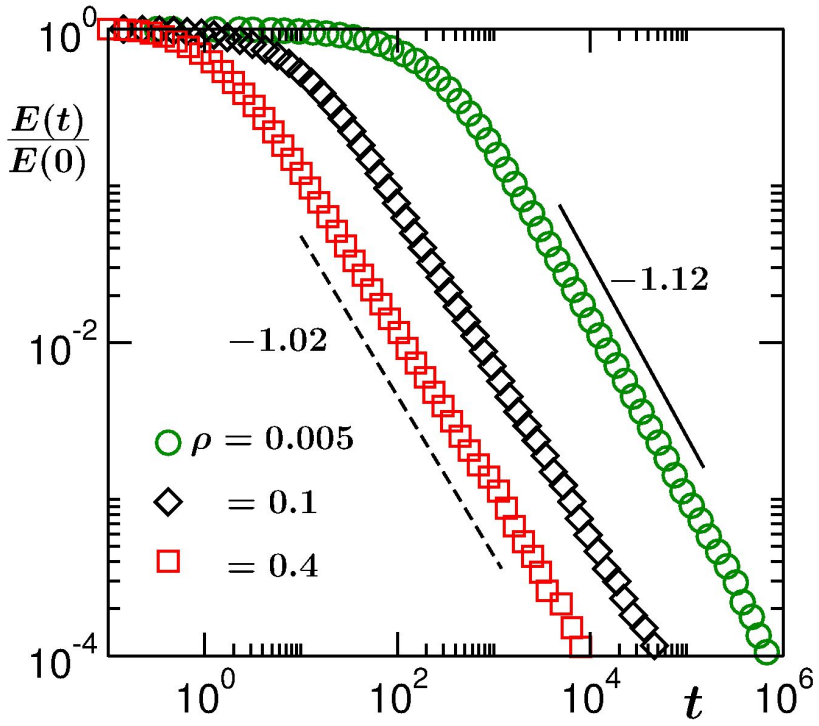

Figure 5.2: Log-log plot of energy as a function of time, for different starting densities (mentioned in the figure). The solid and dashed lines represent power-law decays. Corresponding exponents are mentioned in the figure. All results correspond to BAM in $d = 2$. These and other quantitative results in this dimension (for the BAM) are obtained for $N = 10^5$.

In Fig. 5.2 we plot the energy for three different initial densities, viz., $\rho = 0.005, 0.1$ and 0.4, vs time, on a log-log scale. Fig. 5.3 shows the log-log plot of the growth of mass for the same three starting densities. As seen, the exponents for the energy decay and growth of mass, i.e., θ and ζ, respectively, for different densities differ from each other as well as from the Carnevale *et al.* [1] value 1 (recall that we are working in $d = 2$). The deviation is quite significant when ρ is small. Value of ζ increases towards unity with the increase of the density [4]. On the other hand, θ decreases from a higher value, towards unity, as the density of the system increases [4]. This already

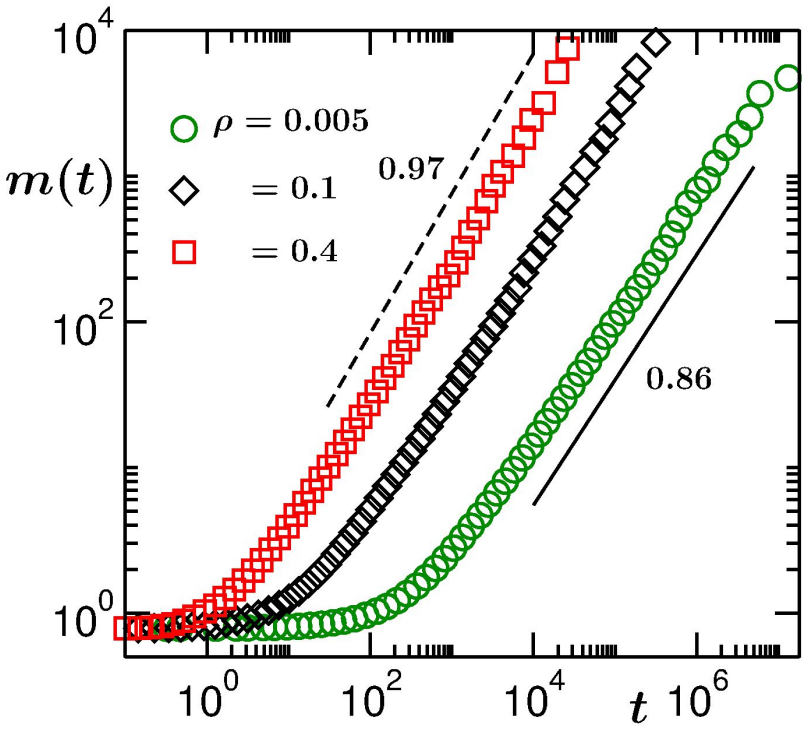

Figure 5.3: Log-log plot of mass as a function of time, for different starting densities, in $d = 2$, for the BAM. The solid and dashed lines represent power-law growths with exponents 0.86 and 0.97, respectively.

provides hint on the validity of hyper-scaling relation [4]. However, to confirm that we need more accurate quantitative analysis.

For this purpose, we calculate the instantaneous exponent θ_i, for the decay of E, defined as [26]

$$\theta_i = -\frac{d(\ln E)}{d(\ln t)}. \tag{5.18}$$

In Fig. 5.4, we plot θ_i as a function of E. We extract the asymptotic value θ from the convergence of θ_i in $t \to \infty$ or $E \to 0$ limit. Indeed θ exhibits density dependence. For the sake of clarity, here we show the plots for $\rho = 0.005$ and

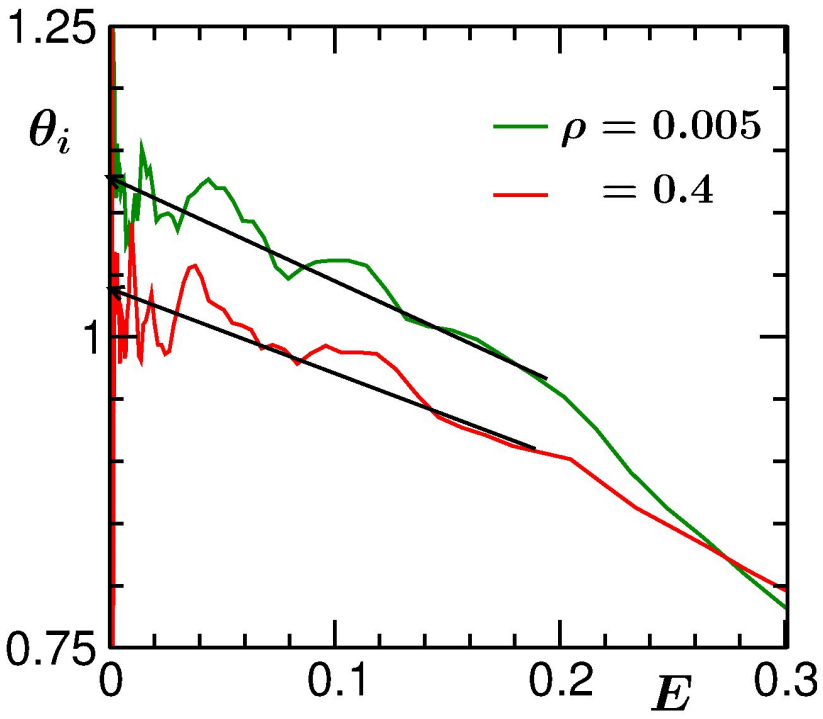

Figure 5.4: Plot of the instantaneous exponent θ_i, vs E, for two values of the starting density. The results correspond to BAM in $d = 2$. Solid straight lines are guides to the eye.

0.4 only. Similar exercise has also been performed for the growth of mass. In Fig. 5.5 we plot the instantaneous exponent ζ_i, for the growth of mass, defined as [26]

$$\zeta_i = \frac{d(\ln m)}{d(\ln t)}, \tag{5.19}$$

as a function of $1/m$, for $\rho = 0.005$ and 0.4. Here also, the asymptotic values vary with the change in density. The exponents θ and ζ, obtained from these exercises, for different starting densities, are quoted in table 5.1.

Carnevale *et al.* [1] predict that the energy decay and the growth of mass are inversely proportional to each other. Our results show that the exponents, which we have been accurately quantified via the calculation of instantaneous

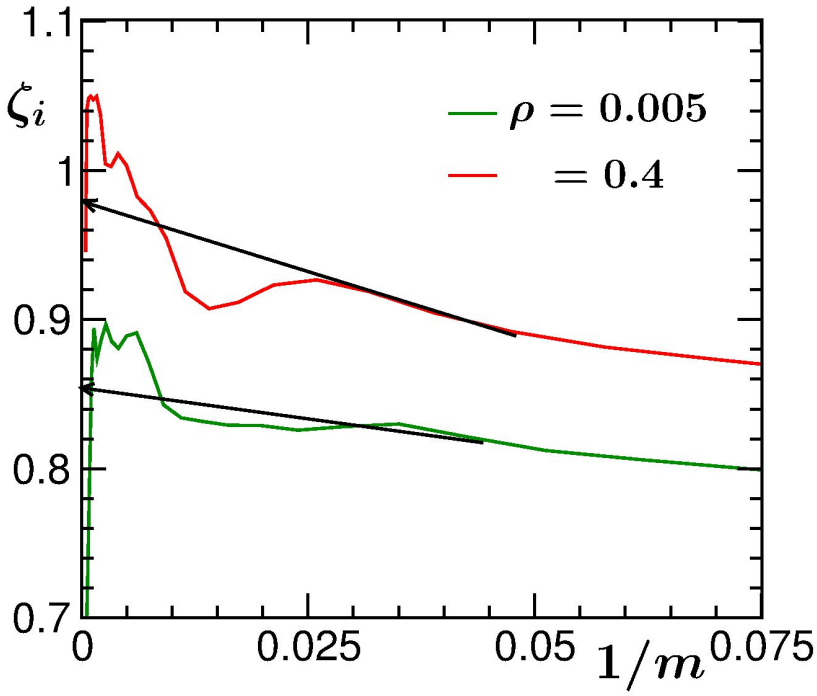

Figure 5.5: Plot of the instantaneous exponent ζ_i, vs $1/m$, for two values of the starting density. The results are for $2D$ BAM. Solid straight lines are guides to the eye.

exponents [26], are nonuniversal and strongly depend upon the density of the particles in the system. The predictions are only valid at higher densities. At lower densities they deviate significantly. But the simulation results follow a hyperscaling relation [4]: $\theta + \zeta = 2$, in $d = 2$. See the numbers quoted in the last column of table 5.1. While these results of ours are consistent with previous reports [4], such accurate analyses were not performed earlier. On the other hand, in $d = 3$ simulation study to confirm the validity of the hyperscaling relation was not done before. In the following subsection we present these results.

Table 5.1: Values of θ and ζ are listed for different initial particle densities for $2D$ BAM.

Density	θ	ζ	$\theta + \zeta$
0.005	1.12	0.86	1.98
0.1	1.06	0.92	1.98
0.3	1.08	0.94	2.02
0.4	1.02	0.98	2.0

5.4.2 BAM in d=3

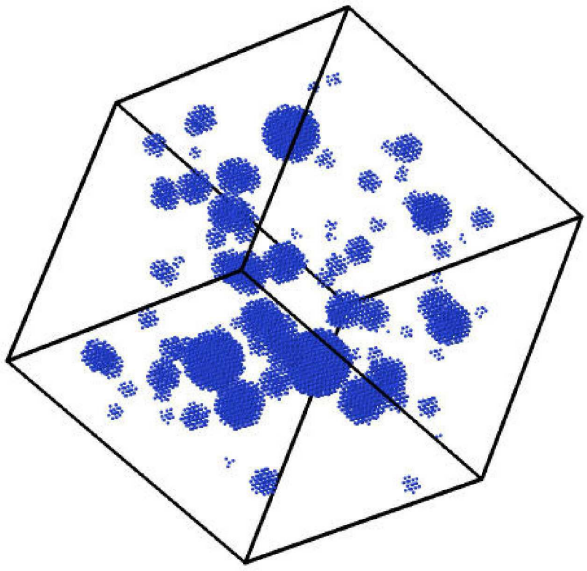

Figure 5.6: An evolution snapshot for the $3D$ BAM, from $t = 100$. The starting particle density is 0.1. The linear dimension of the cubic box is $L = 64$.

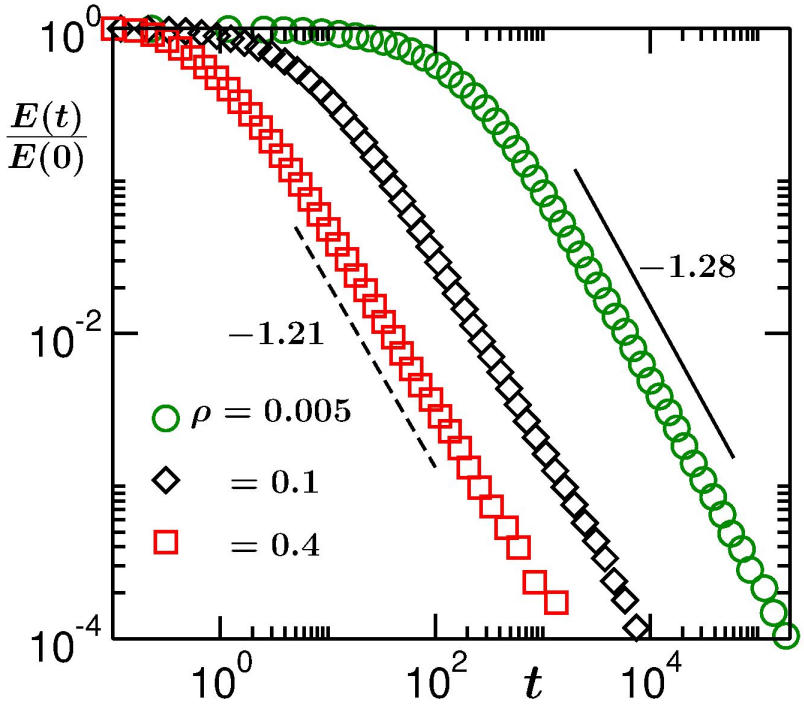

Figure 5.7: Log-log plot of energy as a function of time, for the $3D$ BAM. Results for three different densities are included. The solid and dashed lines are power-laws, exponents being mentioned in the figure. In this dimension all the quantitative results are obtained from simulations in cubic boxes with $N = 10^5$.

First, in Fig. 5.6 we show a snapshot for the three-dimensional BAM evolution. In Fig. 5.7 we plot the energy as a function of time for various different choices of the initial density of particles. Carnevale *et al.*'s [1] prediction for the exponent for the energy decay as well as that for the growth of mass is 6/5 in this space dimension. The values of the exponent θ, as seen in Fig. 5.7, for energy decay, do not obey this theoretical number for all densities. As in the $2D$ case, here also θ decreases from a higher value towards 6/5, as the density of the system increases. In Fig. 5.8, we plot average mass $m(t)$ of the clusters as a function of time, for the same choices

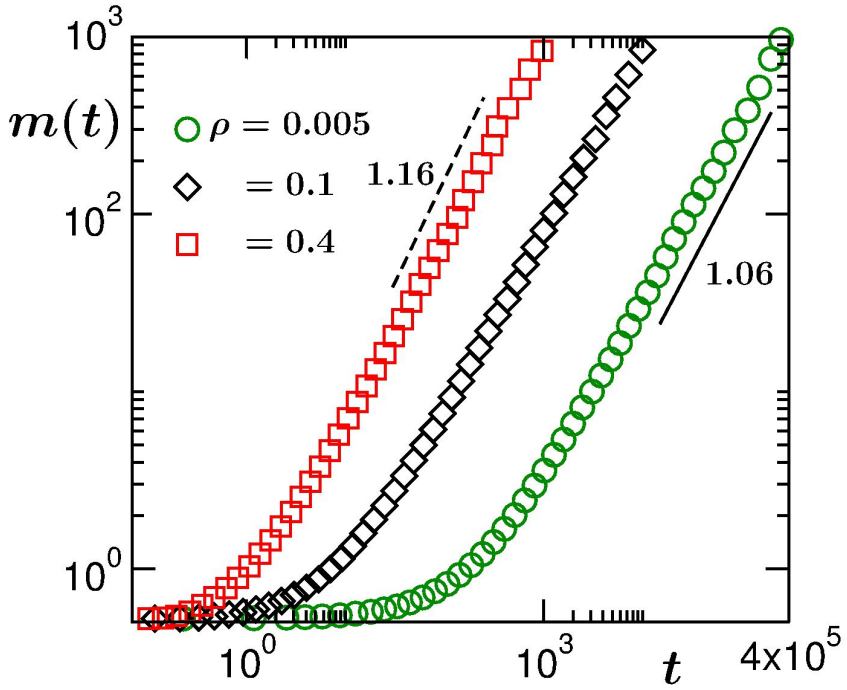

Figure 5.8: Log-log plot of mass, for the $3D$ BAM, as a function of time, for different densities (mentioned in the figure). The solid and dashed lines stand for power-law growths with exponent values 1.06 and 1.16.

of the initial particle density. Values of the power-law exponents have been mentioned next to the respective data sets. Unlike for the energy decay, here, for the growth of mass, the value of the exponent ζ increases towards the value 6/5 with the increase of the density in the system. This fact is also similar to the case of $d = 2$.

For more accurate quantification of the exponents, for the energy decay as well as the growth of mass, we calculate the instantaneous exponents [26] θ_i and ζ_i, defined above, and plot them vs E and $1/m$, respectively, in Fig. 5.9 and Fig. 5.10, for $\rho = 0.005$ and 0.4. The asymptotic values estimated from these plots of instantaneous exponents are quoted in Table 5.2. It is observed that, like in $d = 2$, the exponents are strongly density dependent.

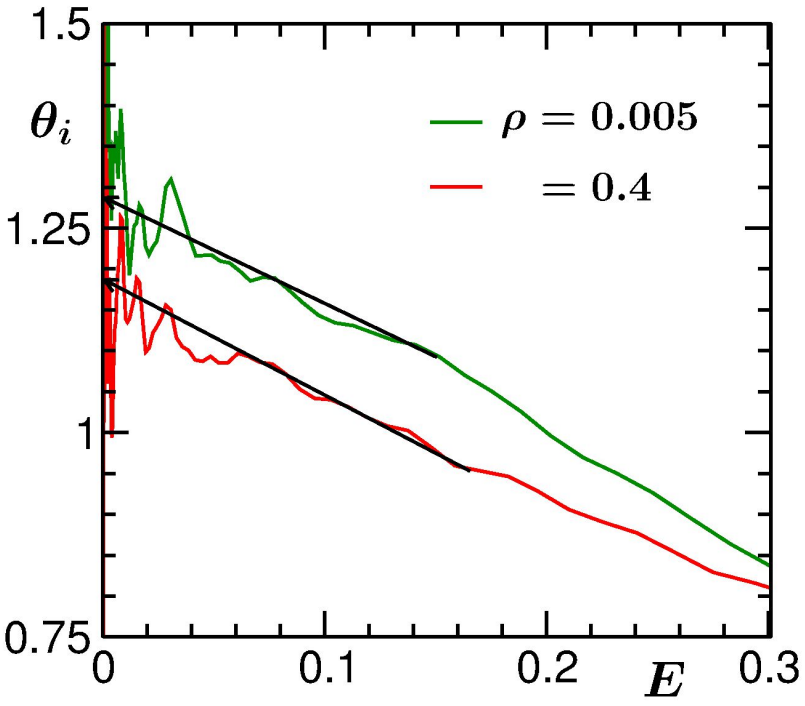

Figure 5.9: Plot of the instantaneous exponent θ_i, vs E, for the $3D$ BAM. The solid straight lines are guides to the eye. We have shown results from two values of ρ.

However, they obey the hyperscaling relation [4], i.e., $3\theta + 2\zeta = 6$.

5.4.3 The case of GGM

In Fig. 5.11 we show a representative snapshot from the evolution in GGM in $d = 3$. The snapshot shows high and low density regions, like the phase separation [27] during a vapor-liquid transition. In this subsection, the objective is to investigate if there exists any dimension dependence in the decay of energy and growth of mass in the GGM.

In Fig. 5.12 we show plots for the decay of energy, in $d = 1$, 2 and 3, for the GGM. Note that the axes are scaled to bring all the plots within

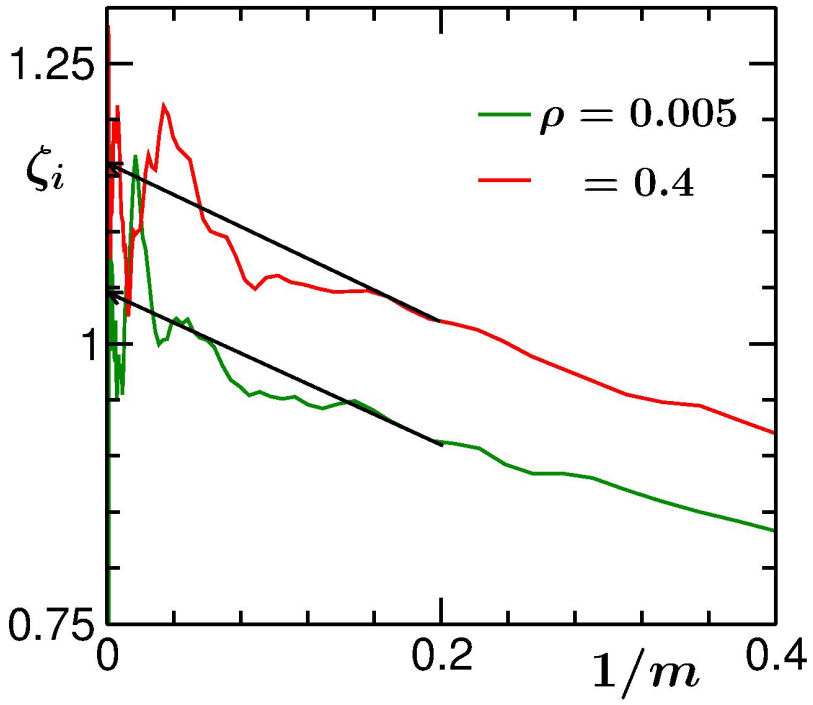

Figure 5.10: Plot of the instantaneous exponent ζ_i, vs $1/m$, for the $3D$ BAM. The solid straight lines are guides to the eye. Results for two densities are shown.

ranges that can help to make the crucial features identifiable for all values of d. Clearly, the decay rate is different for different dimensions. Interestingly, the exponents are in nice agreement with $2d/d+2$, predicted by Carnevale *et al.* [1]. (At much later time (not shown) the decays are faster which can be related to finite size or other effects.) However, from previous studies on growth of mass, we got hint that this agreement of energy decay with the prediction of Carnevale *et al.* [1] may be accidental. To make a more concrete statement on this aspect, below we look at the growth picture.

In Fig. 5.13 we present plots of m vs t, on a log-log scale, for all the three dimensions. We show data only in the scaling regime [27]. Furthermore,

Table 5.2: Values of θ and ζ for different initial particle densities. All results are for $3D$ BAM.

Density	θ	ζ	$3\theta + 2\zeta$
0.005	1.28	1.06	5.96
0.1	1.24	1.10	5.92
0.4	1.21	1.17	5.97

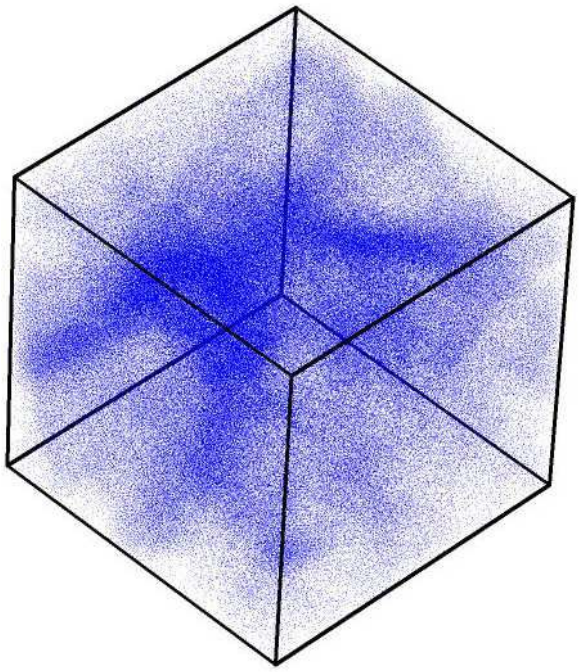

Figure 5.11: An evolution snapshot for the $3D$ GGM with $e = 0.8$. The density of particles is 0.18 and the linear dimension of the simulation box is $L = 120$.

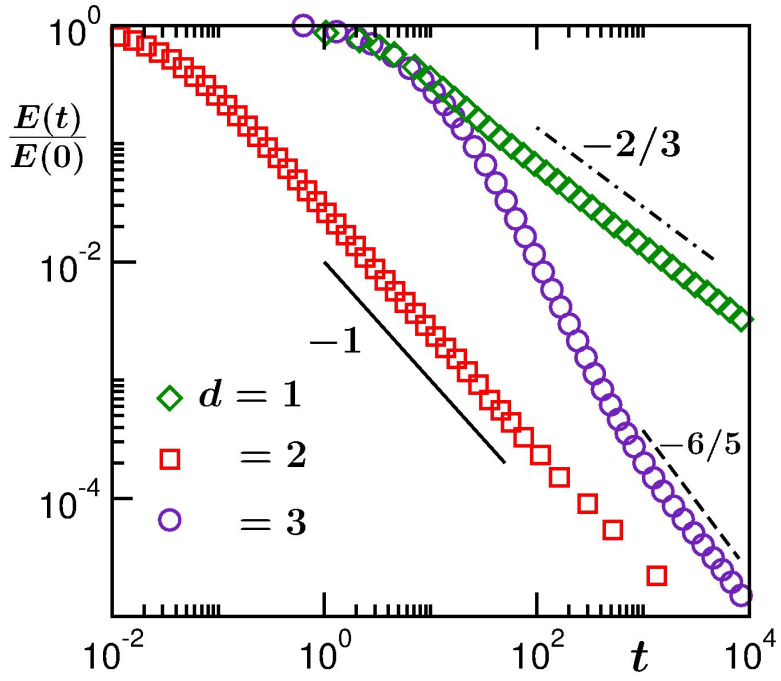

Figure 5.12: Log-log plot of the decay of energy in GGM in $d = 1$, 2 and 3. The dashed-dotted, dashed and solid lines correspond to power-laws, exponents being mentioned next to them. The results are for $\rho = 0.3$, 0.37, 0.18 and $L = 32768$, 512, 120 for $d = 1$, 2 and 3, respectively.

data from different dimensions have been multiplied by appropriate factors to bring onto the scales of the graph. It appears, all the data sets follow power-laws [27] with very similar exponent. This weaker dependence of mass not only contradicts the Carnevale *et al.*'s [1] theory, it also suggests absence of any hyperscaling relation of the type obeyed by the BAM results.

5.5 Conclusion

Via event-driven molecular dynamics simulations we have studied nonequilibrium dynamics in ballistic aggregation (BAM) [1, 4] and granular gas

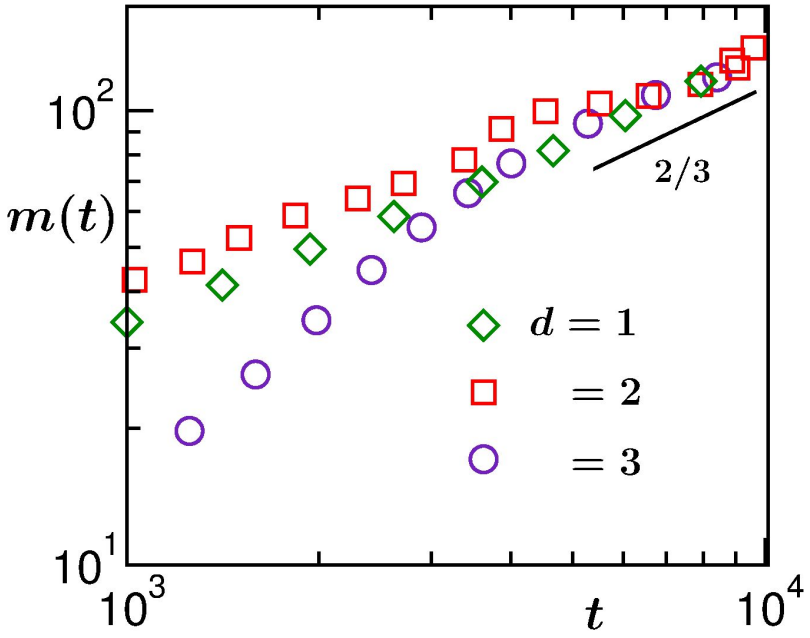

Figure 5.13: Log-log plot of the growth of the average mass in all the three dimensions for GGM. The data sets have been scaled to bring them onto the scales of the graph. Solid line there corresponds to a power-law with an exponent 2/3.

(GGM) [18] models. The focus was on the energy decay and the growth of mass. The corresponding results are compared with available theoretical predictions [1, 4].

We observe that for both the models the above mentioned quantities exhibit power-law behavior as a function of time. For the BAM, the corresponding exponents exhibit strong density dependence. Nevertheless, these exponents satisfy a hyperscaling relation [4] . With the increase of density, the energy and mass get inversely related to each other, the exponent being strongly dimension dependent. This is consistent with the prediction of Carnevale *et al.* [1]

For the GGM we observe that the energy decay satisfies the prediction of

Carnevale *et al.* at all dimensions [1]. However, this is not inversely related to the growth of mass. In fact the latter exhibits no dimension dependence.

Bibliography

[1] G.F. Carnevale, Y. Pomeau, and W.R. Young, Phys. Rev. Lett. **64**, 2913 (1990).

[2] E. Ben-Naim, S. Redner, and F. Leyvraz, Phys. Rev. Lett. **70**, 1890 (1993).

[3] E. Ben-Naim, P. Krapivsky, and S. Redner, Phys. Rev. E **50**, 822 (1994).

[4] E. Trizac and J.-P. Hansen, J. Stat. Phys. **82**, 1345 (1996).

[5] L. Frachebourg, Phys. Rev. Lett. **82**, 1502 (1999).

[6] J. Piasecki, E. Trizac, and M. Droz, Phys. Rev. E **66**, 066111 (2002).

[7] N.V. Brilliantov, A.S. Bodrova, and P.L. Krapivsky, J. Stat. Mech.: Th. and Expt. **06** P06011 (2009).

[8] F. Spahn, N. Albers, M. Sremcevic, and C. Thornton, Europhys. Lett. **67**, 545 (2004).

[9] N.V. Brilliantov, P.L. Krapivsky, A. Bodrova, F. Spahn, H. Hayakawa, V. Stadnichuk, and J. Schimidt, Proc. Nat. Acad. Sci. **112**, 9536 (2015).

[10] R.R. Rogers and M.K. Yao, *A short course in Cloud Physics*, 3rd ed. (Butterworth Heinemann, Oxford, 1989).

[11] J. Midya and S.K. Das, Phys. Rev. Lett. **118**, 165701 (2017).

[12] E. Trizac and P.L. Krapivsky, Phys. Rev. Lett. **91**, 218302 (2003).

[13] S.N. Pathak, Z. Jabeen, D. Das, and R. Rajesh, Phys. Rev. Lett. **112**, 038001 (2014).

[14] S.Paul and S.K. Das, (to appear in Phys. Rev. E, 2017).

[15] M. Shinde, D. Das, and R. Rajesh, Phys. Rev. E **79**, 021303 (2009).

[16] E. Ben-Naim, S.Y. Chen, G.D. Doolan and S. Render, Phys. Rev. Lett. **83**, 4069 (1999).

[17] X. Nie, E. Ben-Naim and S. Chen, Phys. Rev. Lett. **89**, 204301 (2002).

[18] I. Goldhirsch and G. Zanetti, Phys. Rev. Lett. **70**, 1619 (1993).

[19] S.N. Pathak, D. Das, and R. Rajesh, Europhys. Lett. **107**, 44001 (2014).

[20] S.K. Das and S. Puri, Europhys. Lett. **61**, 749 (2003).

[21] S.K. Das and S. Puri, Phys. Rev. E **68**, 011302 (2003).

[22] S. Paul and S.K. Das, Europhys. Lett. **108**, 66001 (2014).

[23] N.V. Brilliantov and T. Poeschel, *Kinetic Theory of Granular Gases* (Oxford University press, Oxford, 2004).

[24] D.C. Rapaport, *The Art of Molecular Dynamics Simulations* (Cambridge University Press, Cambridge, England, 2004).

[25] M.P. Allen and D.J. Tildesley, *Computer Simulations of Liquids* (Clarendon, Oxford, 1987).

[26] D.A. Huse, Phys. Rev. B **34**, 7845 (1996).

[27] A.J. Bray, Adv. Phys. **51**, 481 (2002).

Chapter 6

A comparative study of kinetics of phase separation in passive and active matter systems

6.1 Introduction

There has been much research interest in the understanding of nonequilibrium structure and dynamics during phase transitions [1–13]. While significant progress has been made with respect to the kinetics of phase separation in passive systems [1–13], in the domain of active matter [14–37], where constituent particles are self-propelling, the focus is rather recent, though intense. In the case of passive matter, following a quench from high temperature homogeneous configuration to a temperature inside the miscibility gap, as a system approaches the phase-separated new equilibrium, the average size (ℓ) of particle-rich and particle-poor domains typically grows algebraically,

with time (t), as [1–4]

$$\ell \sim t^{\alpha}. \tag{6.1}$$

The patterns, formed by the above mentioned domains, exhibit scaling property [3]

$$C(r,t) \equiv \tilde{C}(r/\ell), \tag{6.2}$$

where $C(r,t)$ is a two-point equal time correlation function, defined as [3]

$$C(r,t) = \langle \psi(\vec{r},t)\psi(\vec{0},t)\rangle - \langle \psi(\vec{r},t)\rangle\langle \psi(\vec{0},t)\rangle, \tag{6.3}$$

ψ being a space ($\vec{r}$) and time dependent order parameter field and $\tilde{C}$ is a time independent master function. The scalar notation r, the separation between two points, is used in the argument of C with the understanding that there exists structural isotropy. The scaling property of Eq. (6.2) is related to the fact that the growth is self-similar in nature [3], i.e., apart from a change in the global length scale, the patterns at two different times are similar to each other, in a statistical sense. In the passive situation, a good degree of understanding has been obtained [1–4] with respect to the analytical forms of the correlation function and values of the growth exponent α, based on the conservation of order parameter, transport mechanism, etc.

In the case of active matter there has been growing interest [14–17, 20–27, 35, 36] in understanding of the above mentioned aspects. However, most studies, for this purpose, use models that do not exhibit phase transition in the passive limit. In such a situation, it becomes difficult to quantify the effects of activity. Following a recent work [36], we consider a model that has

a passive limit in which the system undergoes phase transition. In this earlier work [36] focus was on the understanding of pattern, growth and aging in space dimension $d = 3$, with high enough particle density so that the resulting "vapor-liquid" transition exhibit percolating nonequilibrium structure. In this work we undertake a comprehensive study to quantify the influence of self-propelling activity on a "vapor-solid" transition in $d = 2$, for disconnected morphology. We report important results on how the structure and growth dynamics change due to introduction of self-propulsion.

The rest of the chapter is organized as follows. In Section 6.2 we discuss the model and methods. Results are presented in Section 6.3. Finally, Section 6.4 concludes the chapter with a brief summary and outlook.

6.2 Models and Methods

In this study, the passive interaction among the particles has been modeled via the potential [38–41]

$$u(r) = U(r) - U(r_c) - (r - r_c)\left(\frac{dU}{dr}\right)_{r=r_c}, \tag{6.4}$$

where

$$U(r) = 4\epsilon\Big[\Big(\frac{\sigma}{r}\Big)^{12} - \Big(\frac{\sigma}{r}\Big)^{6}\Big] \tag{6.5}$$

is the standard Lennard-Jones (LJ) potential, ϵ and σ being the strength of interaction and diameter of particles, respectively, r the inter-particle distance and r_c $(= 2.5\sigma)$ being a cut-off distance within which particles interact. The phase diagram in the temperature (T) - density (ρ) plane for this

passive model has been calculated earlier [41] for $d = 2$ and the obtained values for the critical temperature (T_c) and critical (number) density (ρ_c) are $\simeq 0.41\epsilon/k_B$ and $\simeq 0.37$, respectively, k_B being the Boltzmann constant. We have introduced the activity in the system in the Vicsek [32] manner in which particles try to align their motion along the average direction,

$$\vec{D}_n = \frac{\sum_j \vec{v}_j}{|\sum_j \vec{v}_j|}, \tag{6.6}$$

of their neighbors contained within the circle of radius r_c. Essentially, during the course of evolution, at each time step, the particles will get directional impact along $\vec{D}_n$, in addition to the passive interaction.

We perform time-step driven molecular dynamics (MD) simulations [38, 39] in $2D$ boxes of linear dimension $L\sigma$, with periodic boundary conditions applied in both the directions. The dynamical equations are solved by using velocity Verlet algorithm [38]. To keep the temperature of the system constant, we have used the Langevin thermostat [38, 39]. Thus, we have solved the equation (for particle i) [30, 31, 36, 38]

$$m\ddot{\vec{r}}_i = -\nabla U_i - \gamma m\dot{\vec{r}}_i + \sqrt{(6\gamma k_B T m)}\vec{R}_i(t) + \vec{f}_i, \tag{6.7}$$

where m is the mass (same for all the particles), γ is the damping coefficient, U_i is the potential (passive interaction) energy of particle i, $\vec{R}_i$ is random noise, $\vec{f}_i$ is the active force implemented via the Vicsek [32] rule and T is the temperature to which the system is quenched. The random noise $\vec{R}_i$ is

δ-correlated over space and time, and can be written as

$$\left\langle R_i^{\mu}(t) R_j^{\nu}(t') \right\rangle = \delta_{\mu\nu}\delta_{ij}\delta(t-t'), \tag{6.8}$$

where t and t' stand for two different times, i and j are particle indices, and μ and ν represent the Cartesian axes. The self-propelling force $\vec{f_i}$ can be written as

$$\vec{f_i} = f_A \vec{D}_n, \tag{6.9}$$

where f_A is the magnitude and $\vec{D}_n$ is the direction mentioned above.

Without the last term, solution of Eq. (6.7) gives the velocity of the particles in the passive limit ($\vec{v}_i^{\,\mathrm{pas}}(t+\Delta t)$), where Δt is the time step of integration. In our simulation, we have used $\Delta t = 0.01\tau$, τ $(= \sqrt{m\sigma^2/\epsilon})$ being the LJ unit of time. Following this, the particle velocities were further updated by incorporating $\vec{f_i}$. However, if Eq. (6.9) is used for $\vec{f_i}$ the direction of motion as well as the magnitude will change which will raise the overall temperature of the system. To keep the temperature of the system constant we normalize the magnitude of velocity to its passive value, keeping the updated direction unchanged [36].

For the sake of convenience, we set the values of m, σ, ϵ, k_B and γ to unity. All our results for the active case will be presented for $L = 1024$, with periodic boundary conditions. The initial positions and velocities of all the particles have been taken randomly. Then the dynamics of the system has been studied after quenching it to a temperature T below T_c, with overall density ($\rho = N/L^2$, N being the total number of particles) $= 0.05$. Unless otherwise mentioned, results will be presented for $T = 0.1$. We obtained

results for two values of f_A, viz., $f_A = 0$ and 1, $f_A = 0$ being the passive model. Quantitative differences between the results from the active and passive cases have been pointed out.

For the calculation of the correlation function, we map the off-lattice configurations to a lattice one. Each point on the lattice has been assigned an order-parameter (ψ) value. The value of ψ is $+1$ or -1 depending on whether the local density ($\rho_{\rm loc}$), which can be calculated from the number of particles present within a small area around that point, is higher or lower than a cut-off value $\rho_{\rm cut}$. In our studies, we choose $\rho_{\rm cut} = 0.5$. The average mass (m) of the clusters can be calculated from the continuum configuration, by appropriately identifying the clusters.

6.3 Results

We divide the section into two sub-sections. To obtain a quantitative picture on the effects of self-propulsion, first we discuss results from pure passive model. These are presented in the first subsection. The results from the active case are presented in the second one.

6.3.1 Passive case

Given that our objective is to study the situation when domains of the high density phase do not percolate, we stick to a rather low value of the overall density, viz., $\rho = 0.05$, which is very close to the vapor branch of the coexistence curve. In Fig. 6.1(a) we show snapshots from the evolution of a system which was quenched from a homogeneous density state to $T = 0.1$. At

early enough time the droplets have circular appearance. With the progress of time, as the size of these droplets increases, the shape keeps deviating from the above mentioned circular symmetry. The snapshot at the latest presented time is very much fractal.

To understand the reason behind the formation of such fractal structure, in the following we describe the mechanism of growth. Because of the choice of very low temperature, the high density phase is in crystalline state. Given that the temperature of the evolving system is controlled via a non-hydrodynamics preserving thermostat the solid state domains or clusters are essentially static. Growth occurs via the deposition of particles on these clusters from the vapor phase. Having been deposited, these particles practically stick to the boundaries of the clusters. This is because of the low mobility of the cluster constituents in the very low temperature solid phase. Of course, during the growth process the clusters try to obtain a circular shape, to minimize the interfacial free energy, via rearrangement of particles. However, because of the solid state (see Fig. 6.1(b) where we show an enlarged part of a domain) and very low temperature, the mobility of the constituent particles is very low, as mentioned above. The corresponding time scale (τ_1) of the relaxation is thus much longer than the time scale (τ_2) of diffusive deposition of particles from the vapor phase. Therefore, once the structure deviates from the circular shape, because of addition of particles, quick regaining of the structure does not become possible. Furthermore, collision of the particles, while being deposited from the vapor phase, with the clusters, can induce rotations of the clusters. This makes the deposition more probable in the elongated direction, resulting in well grown fractal structures [13].

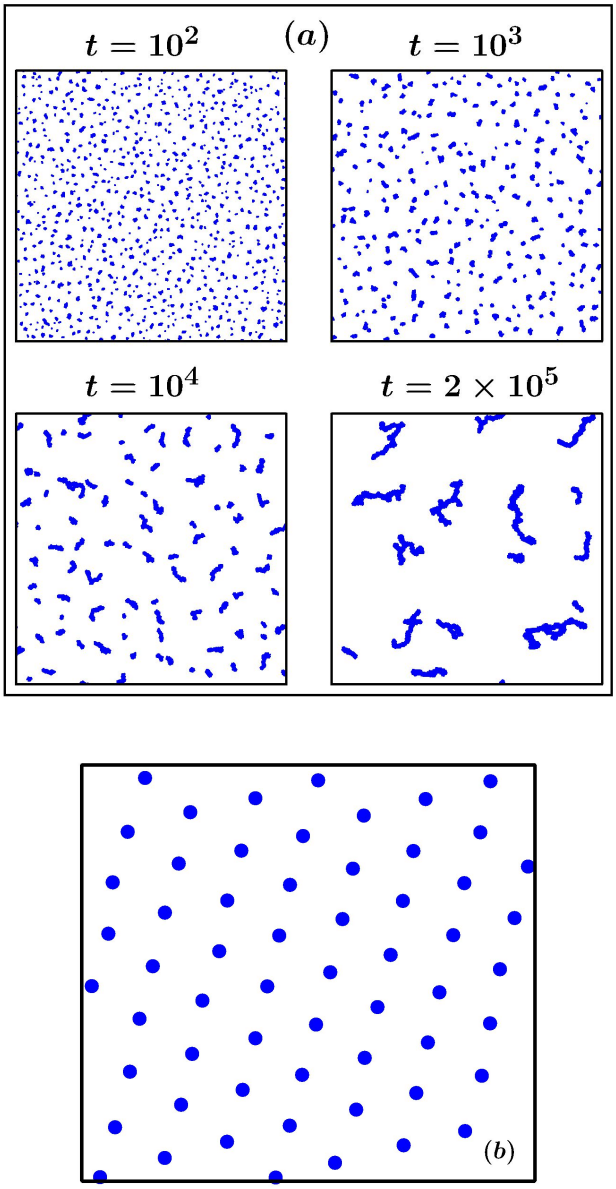

Figure 6.1: (a) Evolution snapshots from four different times for the passive model. The dots mark the locations of the particles. (b) Part of a solid-state cluster.

To calculate the fractal dimension, in Fig. 6.2(a) we plot the average mass, m, of the clusters, as a function of the average radius of gyration, R_g. For this purpose the cluster boundaries were appropriately identified.

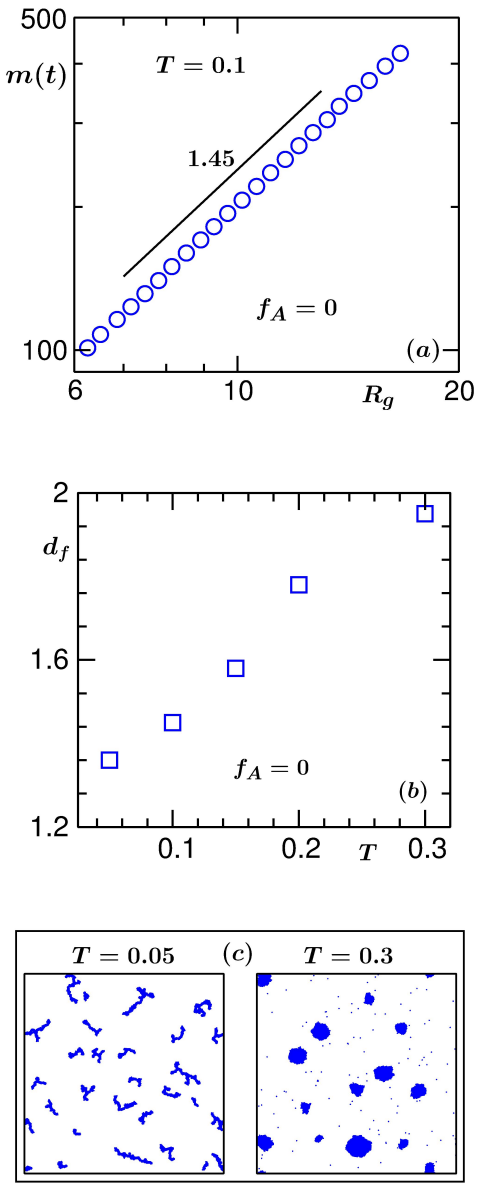

Figure 6.2: (a) Average mass of clusters is plotted vs the average radius of gyration, on a log-log scale. The solid line represents a power law, exponent being mentioned in the figure. (b) Plot of fractal dimension d_f as a function of temperature. (c) Evolution snapshots for two different temperatures, values of which are mentioned in the figure. All results correspond to the passive model.

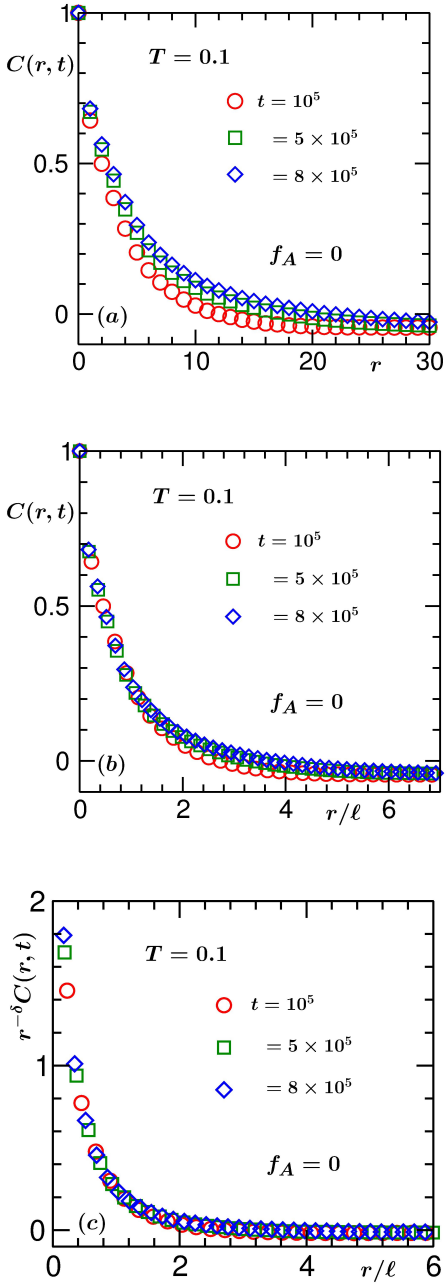

Figure 6.3: (a) Two-point equal time correlation function is plotted vs distance r. Data from three different times are shown. (b) $C(r,t)$ from different times are plotted vs r/ℓ. (c) Scaling plot of $C(r,t)$ after taking into account the correction factor due to fractality of the structure. All results are from the passive model.

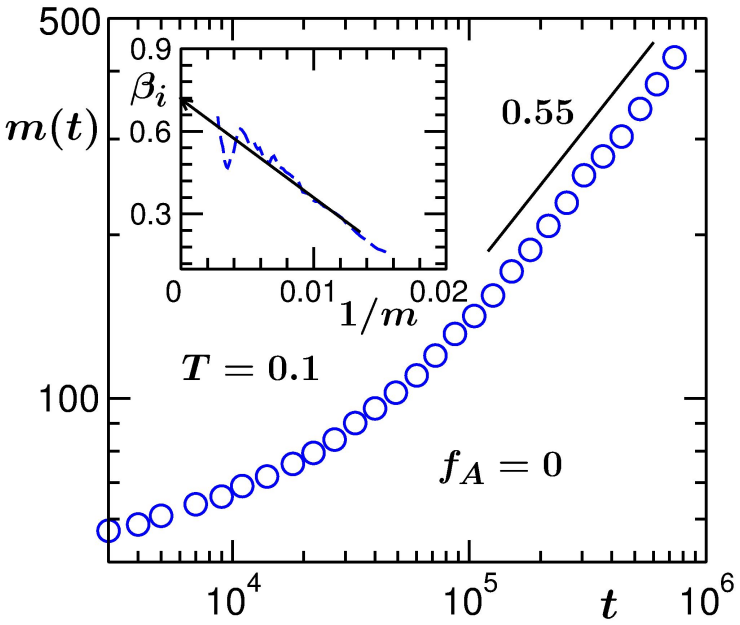

Figure 6.4: Log-log plot of m vs t, for the passive model. The solid line represents a power-law with exponent 0.55. Inset shows β_i, the instantaneous exponent, as a function of $1/m$. The solid line is a guide to the eye.

Number of particles in such a closed boundary corresponds to the mass (m_c) of the cluster. The average value was obtained from the first moment of the corresponding distribution. The radius of gyration of a cluster was estimated as [42],

$$R_g^c = \Big[\frac{1}{m_c}\sum_{i=1}^{m_c}(\vec{r}_i - \vec{r}_{\rm cm})^2\Big]^{1/2}, \tag{6.10}$$

where $\vec{r}_{\rm cm}$ is the location of the centre of mass of the cluster:

$$\vec{r}_{\rm cm} = \frac{1}{m_c}\sum_{i=1}^{m_c}\vec{r}_i. \tag{6.11}$$

Again the average value was estimated from the first moment of the distribution of R_g^c. On a log-log scale, the plot in Fig. 6.2(a) has a linear appearance,

in the large mass, i.e., long time limit. This implies a power-law behavior

$$m \sim R_g^{d_f}, \tag{6.12}$$

d_f being the fractal dimension [43, 44]. The data set appears consistent with the solid line that has the exponent $d_f = 1.45$. Such small value was observed in Brownian dynamics simulations as well [45, 46].

If the fractal structure is a result of the separation between the time scales τ_1 and τ_2, we expect this to have a temperature dependence. This is because, with the increase of the latter, τ_1 decreases, whereas τ_2 increases, because of decreasing cluster rigidity and increasing density in the vapor phase, respectively. In Fig. 6.2(b) we plot d_f as a function of T. Clearly, d_f increases with T. For T close to the triple point, which is around 0.3 for this model, it appears, d_f is approaching d (= 2). For visual illustration, in Fig. 6.2(c) we have shown two typical snapshots, one from very low and the other from a reasonably high temperature. While extremely filament like structure is prominent at the lower temperature, all the clusters at the higher temperature have nearly circular shape. Rest of the results are presented from $T = 0.1$.

In Fig. 6.3(a) we show plots of the two-point equal time correlation function from different times since quench, with the variation of distance. Slower decay with increasing time implies growth in the system. To verify the scaling property of Eq. (6.2), in Fig. 6.3(b) we show a scaling plot, by dividing the distance axis by the average length of the domains, obtained from the decay of $C(r, t)$ to a particular value (0.25). The data collapse at

large values of r/ℓ does not appear good. This is because of the fractality. In such situations, appropriate scaling form is [43, 44]

$$C(r,t) \equiv r^{\delta}\tilde{C}(r/\ell), \tag{6.13}$$

where $\delta = d - d_f$. In Fig. 6.3(c) we have obtained excellent collapse of data by using the above form.

For such fractal structures, it is appropriate to look at the time dependence of average mass to quantify the growth. An alternative is, of course, to calculate R_g. In Fig. 6.4, we have shown m as a function of t, on a log-log scale. The data at late time tend to appear linear, implying power-law growth. Here we expect $m \sim t^{\beta}$ with $\beta = 2/3$, since the growth occurs via diffusive deposition of particle, referred to as the Lifshitz-Slyozov mechanism [5]. However, the exponent appears significantly lower than the expected value (see the solid line). This is perhaps because of the fact that there is delayed nucleation and there exists an off-set length or mass when the system enters the scaling regime. In such situations, instead of extracting the exponent from the log-log plot, one should adopt more accurate exercise. In the inset of this figure we plot the instantaneous exponent [47]

$$\beta_i = \frac{d(\ln m)}{d(\ln t)}, \tag{6.14}$$

as a function of $1/m$. The corresponding data set converges to approximately $\beta = 0.72$, very close to the expected value.

6.3.2 Active case

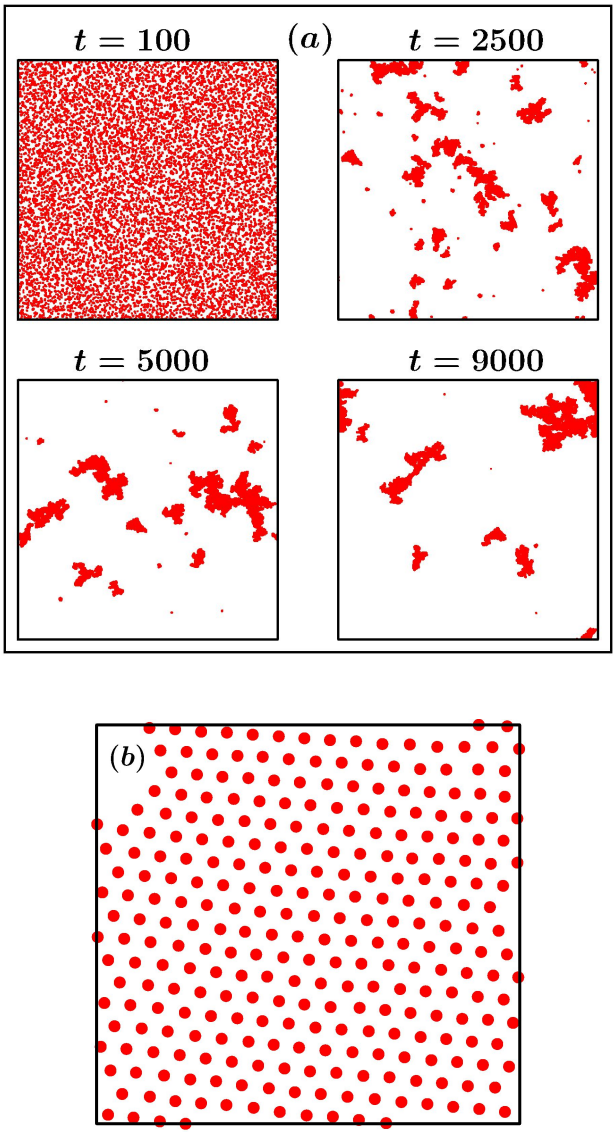

Figure 6.5: (a) Evolution snapshots for the active model with $f_A = 1$. (b) A portion of a cluster.

In Fig. 6.5(a) we show snapshots from four different times, for $f_A = 1$. A comparison with Fig. 6.1(a) reveals that the fractality is lower in this case, even though the temperature is same. A small part of a cluster is shown in

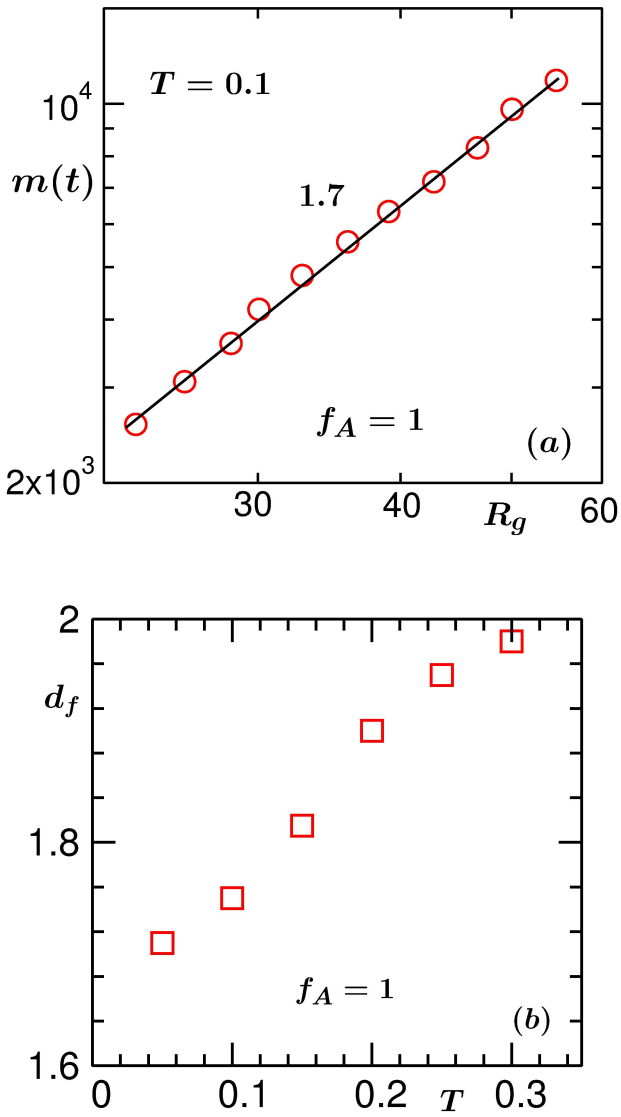

Figure 6.6: (a) Log-log plot of m vs R_g. The solid line is a power-law with $d_f = 1.7$. (b) Temperature dependence of d_f. All results are for $f_A = 1$.

Fig. 6.5(b). It shows that the crystalline structure still exists. To estimate the fractal dimension, in Fig. 6.6(a) we have shown a log-log plot of m vs R_g. The linear look of the data set indicates power-law behavior and the exponent is $\simeq 1.7$. Thus the structure is indeed less fractal than the passive case. The temperature dependence of d_f is presented in Fig. 6.6(b). Such

reduction in fractality can be due to the fact that the Vicsek [32] activity keeps the particles inside the clusters mobile, with respect to the centres of mass. Thus the timescales τ_1 and τ_2 are comparable in this case.

In Fig. 6.7 we show a scaling plot of $C(r,t)$, by taking data from three different times. The collapse appears reasonably good when the correlation functions are plotted vs r/ℓ. The better quality scaling with respect to the variable r/ℓ, compared to the passive case, is because of the higher fractal dimension. Next we move to quantify the growth.

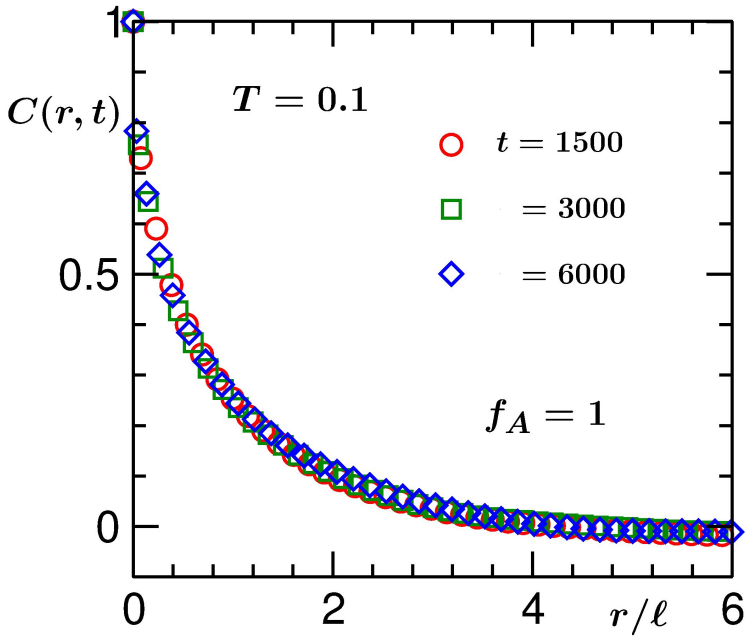

Figure 6.7: $C(r,t)$, from three different times, are plotted vs r/ℓ, for $f_A = 1$.

Unlike the passive case, here the clusters can move, because of the activity. This may lead to growth via cluster coalescence mechanism. For diffusive motion of the clusters, Binder and Stauffer [6–8] pointed out that the growth exponent β should be 1, if, of course, the clusters have spherical or circular symmetry. This exponent can be obtained from the solution of the equation

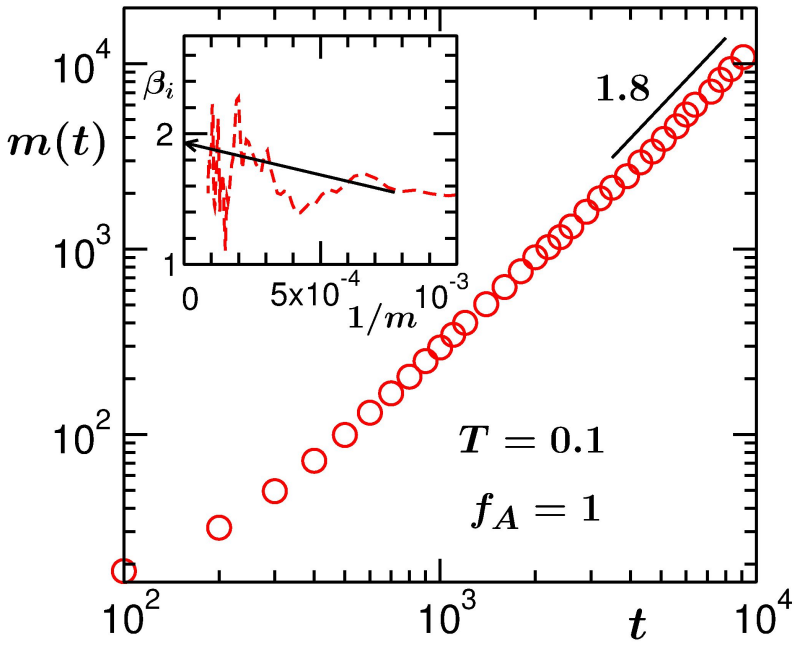

Figure 6.8: For $f_A = 1$, average mass is plotted vs time, on a log-log scale. The solid line is a power-law, exponent being mentioned next to it. Inset shows β_i as a function of $1/m$. The solid line there is a guide to the eye. All results are for $f_A = 1$.

[8]

$$\frac{dn}{dt} = -Cn^2, \tag{6.15}$$

where n is the cluster density ($\propto \frac{1}{m}$) and C is a constant whose value depends upon the diffusion constant and the average radius of the clusters.

In Fig. 6.8 we present a plot of m as a function of time. On a log-log scale the data appear consistent with a power-law. However the exponent is much higher than unity (see also the plot of instantaneous exponent β_i vs $1/m$, in the inset), that is expected for diffusive coalescence mechanism [6–8]. A possibility for such a drastic disagreement can be the fractality in the structure, in addition to the fact that the motion of the droplets is much

faster than simple diffusion. To investigate the latter we calculate the mean-squared-displacement ($\mathrm{MSD_{CM}}$) of the centre of mass of the clusters [40].

In Fig. 6.9 we show a log-log plot of the $\mathrm{MSD_{CM}}$, as a function of time, for a typical cluster. The data exhibit a robust quadratic behavior, perhaps the $\mathrm{MSD_{CM}}$ is slightly faster than t^2. In the inset of this figure we also show the number of particles in a few clusters, with the progress of time. Nearly constant behavior rules out the possibility of Lifshitz-Slyozov particle diffusion mechanism.

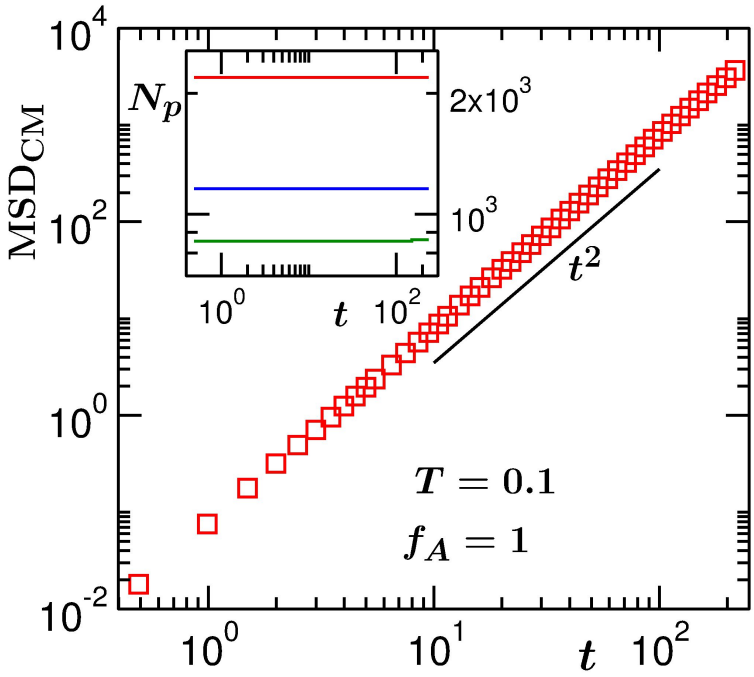

Figure 6.9: Mean-squared-displacement of the centre of mass of a cluster, for $f_A = 1$, is plotted as a function of time, on a log-log scale. The solid line is proportional to t^2. The inset shows the number of particles in a few different clusters, as a function of translated time, before they undergo collisions.

Having been encouraged by the quadratic time dependence of the $\mathrm{MSD_{CM}}$, below we consider the theory of ballistic aggregation [48–50] to understand

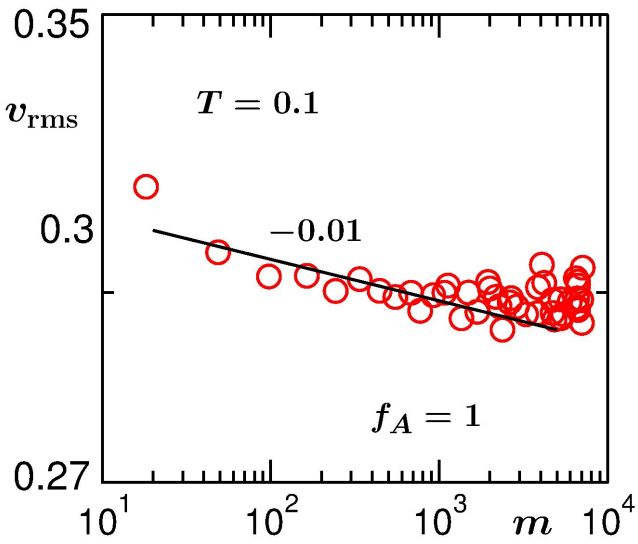

Figure 6.10: Log-log plot of the root-mean-squared velocity of the clusters as a function of mass, for $f_A = 1$. The solid line has a power-law exponent -0.01.

the high value of growth exponent, $\beta \simeq 2$. Note that such approach is not new in active matter context [27]. For that purpose one writes the kinetic equation [13]

$$\frac{dn}{dt} = - \text{ “collision cross-section” } \times v_{\rm rms} \times n^2, \tag{6.16}$$

where $v_{\rm rms}$ is the root mean squared velocity of the clusters. In $d = 2$, the collision cross-section is the radius of gyration which has the mass dependence $R_g \sim m^{1/d_f}$. Taking $n \propto \frac{1}{m}$ and $v_{\rm rms} \sim m^{-z}$, one arrives at

$$\frac{dm}{dt} = m^{\frac{1-zd_f}{d_f}}, \tag{6.17}$$

solution of which provides

$$m \sim t^{\beta}, \quad \beta = \frac{d_f}{d_f(z+1)-1}. \tag{6.18}$$

Given that $d_f \simeq 1.7$ and β is close to 2, the value of z should be approximately 0.1, much smaller than 0.5, expected for random cluster motion. In Fig. 6.10 we show $v_{\rm rms}$ as a function of m. Indeed, the value appears rather low. The discrepancy that is observed with the expectation, can be understood via more accurate analysis of simulation data with much better statistics. For example, as mentioned above, it is possible that $\mathrm{MSD}_{\rm CM}$ exhibits slightly stronger time dependence. While such a trend is already visible in the presented plot, more accurate estimate requires better statistics. Here note that, since in our active matter system energy is being continuously injected, it is not surprising that $v_{\rm rms}$ will be nearly independent of mass.

6.4 Conclusion

We have presented extensive molecular dynamics simulation results from the comparative studies of kinetics of phase separation in passive and active matter systems. The passive system is the limiting case of a general active matter model. This way it is easier to identify the effects of activity. The passive inter-particle interaction in the model is described by the Lennard-Jones potential [38–40]. The self-propulsion is introduced via the well known Vicsek model [32] where phase transition occurs due to cooperative motion.

In our molecular dynamics simulation, the temperature was controlled via

a Langevin thermostat [38]. In the passive limit this provides growth of solid clusters via particle diffusion mechanism. In the active case, on the other hand, the clusters grow via (nearly) ballistic aggregation mechanism [13, 48–50] that provides much higher growth exponent compared to the Lifshitz-Slyozov [5] value. This we have tried to understand via a nonequilibrium kinetic theory for ballistic aggregation by incorporating the fractality of the structure of the clusters.

It is expected that hydrodynamics [38] will play role in the growth process. However, the thermostat that was used in our simulations is a stochastic one. In future it will be interesting to perform similar studies with a hydrodynamics preserving thermostat [38]. Also, the effects of fractality can be checked by varying the temperature.

Bibliography

[1] A. Onuki, *Phase Transition Dynamics* (Cambridge University Press, Cambridge, England, 2002).

[2] K. Binder, in *Phase Transformation of Materials*, edited by R.W. Cahn, P. Hansen, and E.J. Kramer (VCH, Weinheim, 1991), p. 405, Vol. 5.

[3] A.J. Bray, Adv. Phys. **51**, 481 (2002).

[4] R.A.L. Jones, Soft Condensed Matter (Oxford niversity press, Oxford, 2008).

[5] I.M. Lifshitz and V.V. Slyozov, J. Phys. Chem. Solids **19**, 35 (1961).

[6] K. Binder and D. Stauffer, Phys. Rev. Lett. **33**, 1006 (1974).

[7] K. Binder, Phys. Rev. B **15**, 4425 (1977).

[8] E.D. Siggia, Phys. Rev. A **20**, 595 (1979).

[9] H. Furukawa, Phys. Rev. A **31**, 1103 (1985).

[10] H. Furukawa, Phys. Rev. A **36**, 2288 (1987).

[11] S. Roy and S.K. Das, Soft Matter **9**, 4178 (2013).

[12] R. Shimizu and H. Tanaka, Nature Comm. **6**, 7407 (2015).

[13] J. Midya and S.K. Das, Phys. Rev. Lett. **118**, 165701 (2017).

[14] M. C. Marchetti, J. F. Joanny, S. Ramaswamy, T. B. Liverpool, J. Prost, M. Rao, and A. Simha, Rev. Mod. Phys. **85**, 1143 (2013).

[15] S. Ramaswamy, Annu. Rev. Condens. Matter Phys. **1**, 323 (2010).

[16] M.E. Cates and J.Tailleur, Annu. Rev. Condens. Matter Phys. **6**, 219(2015).

[17] S. Mishra and S. Ramaswamy, Phys. Rev. Lett. **97**, 090602 (2006).

[18] J.M. Belmonte, G.L. Thomas, L.G. Brunnet, R.M.C. de Almeida, and H. Chaté, Phys. Rev. Lett. **100**, 248702 (2008).

[19] S. Mishra, A. Baskaran, and M.C. Marchetti, Phys. Rev. E **81**, 061916 (2010).

[20] M.E. Cates, D. Marrenduzzo, I. Pagonabarraga, and J. Tailleur, Proc. Natl. Acad. Sci. U.S.A. **107**, 11715 (2010).

[21] G.S. Redner, M.F. Hagan, and A. Baskaran, Phys. Rev. Lett. **110**, 055701 (2013).

[22] G.S. Redner, A. Baskaran, and M.F. Hagan, Phys. Rev. E **88**, 012305 (2013).

[23] A. Wysocki, R.G. Winkler, and G. Gompper, Europhys. Lett. **105**, 48004 (2014).

[24] E. Méhes, E. Mones, V. Németh, and T. Vicsek, PLOS ONE **7**, e31711 (2012).

[25] F. Peruani and M. Bär, New J. Phys. **15**, 065009 (2013).

[26] S. Mishra, S. Puri, and S. Ramaswamy, Philos. Trans. R. Soc., A**372**, 20130364 (2014).

[27] P. Cremer and H. Löwen, Phys. Rev. E **89**, 022307 (2014).

[28] J. Schwarz-Linek, C. Valeriani, A. Cacciuto, M. E. Cates, D. Marenduzzu, A.N. Morozov, and W.C.K. Poon, Proc. Natl. Acad. Sci. U.S.A. **109**, 4052 (2012).

[29] J. Palacci, S. Sacanna, A.P. Steinberg, D.J. Pine, and P.M. Chaikin, Science **339**, 936 (2013).

[30] S.K. Das, S.A. Egorov, B. Trefz, P. Virnau, and K. Binder, Phys. Rev. Lett. **112**, 198301 (2014).

[31] B. Trefz, S.K. Das, S.A. Egorov, P. Virnau, and K. Binder, J. Chem. Phys. **144**, 144902 (2016).

[32] T. Vicsek, A. Czirôk, E. Ben-Jacob, I. Cohen, and O. Schochet, Phys. Rev. Lett. **75**, 1226 (1995).

[33] A. Czirôk and T. Vicsek, Phys. A **281**, 17 (2000).

[34] G. Baglietto, E.V. Albano, and J. Candia, Interface Focus **2**, 708 (2012).

[35] H. Chaté, F. Ginelli, G. Grégoire, F. Peruani, and F. Raynand, Eur. Phys. J. B **64**, 451 (2008).

[36] S.K. Das, J. Chem. Phys. **146**, 044902 (2017).

[37] D. Loi, S. Mossa, and L.F. Cugliandolo, Soft Matter **7**, 10193 (2011).

[38] D. Frenkel and B. Smit, *Understanding Molecular Simulations: From Algorithm to Applications* (Academic Press, California, 2002).

[39] M. P. Allen and D.J. Tildesley, *Computer Simulations of Liquids* (Clarendon, Oxford, 1987).

[40] J. -P. Hansen and I.R. McDonald, *Theory of Simple Liquids* (Academic press, London, 2008).

[41] J. Midya and S.K. Das, J. Chem. Phys. **146**, 024503 (2017).

[42] H. Goldstein, C.P. Poole, and J.F. Safko, *Classical Mechanics* 3rd Ed. (Addison-Wesley, 2001).

[43] T. Vicsek, *Fractal Growth Phenomena* (World Scientific, Singapore, 1992).

[44] T. Vicsek, M. Shlesinger, and M. Matushita, editors, *Fractals in Natural Sciences* (World Scientific, Singapore, 1994).

[45] F. Sciortino and P. Tartaglia, Phys. Rev. Lett. **74**, 282 (1995).

[46] F. Sciortino, A. Belloni, and P. Tartaglia, Phys. Rev. E **52**, 4068 (1995).

[47] D.A. Huse, Phys. Rev. B **34**, 7845 (1996).

[48] G.F. Carnevale, Y. Pomeau, and W.R. Young, Phys. Rev. Lett. **64**, 2913 (1990).

[49] E. Trizac and P.L. Krapivsky, Phys. Rev. Lett. **91**, 218302 (2003).

[50] E. Trizac and J.-P. Hansen, J. Stat. Phys. **82**, 1345 (1996).

Zimbra **subhajitpaul@jncasr.ac.in**

EPL - permission for Copyright

From : Editorial Office <editorial.office@epletters.net> Tue, Jun 06, 2017 06:06 PM
Subject : EPL - permission for Copyright
To : Subhajit Paul <subhajitpaul@jncasr.ac.in>

Dear Mr. Paul,

Many thanks for your message.
In answer to your request, we are pleased to inform you that you are allowed to use:

the material you need from

Subhajit Paul and Subir K. Das

"Dynamics of clustering in freely cooling granular fluid"

EPL 108 (2014) 66001, https://doi.org/10.1209/0295-5075/108/66001

The references of the sources must be given (title, year, issue).
Thank you.

Sincerely yours,

Frederic Burr
EPL Staff Editor

_____

Le 5 juin 2017 à 13:36, Subhajit Paul

<subhajitpaul@jncasr.ac.in> a écrit :

Dear Sir,

I am Subhajit Paul, a final year Ph.D student under the supervision of Prof. Subir K. Das, in the Theoretical Sciences Unit of Jawaharlal Nehru Centre for Advanced Scientific Research, Jakkur P.O., Bangalore, India. I have a publication in Europhys. Letters in 2014.
Currently I am writing my thesis and want to include the

results (including text) presented in that paper in the thesis. Below I mention the details of that publication:

Dynamics of clustering in freely cooling granular fluid, EPL, Vol. 108, Page- 66001, 2014.

I will be highly obliged if you kindly permit me to use those results in my thesis.
Looking forward for your reply.

Thanks and regards,
Subhajit Paul.

--
Subhajit Paul
Soft matter and statistical mechanics lab
Theoretical Sciences Unit
JNCASR, Bangalore-560064
Ph. - (080)22082962

APS Copyright Policies and Frequently Asked Questions

What is copyright? http://www.copyright.gov/
Copyright is a form of legal protection for original works of authorship. Copyright covers both published and unpublished works.

What does copyright protect?
Copyright, a form of intellectual property law, protects original works of authorship including literary, dramatic, musical, and artistic works, such as poetry, novels, movies, songs, computer software, and architecture. Copyright does not protect facts, ideas, systems, or methods of operation, although it may protect the way these things are expressed. See Circular 1, Copyright Basics, section "What Works Are Protected", see http://www.copyright.gov/circs/circ1.html#wwp

How is a copyright different from a patent or a trademark?
Copyright protects original works of authorship, while a patent protects inventions or discoveries. Ideas and discoveries are not protected by the copyright law, although the way in which they are expressed may be. A trademark protects words, phrases, symbols, or designs identifying the source of the goods or services of one party and distinguishing them from those of others.

What is the difference between copyright infringement and plagiarism?
Copyright infringement occurs when an author's work is reused or republished without the permission of the copyright owner, whether or not author attribution accompanied the reuse.

Plagiarism occurs when an author's work has been reused or republished in such a manner as to make it appear as someone else's work, e.g., without quotation marks and citation of the original work.

Why should I transfer copyright to APS?
Like many other scientific publishers, the American Physical Society (APS) requires authors or their employers to provide transfer of copyright prior to publication. This permits APS to publish the article and to defend against improper use (or even theft) of the article. It also permits APS to mount the article online and to use the article in other forms or media, such as PROLA. By the APS transfer agreement, authors and their employers retain substantial rights in the work, as specified in the agreement (http://forms.aps.org/author/copytrnsfr.pdf) and discussed in this document.

Why should I transfer copyright to APS before the article is accepted for publication by an APS journal?
Transferring copyright early in the process avoids the possibility of delaying publication if the transfer has to be obtained later in the process. By

the terms of the copyright transfer agreement itself, it has no effect until the paper is accepted by an APS journal. The author retains the copyright until acceptance, and has the full freedom, for example, to withdraw the paper from consideration by an APS journal and submit it elsewhere.

Does transferring copyright affect my patent rights?
No. Copyright is separate from any patent rights, and the APS transfer agreement specifically states that patent rights are not affected. However, you should be aware that submitting a manuscript to a journal without first taking steps to protect your patent rights (e.g., filing for a patent) could endanger those rights. Consult your patent attorney.

As the author of an APS-published article, may I post my article or a portion of my article on my own website?
Yes, the author or the author's employer may use all or part of the APS published article, including the APS-prepared version (e.g., the PDF from the online journal) without revision or modification, on the author's or employer's website as long as a fee is not charged. If a fee is charged, then APS permission must be sought. In all cases, the appropriate bibliographic citation and notice of the APS copyright must be included.

What happens if the author has posted an APS-published article on a free access e-print server or on the authors' or institutions' web page and subsequently a fee is imposed for access to those sites?
When a fee is imposed, the author must either obtain permission from APS or withdraw the article from the e-print server or Institutional Repository.

As the author of an APS-published article, may I post my article or a portion of my article on an e-print server?
The author has the right to post and update the article on a free-access e-print server using files prepared and formatted by the author. Any such posting made or updated after acceptance of the article for publication by APS shall include a link to the online abstract in the APS journal or to the entry page of the journal. In all cases, the appropriate bibliographic citation and notice of the APS copyright must be included. If the author wishes to use the APS-prepared version (e.g., the PDF from the online journal) on an e-print server other than authors' or employer's website, then APS permission must be sought. Similarly, if the author wishes to post the article (any version) on an e-print server that charges a fee for use, APS permission must be sought.

As the author of an APS-published article, can I post my article or a portion of my article on a web resource like wikipedia or quantiki?
Sites like wikipedia and quantiki are strict about permissions and require that authors hold copyright to articles that they post there. In order to allow authors to comply with this requirement, APS permits authors to hold copyright to a "derived work" based on an article published in an APS journal as long as the work contains at least 10% new material not covered by APS's copyright and does not contain more than 50% of the text (including equations) of the original article.

As the author of an APS-published article, will I hold copyright to a "derived work", as described above, even if the original article was published prior to 1 October 2008?
Yes. The APS will extend this author right to all papers published in APS journals.

As the author (or the author's employer) of an APS-published article, may I use copies of part or all of my article in the classroom?
Yes, the author or his/her employer may use all or part of the APS-prepared version for educational purposes without requesting permission from the APS as long as the appropriate bibliographic citation is included.

As the author of an APS-published article, may I use figures, tables, graphs, etc. in future publications?
Yes, as the author you have the right to use figures, tables, graphs, etc. in subsequent publications using files prepared and formatted by you or the APS-prepared versions. The appropriate bibliographic citation must be included.

As the author of an APS-published article, may I include my article or a portion of my article in my thesis or dissertation?
Yes, the author has the right to use the article or a portion of the article in a thesis or dissertation without requesting permission from APS, provided the bibliographic citation and the APS copyright credit line are given on the appropriate pages.

As the author of an APS-published article, may I give permission to a colleague or third party to republish all or part of the article in a print publication?
Yes, as the author you can grant permission to third parties to republish print versions of the article provided the APS-prepared version (e.g., the PDF from the online journal, or a copy of the article from the print journal) is not used for this purpose, the article is not published in another journal, and the third party does not charge a fee. The appropriate bibliographic citation and notice of the APS copyright must be included.

As the author of an APS-published article, may I give permission to a colleague or third party to republish all or part of the article in an online journal, book, database compilation, etc.?
Authors should direct the third party request to APS.

As the author of an APS-published article, may I provide a PDF of my paper to a colleague or third party?
The author is permitted to provide, for research purposes and as long as a fee is not charged, a PDF copy of his/her article using either the APS-prepared version or the author prepared version.

As a third party (not an author), may I republish an article or portion of an article published by APS?
Yes, APS will grant permission to republish articles or portions of articles (e.g., tables, graphs, excerpts) published by APS. Depending on the reuse and medium APS has the right to grant permission subject to APS terms and conditions and a fee may be assessed.

As a third party, may I use articles published by APS for lecture and classroom purposes?
Yes, you may use photocopied articles published by APS for lecture and classroom purposes for a single semester without asking permission from APS. However, if the article becomes part of your course material beyond one semester, you must obtain permission from APS. Also, there is no limitation on the use of APS articles using links to the material accessible through institutional subscriptions.

How do I request permission to republish APS-copyrighted material?
To request permission to republish APS-copyrighted material, please provide the following information:

1. Title of journal
2. Title of article
3. Name of author
4. Volume number, page number (or article identifier), year
5. Indicate if you are requesting to republish in print, online, CD-ROM, and/or other format

6. Indicate if you wish to republish all or portion of article; if a portion describe the specific material, e.g., figure numbers, excerpt
7. Indicate how the material will be used, e.g., in a book, journal, proceeding, thesis, etc.
8. Indicate the title of the article/thesis/chapter etc., and the name of the publication in which your work will appear
9. Indicate the name of the publisher
10. Indicate whether or not a fee will be charged for the publication

*To prevent clerical error, please include all requests in a single email or letter.

All permission requests must be in writing (email is acceptable). Blanket permissions are not granted. Please note all requests are subject to APS terms and conditions and a fee may be assessed.

Please allow 5-7 business days for us to respond to a permission request provided all the above information is provided at the time of the request.

Send all permission requests to:

Associate Publisher
American Physical Society
One Physics Ellipse
College Park, MD 20740
Email: assocpub@aps.org

If your questions have not been addressed and you need further assistance, please call: 301-209-3283.

How do I provide a proper bibliographic citation and notice of the APS copyright?
Provide the following information in this order:

Authors names, journal title, volume number, page number (or article identifier), year of publication. "Copyright (year) by the American Physical Society."

Further information
For further information about copyright in general, please refer to the Library of Congress FAQ at: http://www.copyright.gov/help/faq/

Journals published by the American Physical Society can be found at http://publish.aps.org/

FAQ Version: October 1, 2008